INFORMATION TO USERS

This manuscript has been reproduced from the microfilm master. UMI films the text directly from the original or copy submitted. Thus, some thesis and dissertation copies are in typewriter face, while others may be from any type of computer printer.

The quality of this reproduction is dependent upon the quality of the copy submitted. Broken or indistinct print, colored or poor quality illustrations and photographs, print bleedthrough, substandard margins, and improper alignment can adversely affect reproduction.

In the unlikely event that the author did not send UMI a complete manuscript and there are missing pages, these will be noted. Also, if unauthorized copyright material had to be removed, a note will indicate the deletion.

Oversize materials (e.g., maps, drawings, charts) are reproduced by sectioning the original, beginning at the upper left-hand corner and continuing from left to right in equal sections with small overlaps.

Photographs included in the original manuscript have been reproduced xerographically in this copy. Higher quality 6" x 9" black and white photographic prints are available for any photographs or illustrations appearing in this copy for an additional charge. Contact UMI directly to order.

Bell & Howell Information and Learning
300 North Zeeb Road, Ann Arbor, MI 48106-1346 USA
800-521-0600

SPECTROSCOPIC STUDIES OF METAL SORPTION REACTIONS TO SOIL MINERALS

by

Evert J. Elzinga

A dissertation submitted to the Faculty of the University of Delaware in partial fulfillment of the requirements for the degree of Doctor of Philosophy in Plant and Soil Sciences

Summer 2000

© 2000 Evert J. Elzinga
All Rights Reserved

UMI Number: 9982684

Copyright 2000 by
Elzinga, Evert Jan

All rights reserved.

UMI®

UMI Microform 9982684
Copyright 2001 by Bell & Howell Information and Learning Company.
All rights reserved. This microform edition is protected against
unauthorized copying under Title 17, United States Code.

Bell & Howell Information and Learning Company
300 North Zeeb Road
P.O. Box 1346
Ann Arbor, MI 48106-1346

SPECTROSCOPIC STUDIES OF METAL SORPTION REACTIONS TO SOIL MINERALS

by

Evert J. Elzinga

Approved: Donald L. Sparks

Donald L. Sparks, Ph.D.
Chair of the Department of Plant and Soil Sciences

Approved: John C. Nye

John C. Nye, Ph.D.
Dean of the College of Agriculture and Natural Resources

Approved:

Conrado M. Gempesaw II, Ph.D.
Vice Provost for Academic Programs and Planning

I certify that I have read this dissertation and that in my opinion it meets the academic and professional standard required by the University as a dissertation for the degree of Doctor of Philosophy.

Signed: 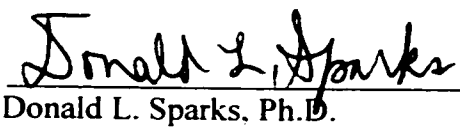

Donald L. Sparks, Ph.D.
Professor in charge of dissertation

I certify that I have read this dissertation and that in my opinion it meets the academic and professional standard required by the University as a dissertation for the degree of Doctor of Philosophy.

Signed: 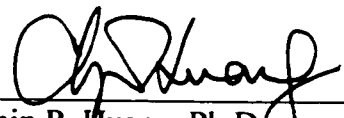

Chin P. Huang, Ph.D.
Member of dissertation committee

I certify that I have read this dissertation and that in my opinion it meets the academic and professional standard required by the University as a dissertation for the degree of Doctor of Philosophy.

Signed: 

Yan Jin, Ph.D.
Member of dissertation committee

I certify that I have read this dissertation and that in my opinion it meets the academic and professional standard required by the University as a dissertation for the degree of Doctor of Philosophy.

Signed: 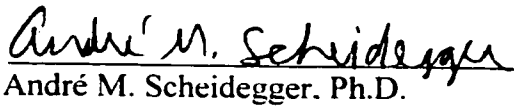

André M. Scheidegger, Ph.D.
Member of dissertation committee

ACKNOWLEDGMENTS

Dr. D.L. Sparks for his support throughout the pursuit of this degree. Jerry Hendricks and all the members of the UDel Soil Chemistry Research group for their friendship and assistance during this research. The members of my dissertation committee for some nice challenges. The X-11A beamline staff at the NSLS for assistance in EXAFS data acquisition, and Kathy Olsen for ICP analyses.

TABLE OF CONTENTS

LIST OF TABLES

LIST OF FIGURES

ABSTRACT

Kinetic and equilibrium studies were conducted on Ni and Pb sorption to pyrophyllite, montmorillonite, illite, amorphous silica, and goethite, using X-ray absorption spectroscopy (XAS) and attenuated total reflectance fourier transform infrared spectroscopy (ATR-FTIR) to characterize sorption reactions on a molecular level. In all systems, competition between different modes of metal uptake was observed, with the final metal speciation being controlled by system parameters such as pH, ionic strength, reaction time, the presence of competing mineral surfaces, and the presence of co-adsorbing oxyanions.

In a study of Ni sorption in a 1:1 pyrophyllite-montmorillonite clay mineral mixture, using XAFS to assess the distribution of sorbed Ni over the mixture components, Ni uptake was found to occur via both adsorption on the montmorillonite phase and Ni-Al hydroxide precipitation associated with the pyrophyllite phase. This study showed that Ni-Al hydroxide precipitation may take place on the same time scale as adsorption mechanisms, which is not accounted for in current models describing metal sorption to (clay) minerals.

In another study, Ni sorption to illite was investigated as a function of pH, ionic strength and reaction time, using XAFS to characterize the Ni sorption products formed. Illite is a clay mineral that contains edge sites available for inner-sphere Ni complexation, internal planar sites capable of outer-sphere Ni adsorption, and structural Al that may dissolve to form Ni-Al hydroxide coprecipitates. The Ni speciation was found to be strongly dependent on reaction conditions. At pH>6.25,

Ni-Al hydroxide phases formed, whereas at lower pH values, Ni sorption proceeded via adsorption to illite edge and planar sites. The reaction time affected both the extent and speciation of sorbed Ni at pH>6.25. Continued Ni uptake over time was observed in this pH range, with faster sorption rates as pH increased. XAFS results showed that this was due to continued growth of Ni-Al hydroxide species over time. At a given loading level, however, pH dependent differences were found in the Ni speciation, which was due to differences in either the composition or the amount of the Ni-Al hydroxide phases formed. Lowering the ionic strength raised the overall Ni sorption at any given pH. XAFS data showed that this was due to the formation of outer-sphere Ni sorption complexes.

In a study of Pb sorption to amorphous silica, XAFS was used to characterize the Pb sorption mechanisms as affected by pH and ionic strength. The system pH affected both the extent and the mechanism of Pb sorption. Raising the pH resulted in increased Pb sorption. At low pH (<4.5), significant outer-sphere Pb sorption was observed, along with inner-sphere adsorption to high affinity surface sites. As pH increased from 4.5 to 6.3, Pb inner-sphere adsorption and Pb nucleation became increasingly important, whereas outer-sphere sorption systematically decreased and became negligible at pH>6.0. Although lowering the ionic strength resulted in increased Pb sorption, essentially no differences in Pb speciation at a given pH value were found in systems with low (I=0.005M) and high (I=0.1M) ionic strength. This indicated that the additional Pb sorption resulting from lowered I occurred via both outer- and inner-sphere Pb complexation, as well as Pb nucleation, dependent on pH.

Co-adsorption of Pb and SO_4 to goethite over the pH range 4.5-6.0 was studied using ATR-FTIR to probe the molecular coordination environment of sorbed

SO_4, and XAFS to probe the chemical environment of sorbed Pb. Both the IR and the XAFS results pointed to the formation of the Pb-SO_4 ternary complexes forming at the goethite surface in the pH range studied. Although it was not possible to exactly determine the configuration of the Pb-SO_4-goethite ternary complexes, we were able to limit the choices to a couple of possible options. In addition to the formation of ternary complexes, Pb adsorption also had an electrostatic effect on SO_4 sorption to goethite. These effects were more pronounced at higher pH values and lower Pb additions.

Chapter 1

INTRODUCTION

1.1 Scope of Research

Retention of heavy metal ions on soil mineral surfaces is a crucial process for maintaining environmental quality. A thorough understanding of the sorption mechanisms involved in the interaction between heavy metals and soil mineral surfaces is therefore of fundamental importance. Sorption reactions at solid-water interfaces decrease the solute mobility and often control the fate, bioavailability, and transport of trace metal ions such as Zn, Cd, Ni, and Cu in aquatic and soil environments. Correctly determining the sorption mechanisms of metals on clay and other mineral surfaces is therefore of great importance for understanding the fate of such pollutants in contaminated soils and sediments, and the hazard they present to humans and soil biota.

Metal sorption is defined here broadly as the transfer of metal ions from the solution phase to the solid phase induced by the presence of mineral surfaces. There have been numerous studies on metal sorption in "simple" systems, where only metal

ions and indifferent electrolyte ions are present (*e.g.* Maguire *et al.*, 1981; Kim and Ferguson, 1992; Zachara *et al.*, 1993). The following processes have been suggested to play a role in the overall sorption of metal cations by soil minerals: cation exchange, chemisorption, surface precipitation, and diffusion. The relevance of each of these processes in a sorption experiment is determined by the experimental setup, which is defined by the solid phase/metal combination, the experimental conditions (*e.g.* metal concentration, type and concentration of the background electrolyte, pH), and the reaction time employed.

In ligand containing systems, which soils typically are, metal sorption may be different from "simple" systems due to metal-ligand and/or ligand-surface interactions. The results can not be generalized easily: metal sorption sometimes decreases and sometimes increases depending on the particular metal, ligand, sorbent and pH range being studied.

There is a need to characterize metal sorption reactions to soil mineral surfaces as a function of variables that may control metal speciation in natural soil settings. These include pH, ionic strength, reaction time, the presence of competing surfaces for metal uptake, and the presence of non-inert co-adsorbing oxyanions. Application of in-situ spectroscopic techniques in performing such research is particularly useful, since these provide mechanistic molecular scale information on the sorption reactions studied.

1.2 General Sorption Processes

1.2.1 Cation Exchange

In soil science, the term "cation exchange" is used to characterize the replacement of one adsorbed, readily exchangeable cation by another (Sposito, 1989). Cation exchange is not a chemical reaction in the usual sense, since the bonds broken and formed are long-range electrostatic bonds of low energy (McBride, 1994). Electrostatic bonding of metal ions to clay minerals occurs mainly at planar sites of permanent structural charge and is therefore pH independent. Only for clay minerals with low structural charge (*e.g.* pyrophyllite) does significant electrostatic bonding at the clay edge sites of variable charge take place. In these systems electrostatic bonding is pH dependent (Stumm and Morgan, 1996).

The Me^{n+}-Na^{+} exchange, where Me^{n+} is a metal cation with valence n, can be described as (McBride, 1994):

$$Me^{n+} + nNa^{+}\text{-clay} \leftrightarrow Me^{n+}\text{-clay} + nNa^{+}$$

The selectivity coefficient (K_s) can be written:

$$K_s = ([Na]^n N_{Me}) / ([Me](N_{Na})^n)$$

where [Na] and [Me] represent the molarity of the metals in solution, and N_{Na} and N_{Me} symbolize the fraction of clay exchange sites occupied by Na^{+} and Me^{n+}. Equation (1) shows that multivalent cations effectively displace monovalent cations from clay exchange sites when the monovalent cation concentration is low. Studies on Na^{+}-Me^{2+} exchange reactions on Na^{+}-saturated sorbents such as the Wyoming, Camp Berteau, and Chambers montmorillonites (Peigneur *et al.*, 1975; Inskeep and Baham,

1983; Fletcher and Sposito, 1989) have shown that Na^{+}-Me^{2+} exchange reactions on montmorillonite are relatively insensitive to pH at low pH-values (pH<6) (Peigneur *et al.*, 1975; Zachara *et al.*, 1993). However, at higher pH (pH>6), adsorption of metal cations on layer silicates increases with increasing pH (Peigneur *et al.*, 1975; Schulthess and Huang, 1990; Cowan *et al.*, 1992; Inskeep and Baham, 1983). Papelis and Hayes (1996) studied the sorption of Co^{2+} on montmorillonite, and found that at low ionic strength (*i.e.* low Na^{+} concentrations) Co^{2+} is mainly sorbed as an outer-sphere complex and Co sorption is pH insensitive over the pH-range 3-9.

Ion exchange reactions at surface sites exposed to solution are extremely fast. In fact, the kinetics of cation exchange have not generally been accessible to measurements by conventional methods. Cation exchange on clays without narrow interlayer regions (*e.g.* kaolinites, fully dispersed smectites) appears to be instantaneous (McBride, 1994). With 2:1 clay minerals that contain both external and internal exchange sites, particularly with vermiculite and micas where partially collapsed interlayer sites exist, the kinetics are slower (Sparks, 1995). This is due to the presence of exchange sites of low accessibility on these clay minerals; the actual "chemical" process of cation exchange itself, however, is fast also on these sites.

1.2.2 Chemisorption

Chemisorption (also called specific sorption) involves the formation of a covalent bond between a metal and the clay surface and leads to the formation of an inner-sphere metal complex. The edges of layer silicate clays provide surface sites for

the chemisorption of transition and heavy metals. The sorption site presented to the metal in solution is a valence-unsatisfied OH^- or H_2O ligand bound to a metal ion (Al^{3+} or Si^{4+}). For example, on the octahedral aluminum sites, a trace metal, Me, may bind according to the reaction:

$$>Al\text{-}OH]^{-1/2} + Me(H_2O)_6{}^{n+} \rightarrow >Al\text{-}O\text{-}Me(H2O)_5]^{(n-3/2)+} + H_3O^+$$

This reaction has at least four features that distinguish it from cation exchange (McBride, 1994):

1. Release of n H^+ ions for each Me^{n+} cation chemisorbed
2. A high degree of specificity shown by particular minerals for particular trace metals
3. Tendency toward irreversibility, or at least a desorption rate that is orders of magnitude slower than the adsorption rate
4. A change in the measured surface charge toward a more positive value.

This last feature implies that the adsorbed metal and its charge become part of the mineral surface, thereby shifting the PZC to higher pH.

Numerous studies have demonstrated the importance of chemisorption of metals by clay minerals (*e.g.* McBride *et al.*, 1984; Zachara *et al.*, 1988; Singh and Mattigod, 1992; Cowan *et al.*, 1992; Zachara *et al.*, 1994; Scheidegger *et al.*, 1996a; Papelis and Hayes, 1996). Chemisorption of metals generally becomes more specific as the solution pH increases; *i.e.*, formation of inner-sphere complexes is favored at

elevated pH (Sparks, 1995). Papelis and Hayes (1996) showed that the sorption mechanism of Co on montmorillonite shifts from cation exchange to chemisorption when ionic strength is increased from I=0.001 to I=0.1M.

Chemisorption of metal cations on clay minerals is slower than cation exchange, often increasing gradually over several days. Trace metal cations chemisorbed on clays gradually lose much of their initial lability (as measured by diminishing self-exchange rates) over a period of days. Consequently, trace metal chemisorption on clay minerals is considered to be highly nonreversible (McBride, 1994).

1.2.3 Surface Precipitation

Recent studies using surface spectroscopic and microscopic techniques such as extended X-ray absorption fine structure spectroscopy (EXAFS), X-ray photo electron spectroscopy (XPS), Auger electron spectroscopy, scanning electron microscopy, atomic force microscopy, and TEM have shown that in many cases the sorption of heavy metals on clay and oxide surfaces results in the formation of multinuclear or polynuclear surface complexes (Fendorf *et al.*, 1992a,b, 1993, 1994; Charlet and Manceau, 1993; Fendorf and Sparks, 1994; Junta and Hochella, 1994; O'Day *et al.*, 1994a,b; Scheidegger *et al.*, 1996a,b, 1997, 1998). Such precipitate phases have been commonly observed at surface metal loadings far below a theoretical monolayer, and in a pH range well below the pH where the formation of metal hydroxide precipitates due to bulk precipitation would be expected based on the thermodynamic solubility

product (Charlet and Manceau, 1993; Fendorf *et al.*, 1994; O'Day *et al.*, 1994a; Fendorf and Fendorf, 1996, Scheidegger *et al.*, 1996a,b, 1997, 1998). The formation of these precipitates therefore appears to be somehow related to the presence of mineral surfaces, which has lead to the term surface precipitates. O'Day *et al.* (1994a) suggested the following mechanisms for stabilisation of multinuclear species near mineral surfaces: (1) the solid phase may lower the energy of nucleation by providing sterically similar sites for nucleation; (2) metal concentrations in the electrical double layer are higher than in the bulk solution, which may promote metal precipitation near or at the surface; and (3) the dielectric constant of water near the surface is reduced relative to the bulk solution, and therefore the solubility of solid phases near the surface is lowered relative to the bulk solution.

In the case of Ni sorption on clay mineral surfaces described by Scheidegger *et al.* (1996a,b, 1997, 1998), the formed surface precipitate was identified as a mixed Ni-Al-hydroxide phase. The data suggested that Al released upon dissolution of the clay mineral was part of the surface precipitate, leading to the formation of a co-precipitate. Follow-up studies by Ford *et al.* (1999) and Scheinost *et al.* (1999, 2000) confirmed these findings, and provided evidence for increased resistance to dissolution of the Ni-Al hydroxy phases over time due to silification of the interlayer surface associated with these sheet-like structured phases. The formation of similar phases has been observed for Zn and Co. Recent TEM work by Towle *et al.* (1997) and Thompson *et al.* (1999) has shown that they may form as separate entities not associated with the

mineral surface. Thus, although the Me(II)-Al LDH phases do form as the result of the presence of minerals, they do not necessarily reside at the mineral surface.

1.2.4 Diffusion

With 2:1 clay minerals that contain internal sites, diffusion to these sites may take place. Diffusion is a "physical" process driven by concentration gradients that may continue for weeks or months. Since diffusion removes metal ions from solution it is classified here as a separate sorption process. Diffusion within clay particles is referred to as intra-particle diffusion, and may include diffusion of sorbate occluded in micropores (pore diffusion) and along pore-wall surfaces (surface diffusion), as well as diffusion processes into the bulk of the solid, all of which are activated diffusion processes (Sparks, 1989). Metal ions that diffuse to the internal clay sites may be subject to cation exchange. An example of a system in which diffusion plays a significant role is the Cs/Illite system described by Comans and Hockley (1992). Illite clays contain internal sites to which Cs slowly diffuses. Cesium ions bind to these sites, dehydrate, and thereby collapse the interlayer. As a result, Cs ions get fixed in the illite interlayer region.

1.3 Metal Sorption in Soils

Soils are heterogeneous mixtures of a variety of clay and oxide minerals, and as a result, a variety of sorbents will be competing for uptake of metals added to soil systems. Complexity exists at the single clay and mineral oxide level: many minerals

simultaneously have sites that are capable of inner-sphere metal adsorption, sites that are capable of outer-adsorption, and slowly accessible inter-layer sites. Therefore, competition for metal uptake in soils takes place at two levels: between the surfaces of the different minerals present, as well as between the different surface sites of a single soil mineral. Metal partitioning in soils will be a function of the types of complexation sites present, their affinity for metal uptake, their abundance and accessibility in the system, as well as the rate (kinetics) by which the reaction between metal and surface site proceeds. Important controls on metal partitioning in soils are pH, reaction time, ionic strength, metal concentration, the solids concentrations, and temperature.

In addition to the complexity induced by the presence of a variety of minerals in soils and the different mechanisms by which a single mineral may bind metal ions, soil solutions often contain an array of constituents that may affect the uptake of the metal species being studied. An obvious example is the presence of other metal cations competing with the target metal for sorption sites, which leads to sorption lower than expected based on the results of single metal sorption studies. Other important consituents are inorganic and organic anions. Anions may sorb to mineral surfaces, thereby changing the surface characteristics of field soils, leading to altered metal sorption behavior. Other possible effects of anions include the formation of anion-metal complexes in solution and at the mineral surface, and the formation of metal-anion precipitates. As a result, the effect of anions on metal sorption behavior can not be generalized easily. Metal sorption sometimes increases (*e.g.* Benjamin and

Leckie., 1981; Clark and McBride, 1985; Gunneriusson, 1994, Gunneriusson *et al.*, 1994; Bargar *et al.*, 1998) and sometimes decreases (*e.g.* Davies and Leckie, 1978; Elrashdi and O'Connor, 1982; Boekhold *et al.*, 1993) depending on the particular metal, ligand, adsorbent and pH range being studied. Sposito (1989) classified the general effects of metal-complexing ligands in the soil solution on the adsorption of metal cations to soil minerals as follows:

1. The ligand has a low affinity for the metal and for the adsorbent.
2. The ligand has a high affinity for the metal and forms a soluble complex with it, and this complex has a low affinity for the adsorbent.
3. The ligand has a high affinity for the metal and forms a soluble complex with it, and this complex has a high affinity for the adsorbent.
4. The ligand has a high affinity for the adsorbent, and the adsorbed ligand has a low affinity for the metal.
5. The ligand has a high affinity for the adsorbent, and the adsorbed ligand has a high affinity for the metal.
6. The metal has a high affinity for the adsorbent, and the adsorbed metal has a high affinity for the ligand.

Categories 3 and 5 result directly in enhanced metal adsorption from the presence of ligands by forming metal-ligand ternary complexes, whereas category 4 can result indirectly in enhanced metal adsorption if the adsorbed ligand causes the surface charge to become more negative. Categories 3, 5, and 6 produce the same

kind of surface species (adsorbed metal-ligand complex) and therefore cannot be identified separately on the basis of macroscopic adsorption experiments.

In most published studies of anion impacts on metal sorption to clay minerals and oxides, mechanisms controlling the effect of ligands on metal sorption are suggested based solely on macroscopic observations, for instance by using modeling approaches to interpret sorption data (surface complexation models or speciation calculations for solution phase metals), or by using techniques like radio-labeling the added ligands. Unfortunately, it is not possible to indefinitely infer sorption mechanisms from modeling results or macroscopic observations (Sposito, 1984); spectroscopic techniques that provide molecular scale information should be used for this purpose (Scheidegger and Sparks, 1996).

Only a few spectroscopic studies addressing the impact of anions on metal sorption have been reported in the literature, so clearly, there is a paucity in mechanistic information available on this subject, and more spectroscopic investigations in this area would be useful.

1.4 Research Justification

Knowledge of metal speciation is a prerequisite for determining the mobility and bioavailability of heavy metals in soil environments. Critical are the mechanisms by which the interactions between heavy pollutants are held by soil constituents, since these affect both the extent and the perseverence of metal retention. Many macroscopic and spectroscopic studies exist where metal sorption to clay minerals and

oxides was studied under a limited range of reaction conditions. While these studies have provided useful information on metal sorption reactions to a host of clay minerals and oxides. the heterogeneous nature of many of these soil minerals makes it quite possible that the mechanisms of metal uptake vary as a function of system parameters such as pH. ionic strength. and reaction time. The research presented in this thesis was aimed to a large part at studying the effects of reaction conditions on metal interactions with soil minerals. Additionally. a study was performed where two different mineral surfaces were competing for metal uptake. a simplified situation from field soil settings. where a variety of sorbents compete for metal sorption. In another study, the effect of sulfate. a common inorganic anion in the soil solution of many agricultural fields. was investigated.

In all studies. in-situ spectroscopic techniques. providing molecular scale information on the bonding environment of the target element. were used to characterize the sorption products formed. These techniques provided mechanistic information on the sorption reactions studied.

The clay minerals and oxides used in this research are common constituents in many soils. and the metal species that were investigated (Pb and Ni) are common environmental contaminants.

1.5 Research Objectives

The specific systems studied, and the corresponding research objectives were the following:

1) To characterize Ni sorption in a mineral mixture consisting of pyrophyllite and montmorillonite system using X-ray absorption spectroscopy (XAFS).

2) To characterize the effects of reaction time, pH and ionic strength on the mechanisms of Ni sorption in illite suspensions, using a combination of macroscopic techniques and EXAFS.

3) To determine the effect of SO_4^{2-} on the mechanisms of Pb sorption to goethite using Fourier transform infrared spectroscopy for molecular probing of the sulfate coordination environment, and EXAFS to probe the local coordination of sorbed Pb atoms.

4) To determine the effects of pH and ionic strength on sorption mechanisms of Pb to the amorphous SiO_2 surface using XAFS.

1.6 References

Bargar, J.R., G.E. Brown Jr., and G.A. Parks. 1998. Surface complexation of Pb(II) at oxide-water interfaces: III. XAFS determination of Pb(II) and Pb(II)-chloro adsorption on goethite and alumina. Geochimica et Cosmochimica Acta, 62, 193-207.

Boekhold, S., E.J.M. Temminghoff, and S.E.A.T.M. Van der Zee. 1993. Influence of electrolyte composition and pH on cadmium sorption by an acid sand. Journal of Soil Science, 44, 85-96.

Charlet, L., and A. Manceau. 1993. Structure, formation, and reactivity of hydrous oxide particles: Insights from x-ray absorption spectroscopy. In: J. Buffle and H.P. van Leeuwen (Eds.) Environmental Particles. Lewis Publ., Boca Raton, Florida.

Clark , C.J., and M.B. McBride. 1985. Adsorption of Cu(II) as affected by phosphate. Soil Science, 139, 412-421.

Comans, R.N.J., and D.E. Hockley. 1992. Kinetics of cesium sorption on illite. Geochimica et Cosmochimica Acta, 56, 1157-1164.

Cowan, C.E., J.M. Zachara., S.C. Smith, and C.T. Resch. 1992. Individual sorbent contributions to cadmium sorption on Ultisols of mixed mineralogy. Soil Science Society of America Journal, 56, 1084-1094.

Davies, J.A., and J.O. Leckie. 1978. Effect of adsorbed complexing ligands on trace metal uptake by hydrous oxides. Environmental Science and Technology, 12, 1309-1315.

Elrashdi, M.A., and G.A. O'Connor. 1982. Influence of solution composition on sorption of Zinc by soils. Soil Science Society of America Journal, 46, 1153-1158.

Fendorf, S.E., M. Fendorf, D.L. Sparks, and R. Gronsky. 1992a. Inhibitory mechanisms of Cr(III) oxidation by δ-MnO_2. Journal of Colloid and Interface Science, 153, 37-54.

Fendorf, S.E., D.L. Sparks, M. Fendorf, and R. Gronsky. 1992b. Surface precipitation reactions on oxide surfaces. Journal of Colloid and Interface Science, 148, 295-298.

Fendorf, S.E., and D.L. Sparks. 1994. Mechanisms of Cr(III) sorption on silica. 2. Effect of reaction conditions. Environmental Science and Technology, 28, 290-297.

Fendorf, S.E., G.M. Lamble, M.G. Stapleton, M.J. Kelley, and D.L. Sparks. 1994. Mechanisms of Cr(III) sorption on silica. 1. Cr(III) surface structure derived by extended X-ray absorption fine structure spectroscopy. Environmental Science and Technology, 28, 284-289.

Fendorf, S.E., and M. Fendorf. 1996. Sorption mechanisms of lanthanum on clay oxide minerals. Clays and Clay Minerals, 44, 220-227.

Fletcher, P., and G. Sposito. 1989. The chemical modeling of clay/electrolyte interactions for montmorillonite. Clays and Clay Minerals, 24, 375-391.

Ford, R.G., A.C. Scheinost, K.G. Scheckel, and D.L. Sparks. 1999. The link between clay mineral weathering and the stabilization of Ni surface precipitates. Environmental Science and Technology, 33, 3140-3144.

Gunneriusson, L. 1994. Composition and Stability of Cd(II)-Chloro and -Hydroxo Complexes at the Goethite(α-FeOOH)/water interface. Journal of Colloid and Interface Science, 163, 484-492.

Gunneriusson, L., L. Loevgren, and S. Sjoeberg. 1994. Complexation of Pb(II) at the goethite (α-FeOOH)/water interface: The influence of chloride. Geochimica et Cosmochimica Acta, 58, 4973-4983.

Inskeep, W.P., and J. Baham. 1983. Adsorption of Cd(II) and Cu(II) by Na-montmorillonite at low surface coverage. Soil Science Society of America Journal, 47, 660-665.

Junta, J.L., and M.F. Hochella Jr. 1994. Manganese(II) oxidation at mineral surfaces: A microscopic and spectroscopic study, Geochimica et Cosmochimica Acta, 58, 4985-4999.

Kim, N.D., and J.E. Fergusson. 1992. Adsorption of cadmium by an aquent New Zealand soil and its components. Australian Journal of Soil Research, 30, 159-167.

Maguire, M., J. Slavek, I. Vimpany, F.R. Higginson, and W.F. ickering. 1981. Influence of pH on Copper and Zinc Uptake by soil clays. Australian Journal of Soil Research, 19, 217-229.

McBride, M.B., A.R. Fraser, and J.W. McHardy. 1984. Cu^{2+} interaction with microcrystalline gibbsite. Clays and Clay Minerals, 32, 12-18.

McBride, M.B. 1994. Environmental chemistry of soils. Oxford University Press, New York.

O'Day, P.A., C.J. Chisholm-Brause, S.N. Towle, G.A. Parks, and G.E. Brown Jr. 1996. X-ray absorption spectroscopy of Co(II) sorption complexes on quartz (α-SiO_2) and rutile (TiO_2). Geochimica et Cosmochimica Acta, 14, 2515-2532.

O'Day, P.A., G.E. Brown, Jr., and G.A. Parks. 1994a. Molecular structure and binding sites of cobalt(II) surface complexes on kaolinite from X-ray absorption spectroscopy. Clays and Clay Minerals, 42, 337-355.

O'Day, P.A., G.E. Brown, Jr., and G.A. Parks. 1994b. X-ray absorption spectroscopy of Cobalt (II) multinuclear surface complexes and surface precipitates on kaolinite. Journal of Colloid and Interface Science, 165, 269-289.

Papelis, C., and K.F. Hayes. 1996. Distinguishing between interlayer and external sorption sites of clay minerals using X-ray absorption spectroscopy. Colloids and Surfaces, 107, 89-96.

Peigneur, P., A. Maes, and A. Cremers. 1975. Heterogeneity of charge distribution in montmorillonite as inferred from cobalt adsorption. Clays and Clay Minerals, 23, 71-75.

Scheidegger, A.M., and D.L. Sparks. 1996. A critical assessment of sorption-desorption mechanisms at the soil mineral/water interface. Soil Science, 161, 813-831.

Scheidegger, A.M., G.M. Lamble, and D.L. Sparks. 1996a. Investigation of Ni sorption on Pyrophyllite: An XAFS Study. Environmental Science and Technology, 30, 548-554.

Scheidegger, A.M., M. Fendorf, and D.L. Sparks. 1996b. Mechanisms of Nickel sorption on pyrophyllite: macroscopic and microscopic approaches. Soil Science Society of America Journal, 60, 1763-1772

Scheidegger, A.M., G.M. Lamble, and D.L. Sparks. 1997. Spectroscopic evidence for the formation of mixed-cation hydroxide phases upon metal sorption on clays and aluminum oxides. Journal of Colloid and Interface Science, 186, 118-128.

Scheidegger, A.M. D.G. Strawn, G.M. Lamble, and D.L. Sparks. 1998. The kinetics of mixed Ni-Al Hydroxide formation on clays and aluminum oxides: a time-resolved XAFS study. Geochimica et Cosmochimica Acta, 62, 2233-2245.

Scheinost, A.C., R.G. Ford, and D.L. Sparks. 1999. The role of Al in the formation of secondary Ni precipitates on pyrophyllite, gibbsite, talc and amorphous silica: A DRS study. Geochimica et Cosmochimica Acta, 63, 3193-3203.

Scheinost, A.C., and D.L. Sparks. 2000. Formation of layered single- and double-metal hydroxide precipitates at the mineral/water interface: A multiple scattering analysis. Journal of Colloid and Interface Science, 223, 167-178.

Schulthess, C.P., and C.P. Huang. 1990. Adsorption of heavy metals by silicon and aluminum oxide surfaces on clay minerals. Soil Science Society of America Journal, 54, 679- 688.

Sparks, D.L. 1989. Kinetics of soil chemical processes. Academic Press, Inc. San Diego, CA.

Sparks, D.L. 1995. Environmental Soil Chemistry. Academic Press, New York, NY.

Sposito, G. 1984. The surface chemistry of soils. Oxford University Press, New York, NY.

Sposito, G. 1989. The chemistry of soils. Oxford University Press, New York, NY.

Stumm, W., and J.J. Morgan. 1996. Aquatic Chemistry, Wiley, New York, NY.

Thompson, H.A., G.A. Parks, and G.E. Brown Jr. 1999. Dynamic interactions of dissolution, surface adsorption, and precipitation in an aging cobalt(II)-clay-water system. Geochimica et Cosmochimica Acta, 63, 1767-1779.

Towle, S.N., J.R. Bargar, G.E. Brown Jr., and G.A. Parks. 1997. Surface precipitation of Co(II)(aq) on Al_2O_3. Journal of Colloid and Interface Science, 187, 62-82.

Zachara, J.M., S.C. Smith, J.P. McKinley, and C.T. Resch. 1993. Cadmium sorption on specimen and soil smectites in sodium and calcium electrolytes. Soil Science Society of America Journal, 57, 1491-1501.

Chapter 2

NICKEL SORPTION MECHANISMS IN A PYROPHYLLITE-MONTMORILLONITE MIXTURE

2.1 Abstract

Nickel sorption on pyrophyllite, montmorillonite and a 1:1 pyrophyllite-montmorillonite mixture was studied at pH=7.5 and a reaction time of 40 minutes. The main modes of Ni uptake under these reaction conditions are adsorption on montmorillonite and surface precipitation on pyrophyllite. For the clay mixture, where adsorption on the montmorillonite component and surface precipitation on the pyrophyllite component compete for Ni uptake, X-ray Absorption Fine Structure Spectroscopy (XAFS) was used to estimate the distribution of Ni over the mixture components. This was done by comparison to pyrophyllite-montmorillonite mixtures with known Ni distributions over the mixture components. Nickel uptake on singly reacted pyrophyllite was slightly higher than on singly reacted montmorillonite. This was consistent with the XAFS results for the clay mixture, which suggested that the

pyrophyllite component sorbed slightly more Ni than the montmorillonite component. Our findings suggested that both adsorption and surface precipitation were important mechanisms in the overall Ni uptake in the clay mixture, and that neither sorption mechanism truly out-competed the other in the reaction time of 40 minutes employed. Therefore, both mechanisms should be considered when modeling Ni sorption in similar systems.

2.2 Introduction

Experimental studies on metal sorption mechanisms often focus on pure single-mineral sorbents. However, sorbents in natural systems are complex mixtures of a variety of minerals, and as a result, a variety of sorbents will be competing for uptake of metals added to such systems. Therefore, to successfully model and predict the fate of metals in soils and sediments, insight into the competitiveness of available sorption mechanisms is crucial. In this study, we will focus on adsorption and surface precipitation of metals as competing sorption mechanisms at clay mineral surfaces. Adsorption is defined here as a two-dimensional uptake process due to physical and chemical interactions between the metal ion and the clay surface (Sparks, 1995). On clay minerals such as montmorillonite adsorption can occur both at the edge sites, which leads to inner-sphere metal complexes, and at the planar (internal) sites of the clay mineral, which results in outer-sphere metal complexes. Recent studies using surface spectroscopic and microscopic techniques such as X-ray absorption fine structure spectroscopy (XAFS), X-ray photo electron spectroscopy (XPS), Auger

electron spectroscopy, scanning electron microscopy, atomic force microscopy, and TEM have shown that in many cases the sorption of heavy metals on clay and oxide surfaces results in the formation of three-dimensional multinuclear or polynuclear surface phases (Fendorf *et al.*, 1992a,b; Charlet and Manceau, 1994; Fendorf and Sparks, 1994; Junta and Hochella, 1994; O'Day *et al.*, 1994a,b; Scheidegger *et al.*, 1997, 1998). Such surface phases (surface precipitates) have been observed at surface metal loadings far below a theoretical monolayer, and in a pH range well below the pH where the formation of metal hydroxide precipitates would be expected based on the thermodynamic solubility product (Charlet and Manceau, 1994; Fendorf *et al.*, 1994; O'Day *et al.*, 1994a; Fendorf and Fendorf, 1996; Scheidegger *et al.*, 1997, 1998). In the case of Ni sorption on clay mineral surfaces described by Scheidegger *et al.* (1998), the surface precipitate was identified as a mixed Ni-Al-hydroxide phase.

It is believed that there is a continuum between Ni adsorption and Ni surface precipitation at clay mineral surfaces. At low surface coverage surface complexation dominates, and as surface coverage increases nucleation occurs and distinct entities or aggregates form at the surface. As surface loading further increases surface precipitation becomes the dominant mechanism (Fendorf and Sparks, 1994; Sparks, 1995). Thus, in single mineral sorption systems, surface precipitation and adsorption are thought to be consecutive metal uptake mechanisms. Adsorption is most likely the mechanism responsible for the initial fast stage of Ni sorption, and surface precipitation appears to be an important mechanism controlling the slower stage of Ni uptake.

Time resolved XAFS studies of Ni sorption on pyrophyllite, montmorillonite, and gibbsite, presented by Scheidegger *et al.* (1998), showed that the initiation of mixed Ni/Al-hydroxide surface precipitate formation varies as a function of sorbent type. For example, 40 minutes after Ni addition, the Ni/montmorillonite system was still in the initial stage of Ni uptake (adsorption), while in the Ni/pyrophyllite system surface precipitate formation had begun after 15 minutes, and continued rapidly up to about 3 hours after Ni addition. The sorbed amount of Ni expressed on a mass basis in both systems was about the same after 40 minutes. An interesting consequence is that, in a pyrophyllite-montmorillonite mixture, it may be possible to distinguish between Ni sorption on the montmorillonite and pyrophyllite surfaces using XAFS spectroscopy. Studies on Ni sorption in such a system may give insight as to the sorption of Ni on either surface. XAFS may be a valuable tool in studying such systems, since it can distinguish between adsorption and surface precipitation. Surface precipitation is indicated by the presence of a second neighbor Ni-Ni/Al peak in the Radial Structure Function (RSF) derived from XAFS data, while this peak is absent when adsorption is the main mode of Ni uptake (Papelis and Hayes, 1996; Scheidegger *et al.*, 1998). Therefore, in a mixture of montmorillonite and pyrophyllite, where surface precipitation occurs on the pyrophyllite phase and adsorption on the montmorillonite phase, the second Ni-Ni/Al peak in the RSF can be used to distinguish between Ni surface precipitation on pyrophyllite and Ni adsorption on montmorillonite. The intensity of the Ni-Ni/Al peak in the RSF is related to the loading of surface precipitates at the mineral surface. We hypothesize that since the

intensity of the Ni-Ni/Al peak will be a function of the Ni loading on pyrophyllite, it can be used to estimate the distribution of Ni in a pyrophyllite/montmorillonite mixture.

The objectives of this study were (1) to characterize Ni sorption in a pyrophyllite/montmorillonite mixture; and (2) to quantify the distribution of Ni between the mineral components of a pyrophyllite/montmorillonite mixture using XAFS.

2.3 Materials and Methods

The preparation and characterization of the pyrophyllite and montmorillonite clay minerals used in this study have been described in Scheidegger *et al.* (1997, 1998). The specific surface areas of the materials were determined by both the N_2-BET and the ethylene glycol monoethyl ether (EGME) methods. The surface areas were 96 $m^2 g^{-1}$ (BET) and 95 $m^2 g^{-1}$ (EGME) for pyrophyllite, and 15.2 $m^2 g^{-1}$ (BET) and 697 $m^2 g^{-1}$ (EGME) for montmorillonite. The BET method accounts for the external surface area of the minerals, whereas the EGME method accounts for the external and internal surface area. For montmorillonite, which is a swelling clay mineral, the difference between the EGME and BET surface areas was large, which demonstrates the large internal surface area associated with this clay mineral. For pyrophyllite the variation between the two methods was small, which indicates that no significant amount of swelling clays, such as montmorillonite, was present.

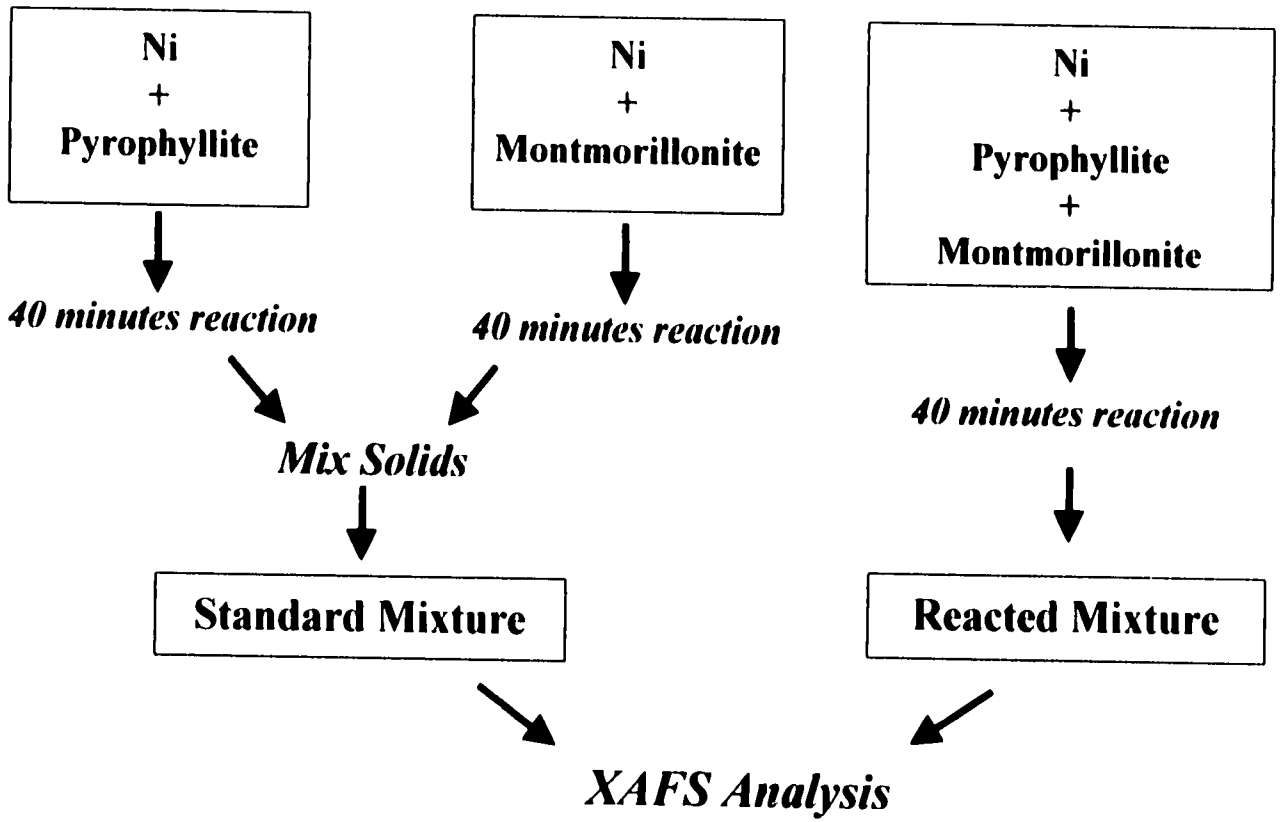

Figure 2.1 Schematic outline of the methods used in this study.

Figure 2.1 depicts a schematic outline of the methods used in this study. The general procedure employed was to prepare a "reacted mixture" and a number of "standard mixtures", and to compare the XAFS data of the reacted mixture versus the standard mixtures. As shown in Figure 1, the reacted mixture was prepared by reacting Ni with a clay suspension consisting of both pyrophyllite and montmorillonite, while the standard mixtures were prepared by mixing pyrophyllite and montmorillonite phases that had separately been reacted with Ni. All mixtures consisted of montmorillonite and pyrophyllite mixed in a 50%-50% dry weight ratio, and had a total Ni loading of 3000 mg kg^{-1}. We assume that the onset of surface precipitation at a mineral surface is dictated by the surface loading, as suggested by Fendorf and Sparks (5). Under the same set of reaction conditions (reaction pH=7.5, 0.1M $NaNO_3$ background electrolyte, initial Ni concentration=2.3 mM) pyrophyllite and montmorillonite reach the same Ni loading level after a reaction time of 40 minutes and at a solids concentration of 10 g L^{-1}. This loading level, expressed on a dry mass basis, is 6000 mg kg^{-1}. Preliminary studies indicated that pyrophyllite shows surface precipitation at Ni loading levels as low as 1500 mg kg^{-1} already, and it therefore is well into the stage of surface precipitation at a Ni loading of 6000 mg kg^{-1}. Montmorillonite on the other hand, is still in the stage of adsorption at a loading level of 6000 mg kg^{-1}. In the most extreme case, Ni added to a mixture of pyrophyllite and montmorillonite will partition to only one surface. In a 50-50 wt-% mixture of pyrophyllite and montmorillonite, a 6000 mg kg^{-1} Ni loading on one component and a 0 ppm Ni loading on the other component results in a total Ni loading of 3000 mg kg^{-1}

for the mixture as a whole. Since pyrophyllite is already well into the stage of surface precipitation at a surface loading of 6000 mg kg^{-1}, whereas montmorillonite is still in the stage of adsorption at this surface loading, we used total mixture loadings of 3000 mg kg^{-1}.

Five standard mixtures with a total Ni loading of 3000 mg kg^{-1} but with different distributions of Ni over the pyrophyllite and montmorillonite components were prepared (Table 2.1). To achieve the Ni sorption levels on the standard mixture components presented in Table 2.1, the initial Ni concentrations (only montmorillonite) and the solid concentrations (both pyrophyllite and montmorillonite) were varied, while all other experimental conditions that affect the Ni surface loading (pH, background electrolyte, and reaction time) were kept the same. The values of the initial Ni concentrations and solid concentrations used for preparation of the mixture components are given in Table 2.1. Solution speciation calculations performed with MINEQL (Westall *et al.*, 1976) suggest that the solubility of $Ni(OH)_2(s)$ at the reaction conditions employed in this study is reached at a Ni concentration of 7.7 mM. Based on these calculations, our systems are undersaturated with respect to $Ni(OH)_2(s)$ in all cases (initial Ni concentrations $\leq$ 2.3 mM). There is, however, a significant variation of reported $\log K_{sp}$ values for $Ni(OH)_2(s)$ in the literature (-10.99 to -18.06; Mattigod *et al.*, 1997), some of which would suggest oversaturation with respect to $Ni(OH)_2(s)$ in our systems at the initial Ni concentrations used. A recent study by Mattigod *et al.* (1997), investigating the solubility of $Ni(OH)_2(s)$ as a function of pH and reaction time, showed that the Ni concentration in a supersaturated solution at

Table 2.1 Nickel loadings on the pyrophyllite and montmorillonite components of the standard mixtures, and the distribution of Ni over the mixture components. Also given are reaction conditions used to prepare the mixture components.

Mixture	$Ni_{pyrophyllite}$				$Ni_{montmorillonite}$			
	Loading[a] (mg kg^{-1})	% of total[b]	[Solid][c] (g L^{-1})	$[Ni]_0$[d] (mM)	Loading[a] (mg kg^{-1})	% of total[b]	[Solid][c] (g L^{-1})	$[Ni]_0$[d] (mM)
(1)	6000	100	10.0	2.3	0	0	-	-
(2)	4000	67	22.5	2.3	2000	33	15.0	0.9
(3)	3000	50	35.2	2.3	3000	50	19.5	1.7
(4)	2000	33	60.1	2.3	4000	67	15.0	2.0
(5)	0	0	-	-	6000	100	10.0	2.3

[a] Ni loading on standard mixture component; [b] contribution (in %) of sorbed Ni on standard mixture component to total sorbed Ni in standard mixture; [c] Solid concentration; [d] Initial Ni concentration.

pH=7.5 (in a 0.01M $NaClO_4$ background) was >3mM even after a reaction time of 90 days. Using XAFS, Scheidegger *et al.* (1998) demonstrated that the Ni removal from solution in Ni/pyrophyllite and Ni/montmorillonite systems under identical reaction conditions as used in our study, was not due to $Ni(OH)_2(s)$ formation in solution at any time during a 15 minute to 3 month reaction time period. Based on these studies, we conclude that in our systems, Ni removal from solution is solely due to Ni sorption to the clay mineral surface, and not due the formation of $Ni(OH)_2(s)$ in solution.

The wet pastes of the pyrophyllite and montmorillonite components of the standard mixtures were not mixed until about five minutes prior to XAFS analysis, and immediately submerged in liquid N_2 to avoid further reactions. The reacted

mixture, which also had a total Ni loading of 3000 mg kg^{-1}, was prepared at an initial Ni concentration of 2.3 mM and a solid concentration of 34.7 g L^{-1}.

The Ni distributions (as % of total Ni) over the pyrophyllite and montmorillonite phases in the standard mixtures as given in Table 2.1 could also have been achieved by mixing pyrophyllite of *e.g.* 6000 mg kg^{-1} with appropriate amounts of *e.g.* 2000 mg kg^{-1} montmorillonite. It should be realized, however, that the intensities of the Ni-Ni/Al peak in the radial structure functions will be a function of two factors: (i) the distribution of Ni over the mixture components (surface precipitates on pyrophyllite, adsorbed species on montmorillonite); and (ii) the surface loading on the pyrophyllite phase. The first factor accounts for the "dilution" of the Ni-Ni/Al signal as a result of the presence of adsorbed species, which is due to the fact that XAFS provides an average bonding environment of total sorbed Ni. The second factor accounts for the structure of the surface precipitates at the pyrophyllite surface. The Ni-Ni/Al peak increases with increasing loading level, indicating the growth of precipitate clusters at the pyrophyllite surface with increasing Ni loading (Scheidegger *et al.*, 1998). By preparing the standard mixtures according to the procedure we used, both factors are accounted for, whereas the alternative procedure only accounts for the dilution effect.

The Ni sorption experiments were carried out in 0.1M $NaNO_3$, and at pH=7.5, maintained using a pH-stat apparatus. The reaction time was 40 minutes and the initial Ni concentrations were as given previously. Hydration of the clays was carried out in two steps. First, the clays were hydrated in background electrolyte for 24 hours

on a reciprocal shaker. Next, the suspension was brought to the desired solids concentration and placed on the pH-stat apparatus. The suspension was vigorously stirred with a magnetic stir bar and purged with N_2 to eliminate CO_2. The pH was maintained at pH=7.5 using 0.1M NaOH. After 2 hours, an appropriate amount of Ni from a 0.1 M $Ni(NO_3)_2$ stock solution was added in stepwise additions within a 3 minute period so as to achieve the desired initial Ni concentration. After a reaction time of 40 minutes after the last Ni addition, the suspension was centrifuged and the supernatant was passed through a 0.2 μm membrane filter. The filtered supernatant was analyzed for Ni by atomic absorption spectrometry. The sorbed amount of Ni was calculated from the difference between initial and final Ni concentrations. Washing the remaining wet pastes to remove entrained electrolyte was not necessary since in all samples the amount of Ni sorbed at the mineral surface was at least 40 times higher than the amount of Ni in the entrained electrolyte. The samples were sealed and stored in a refrigerator to keep them moist for XAFS analysis.

XAFS spectra were recorded at Beamline X-11A of the National Synchroton Light Source, Brookhaven National Laboratory, Upton, NY. The electron storage ring operated at 2.5 GeV with an average beam current of 180 mA. A Si(111) crystal was employed in the monochromator with a sagittally focused beam. A 0.5 mm premonochromator slit width was used. The height of the entrance slit was readjusted as necessary to compensate for vertical motion of the stored electron beam. Higher order harmonics were suppressed by detuning 25% from the maximum beam intensity.

The beam energy was calibrated by assigning the first inflection on the K-absorption edge of a nickel metal foil to an energy of 8333 eV. The spectra were collected in fluorescence mode using a Lytle detector. The samples were placed at a 45° angle to the incident beam, and a wide-angle collector with the ionization chamber was located at 45° off the sample (*i.e.* 90° off the incident beam). Fill-gases used were N_2 for the Lytle detector and Ar for the I_0 detector. A Co filter and Soller slits were placed between the sample and the detector to reduce elastically scattered X-rays entering the fluorescence detector. The spectra were collected at 77 K to reduce damping of the XAFS oscillation by thermal disorder. The samples were packed into stainless steel sample holders, and mounted on a Cu cold finger that was connected to a liquid N_2 reservoir. To eliminate the possibility of an XAFS contribution from impurities in the sample holder, the sample holder was wrapped in Pb foil. To minimize the heat transfer imposed on the cold finger, samples were pre-cooled by immersion into liquid N_2 for several minutes prior to analysis. Scans were collected in triplicate to improve the signal to noise ratio.

Background subtraction and Fourier filtering were accomplished with the program MacXAFS 4.0. The χ function was extracted from the raw data by using a linear preedge background and a spline postedge background, and normalizing the edge to unity. The data were then converted from energy to k space and weighted by k^3 to compensate for the damping of the XAFS amplitude with increasing k. Structural parameters were extracted with fits to the standard EXAFS equation. *Ab*

initio amplitude and phase functions for single shells were calculated using the FEFF6 code, in combination with ATOMS. Reference compounds used were β-$Ni(OH)_2$ (Johnson Mattey Co.), and takovite ($Ni_6Al_2(OH)_{16}CO_3.H_2O$; Kambalda W.A., Australia). The amplitude of the theoretical data was additionally adjusted by a factor determined from fits to the experimental data for the reference compounds. In all cases except standard mixture 5 (Table 2.1), multishell fitting was done in R space over the range ΔR=1.07-3.12 Å with Δk=3.2-13.6 $Å^{-1}$. For standard mixture (5), we used ΔR=1.07-2.30 Å with Δk=3.2-13.6 $Å^{-1}$. The smaller R range for this sample, where all the Ni is sorbed on the montmorillonite component, is due to the absence of a second shell in the radial structure function of this sample. The only constraint used in the fitting procedure was to fix the Debye-Waller factors of the Ni-Ni and Ni-Al shells at 0.005 $Å^2$. The R_{Ni-O} and R_{Ni-Ni} are estimated to be accurate to ±0.02 Å, and the N_{Ni-O} and N_{Ni-Ni} values are estimated to be accurate to ±20%. The estimated accuracies for N_{Ni-Al} and R_{Ni-Al} are ±60% and ±0.06 Å, respectively. The accuracy estimates are based on the results of theoretical fits to spectra of reference compounds of known structure. A discussion on the fitting procedure employed here and the accuracy estimates is given in Scheidegger *et al.* (1998).

2.4 Results and Discussion

Figures 2.2 and 2.3 show the k^3 weighted χ functions (Figure 2.2) and radial structure functions of the reacted mixture and the standard mixtures (Figure 2.3). The

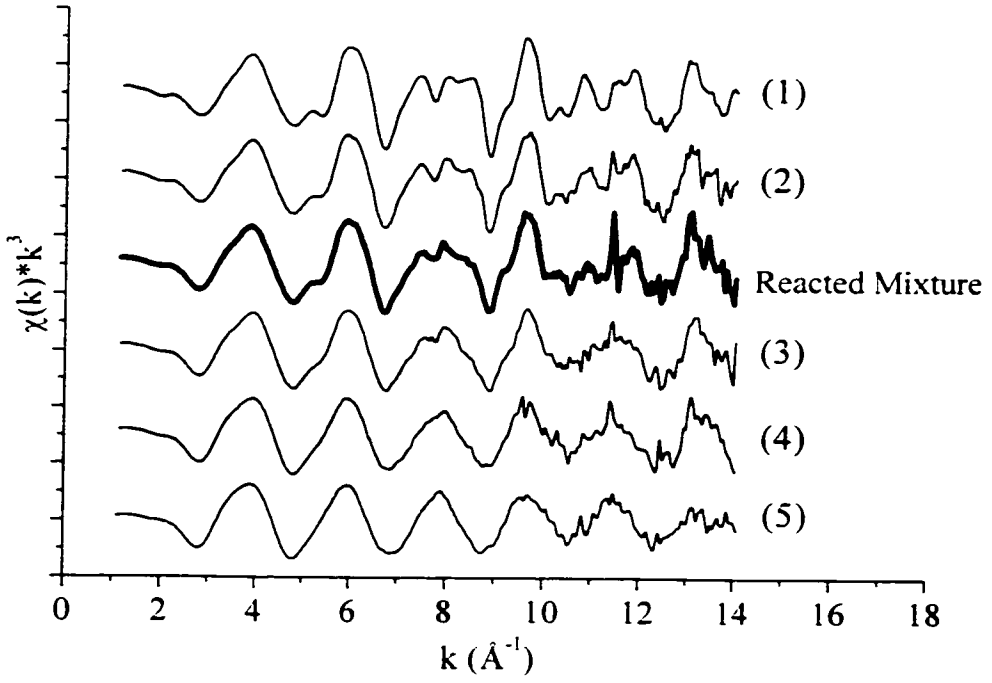

Figure 2.2 The k3 weighted χ functions of the reacted mixture and the standard mixtures. The standard mixtures are numbered as in Table 2.1.

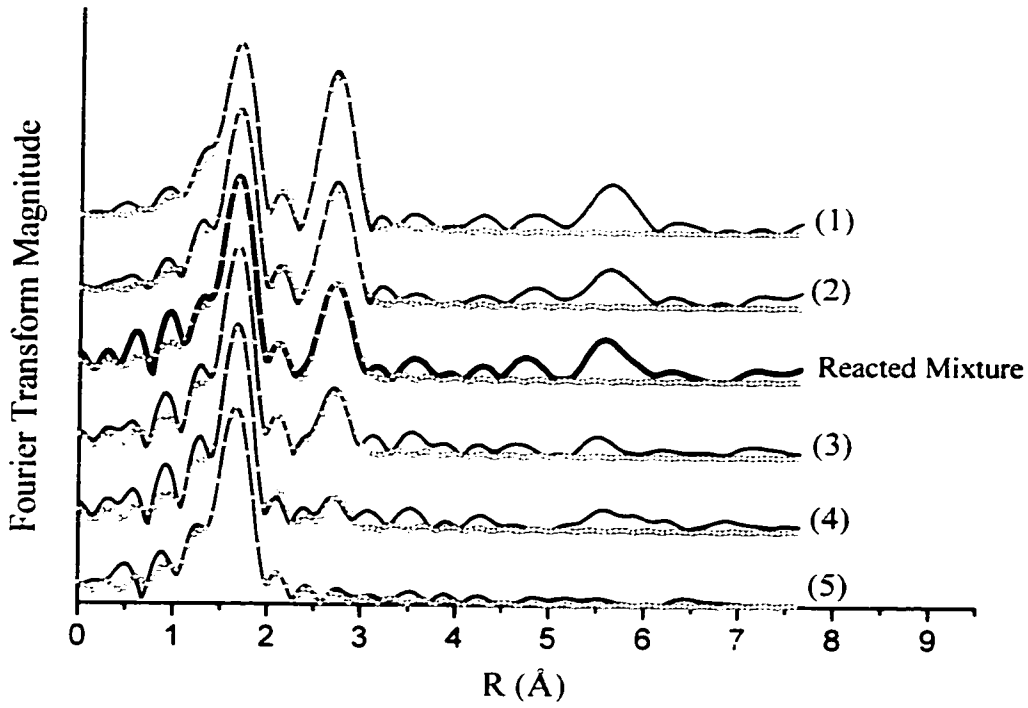

Figure 2.3 Comparison of the measured (solid lines) and the fitted (dotted lines) radial structure functions (uncorrected for phase shift) of the reacted mixture and the standard mixtures. For all radial structure functions, Fourier transformation was performed over Δk=3.2 - 13.6 $Å^{-1}$. The standard mixtures are numbered as in Table 2.1.

solid lines in Figure 2.3 represent the Fourier transforms of the measured data, and the dotted lines those of the theoretical spectra derived with parameters from the fitting procedure. A good agreement between the Fourier transformed XAFS functions and the theoretical fits is observed.

Figure 2.3 shows that the intensity of the first (Ni-O) peak is the same for all mixtures. For the standard mixtures, the intensity of the second (Ni-Ni/Al) peak increases significantly with increasing fraction of Ni loading associated with the pyrophyllite component. The intensity of the second peak of the reacted mixture is smaller than that of standard mixture 2 (67% Ni on pyrophyllite), but larger than that of standard mixture 3 (50% Ni on pyrophyllite). This indicates that in the reacted mixture the amount of Ni sorbed on the pyrophyllite is between 50% and 67% of the total sorbed Ni. Figure 2.2 also shows peaks beyond the second shell at R=5-6 Å. These result from multiple scattering among Ni atoms (O'Day *et al.*, 1994b; Papelis and Hayes, 1996), which was not characterized in the data analysis for this study.

In Table 2.2, the structural parameters derived from the XAFS data are presented. The coordination number N of a given shell is related to the intensity of the shell peak in the radial structure functions. The coordination number of the first shell (N_{Ni-O}) is about 6 for all samples, indicating that Ni is present in an octahedral environment, surrounded by 6 O atoms. The Ni-O bond distance (2.05 Å) is the same in all samples.

The fit results of the second coordination shell show that the number of second neighbor Ni atoms (N_{Ni-Ni}) increases with increasing fraction of Ni associated with the

Table 2.2 Structural parameters derived from XAFS analysis for the reacted mixture and the standard mixtures.

Mixture	Ni-O			Ni-Ni			Ni-Al		
	N[a]	R(Å)[b]	σ^2(Å^2)[c]	N	R(Å)	σ^2(Å^2)[d]	N	R(Å)	σ^2(Å^2)[d]
(1)	6.2	2.05	0.0035	5.3	3.05	0.0050	2.9	3.05	0.0050
(2)	6.1	2.05	0.0032	3.0	3.05	0.0050	1.2	3.06	0.0050
Reacted Mixture	6.1	2.05	0.0030	2.8	3.05	0.0050	1.2	3.12	0.0050
(3)	5.8	2.05	0.0025	2.4	3.04	0.0050	2.1	3.08	0.0050
(4)	5.7	2.05	0.0027	1.3	3.04	0.0050	1.6	3.09	0.0050
(5)	6.3	2.05	0.0033						

[a] Coordination number; [b] Interatomic distance; [c] Debye-Waller factor; [d] The Debye-Waller factors of the Ni-Ni and Ni-Al shells were fixed at 0.0050 Å^2

pyrophyllite phase in the standard mixtures. For the reacted mixture, 2.8 Ni atoms were fit in the second shell. As observed in the RSF's, this number falls between standard mixture 2 (N_{Ni-Ni}=3.0), and standard mixture 3 (N_{Ni-Ni}=2.4). The Ni-Ni bond distance (3.05 Å) is the same in all samples. No trend is observed in the N_{Ni-Al} numbers of the third coordination shell, which also contributes to the second peak in the RSF's. However, the accuracy of N_{Ni-Al} (±60%) is poor as compared to N_{Ni-Ni} (±20%).

We hypothesized that the intensity of the second Ni-Ni/Al peak in the RSF's can be used to estimate the distribution of Ni over the pyrophyllite and montmorillonite components in the reacted mixture. The intensity of the Ni-Ni/Al peak is reflected in the value of N_{Ni-Ni} obtained from the theoretical fit of the XAFS data, and is a measure for the amount of Ni sorbed on the pyrophyllite component.

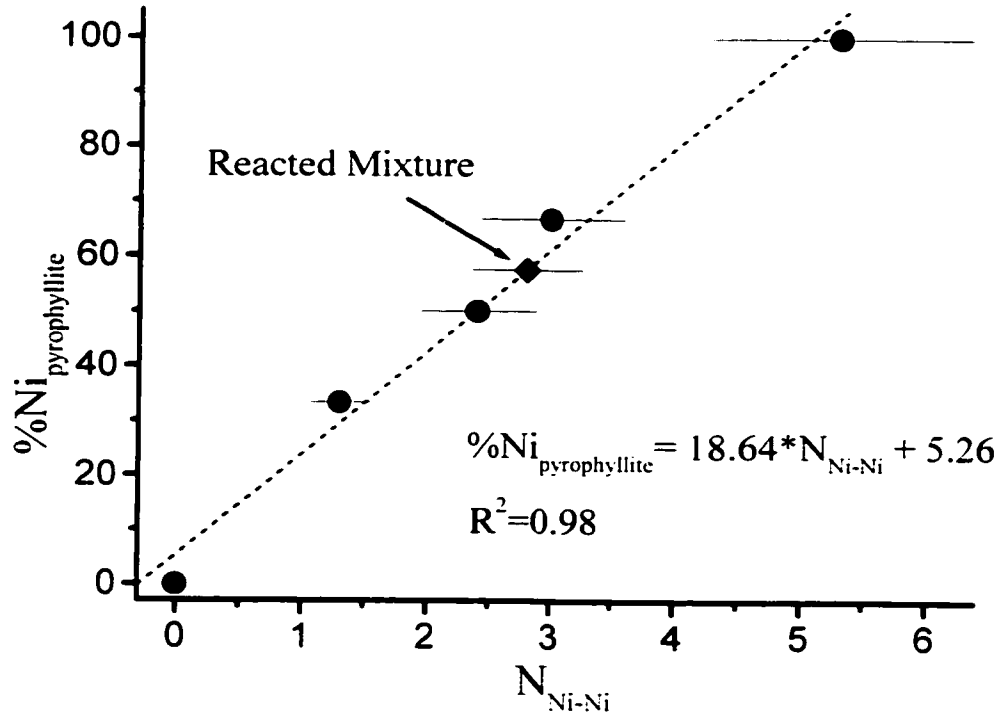

Figure 2.4 Plot of the % of total sorbed Ni associated with the pyrophyllite component as a function of N_{Ni-Ni} derived from XAFS analysis for the standard mixtures. The dashed line represents the best fit to the data. Error bars indicate the accuracy (±20%) of the N_{Ni-Ni} coordination numbers derived from EXAFS data fitting.

Table 2.3 Regression statistics of the relation between $\%Ni_{pyrophyllite}$ and N_{Ni-Ni} derived based on the XAFS results of the 5 standard mixtures.

	Mean	Standard error	p level
Slope	18.64	1.40	0.0009
Intercept	5.26	4.10	0.30

Since the fractions of total Ni associated with the pyrophyllite component ($\%Ni_{pyrophyllite}$) are known for the standard mixtures (Table 2.1), we plotted these values as a function of N_{Ni-Ni} obtained from the theoretical fits to the XAFS data (Figure 2.4). A linear relation between these variables is observed ($\%Ni_{pyrophyllite} = 18.64*N_{Ni-Ni} + 5.26$; $R^2=0.98$). The regression statistics of this equation are presented in Table 2.3. By applying this relation to the reacted mixture ($N_{Ni-Ni}=2.8$; Table 2.2), the total Ni sorbed on the pyrophyllite component in the reacted mixture is estimated at (57.5 ± 8)%, where 57.5% is the mean and ±8% defines the 95% confidence interval of the estimate. This corresponds to a Ni loading of 3450 mg kg^{-1} (95% confidence interval: 2970-3930 mg kg^{-1}) on the pyrophyllite phase, and a Ni loading of 2550 mg kg^{-1} (95% confidence interval: 2070-3030 mg kg^{-1}) on the montmorillonite phase. Thus, the pyrophyllite component sorbs 1.4 times (95% confidence interval: 1.0-1.9) as much Ni as the montmorillonite component, which suggests that it is slightly more competitive for Ni uptake than the montmorillonite component in the reacted mixture under the reaction conditions used.

The initiation of surface precipitation on the pyrophyllite surface occurs at low surface loadings (< 1500 mg kg^{-1}). However, since we used pyrophyllite samples with Ni loadings <6000 mg kg^{-1}, it is likely that also significant amounts of adsorbed Ni were present at the pyrophyllite surface. We were not able to distinguish between adsorbed Ni and Ni present in Ni/Al hydroxide precipitates at the pyrophyllite surface in our XAFS data. The Ni loading on the pyrophyllite phase of the reacted mixture was estimated to be 3450 mg kg^{-1}, which indicates that a substantial amount (>55%) of total Ni sorbed on the pyrophyllite phase in the reacted mixture is in the form of surface precipitates. This suggests that the surface precipitation mechanism at the pyrophyllite surface is more effective for Ni uptake than the adsorption mechanism at the montmorillonite surface in the reacted mixture under the reaction conditions employed in this study.

For further evaluation of the Ni sorption behavior in our mixed system, we carried out two single mineral sorption studies, where montmorillonite and pyrophyllite were separately reacted under the same reaction conditions as the reacted mixture (0.1M $NaNO_3$ background electrolyte; pH=7.5; reaction time=40 minutes, initial Ni concentration=2.3 mM), except for the solids concentration, which was 17.4 g L^{-1}. This solids concentration was used because it is half the total solids concentration of the 50-50 wt-% reacted mixture, and thus equals the solids concentration of either mineral in the reacted mixture. Under these reaction conditions, pyrophyllite reaches a Ni loading level of 4728 mg kg^{-1}, and montmorillonite a Ni loading level of 3952 mg kg^{-1}. As expected, these loading levels

are higher than the estimated loading levels on the pyrophyllite and montmorillonite surface in the reacted mixture (3450 and 2550 mg kg^{-1}, respectively) due to the absence of a competing surface in the singly reacted systems. By taking the ratio of Ni sorption on pyrophyllite to Ni sorption on montmorillonite for the singly reacted systems, it is found that singly reacted pyrophyllite sorbs 1.2 times as much Ni as singly reacted montmorillonite. In the reacted mixture, Ni sorption on pyrophyllite was estimated to be 1.4 times as high as Ni sorption on montmorillonite. The 95% confidence interval of this estimate is 1.0-1.9. The value of 1.2 calculated for the single clay mineral systems falls in this interval, indicating that there are no significant differences in this ratio between the singly reacted systems and the reacted mixture. This suggests that the affinity of Ni for the montmorillonite and pyrophyllite surface is similar in the reacted mixture and the single mineral systems. Nickel surface precipitation on the pyrophyllite phase is found to be more effective than Ni adsorption on the montmorillonite phase in the reacted mixture, which is consistent with the results from the single clay mineral systems. We conclude, therefore, that the mechanisms of adsorption on montmorillonite and surface precipitation on pyrophyllite are competing for Ni uptake in the reacted mixture, and that neither mechanism truly out-competes the other in the reaction time of 40 minutes employed in this study. Thus, when modeling Ni sorption results for systems similar to our pyrophyllite-montmorillonite mixture, both surface precipitation and adsorption should be considered. Over longer reaction times (time scales of days), surface precipitation is expected to occur on both the pyrophyllite and montmorillonite phase

based on the results of Scheidegger *et al.* (1998). At these longer reaction times, therefore, surface precipitation is expected to be the main mode of Ni uptake in the pyrophyllite-montmorillonite mixture.

2.5 Conclusions

In this study we were able to apply XAFS as a tool to distinguish sorption mechanisms on different clay minerals, and to estimate the distribution of Ni between the mineral phases in a 1:1 mixture of pyrophyllite and montmorillonite. The results suggest that the pyrophyllite component is more competitive for Ni uptake than the montmorillonite component. In terms of sorption mechanisms, this suggests that surface precipitation on the pyrophyllite phase is a more effective mechanism for Ni uptake than adsorption at the montmorillonite surface under the reaction conditions used in this study. The partitioning of Ni over the mixture components was found to be similar to what would be expected based on single clay mineral sorption results for the mixture components, which indicated that both adsorption on montmorillonite and surface precipitation on pyrophyllite are important mechanisms for Ni uptake in the clay mixture during the reaction time of 40 minutes employed in this study.

2.6 References

Charlet, L., and A. Manceau. 1994. Evidence for the neoformation of clays upon sorption of Co(II) and Ni(II) on silicates. Geochimica et Cosmochimica Acta, 58, 2577-2582.

Fendorf, S.E., M. Fendorf, D.L. Sparks, and R. Gronsky. 1992a. Inhibitory mechanisms of Cr(III) oxidation by δ-MnO_2. Journal of Colloid and Interface Science, 153, 37-54.

Fendorf, S.E., D.L. Sparks, M. Fendorf, and R. Gronsky. 1992b. Surface precipitation reactions on oxide surfaces. Journal of Colloid and Interface Science, 148, 295-298.

Fendorf, S.E., G.M. Lamble, M.G. Stapleton, M.J. Kelley, and D.L. Sparks. 1994. Mechanisms of Cr(III) sorption on silica. 1. Cr(III) surface structure derived by extended X-ray absorption fine structure spectroscopy. Environmental Science and Technology, 28, 284-289.

Fendorf, S.E., and D.L. Sparks. 1994. Mechanisms of Cr(III) sorption on silica. 2. Effect of reaction conditions. Environmental Science and Technology, 28, 290-297.

Fendorf, S.E., and M. Fendorf. 1996. Sorption mechanisms of lanthanum on clay oxide minerals. Clays and Clay Minerals, 44, 220-227.

Junta, J.L., and M.F. Hochella Jr. 1994. Manganese(II) oxidation at mineral surfaces: A microscopic and spectroscopic study, Geochimica et Cosmochimica Acta, 58, 4985-4999.

Mattigod., S.V., D. Ray, A.R. Felmy, and L. Rao. 1997. Solubility and solubility product of crystalline $Ni(OH)_2$. Journal of Solution Chemistry, 26, 391-403.

O'Day, P.A., G.E. Brown, Jr., and G.A. Parks. 1994a. Molecular structure and binding sites of cobalt(II) surface complexes on kaolinite from X-ray absorption spectroscopy. Clays and Clay Minerals, 42, 337-355.

O'Day, P.A., G.E. Brown, Jr., and G.A. Parks. 1994b. X-ray absorption spectroscopy of Cobalt (II) multinuclear surface complexes and surface precipitates on kaolinite. Journal of Colloid and Interface Science, 165, 269-289.

Papelis, C., and K.F. Hayes. 1996. Distinguishing between interlayer and external sorption sites of clay minerals using X-ray absorption spectroscopy. Colloids and Surfaces, 107, 89-96.

Scheidegger, A.M., G.M. Lamble, and D.L. Sparks. 1997. Spectroscopic evidence for the formation of mixed-cation hydroxide phases upon metal sorption on clays and aluminum oxides. Journal of Colloid and Interface Science, 186, 118-128.

Scheidegger, A.M, D.G. Strawn, G.M. Lamble, and D.L. Sparks. 1998. The kinetics of mixed Ni-Al Hydroxide formation on clays and aluminum oxides: a time-resolved XAFS study. Geochimica et Cosmochimica Acta, 62, 2233-2245.

Sparks, D.L. 1995. "Environmental Soil Chemistry." Academic Press, San Diego, CA.

Westall, J., J.L. Zachary, and F. Morel. 1976. Technical Note 18, Dept. of Civil Eng., MIT.

Chapter 3

REACTION CONDITION EFFECTS ON NI SORPTION MECHANISMS IN ILLITE-WATER SUSPENSIONS

3.1 Abstract

Nickel sorption in illite suspensions was studied as a function of pH (4.5-8.0), reaction time (3h, 24h, and 1 week) and ionic strength (I=0.1M and 0.003M) using X-ray absorption spectroscopy (XAS) to characterize the Ni sorption complexes formed. The formation of Ni-Al layered double hydroxide (LDH) phases was observed at pH values >6.25, with increasing formation of these phases over time, and a faster formation rate with increasing pH. Comparison between samples with the same Ni loading, but different reaction times and pH values, showed larger second neighbor scattering for the samples reacted at higher pH, which had a faster Ni sorption rate. Most likely this was due to a greater importance of Ni-Al LDH precipitation relative to other (mononuclear) Ni sorption mechanisms at higher pH, and/or a higher Al content in the Ni-Al LDH phase formed at lower pH (slower Ni sorption rate).

Lowering the ionic strength resulted in increased Ni sorption over the entire pH range studied. Our XAFS data indicated that this was due to significant outer-sphere Ni sorption occurring at the planar sites at low I, leading to a reduced importance of Ni-Al LDH formation in the overall Ni sorption process at pH>6.50.

3.2 Introduction

Retention of heavy metal ions by soil minerals is a crucial process for maintaining environmental quality in contaminated areas. Sorption reactions at solid-water interfaces decrease solute mobility and often control the fate, bioavailability, and transport of trace metal ions such as Ni in aquatic and soil environments. Correctly determining the mechanisms of metal sorption to clay minerals such as illite is therefore of great importance for understanding the fate of metals in contaminated soils and sediments, and may help in optimizing environmental remediation procedures by accounting for the metal speciation in soils.

Illite is a 2:1 phyllosilicate mineral with tightly held, nonhydrated, interlayer K cations balancing a high layer charge (Fanning *et al.*, 1989). Illitic clays are often an important constituent of the solid phase in alluvial soils and in arid zone soils (Bolt *et al.*, 1979; Fanning *et al.*, 1989). As with many clay minerals, illite contains both planar and edge sites available for metal uptake. Planar sites are due to a net negative structural charge resulting from isomorphic substitution in the octahedral and tetrahedral sheets, and edge sites are due to broken Al-OH and Si-OH bonds at the edges of the clay crystallite (McBride, 1994). The presence of planar sites in illitic

clays presumably results in part from interstratified vermiculite and smectite layers (Srodon and Eberl, 1984), which form if the clay is brought in contact with a solution of low K concentration. Upon prolonged exposure to this solution, the edge-situated interlattice sites become occupied by ions other than K, presumably leading to partial opening of the interlattice space (Bolt *et al.*, 1979).

The different sites available for metal uptake by illite may lead to different Ni retention mechanisms occurring in Ni/illite systems. The planar sites constitute permanent negative charge. Metal interactions with these sites are electrostatic in nature and lead to the formation of outer-sphere metal complexes, *i.e.* the metal ions do not lose their primary hydration spheres upon interaction with the clay mineral surface (Sposito, 1989; Sparks, 1995). At the illite edge sites, both the formation of outer-sphere complexes and chemisorption may occur. Chemisorption leads to the formation of inner-sphere metal complexes through a ligand exchange process, where the metal ions form chemical bonds with the clay mineral surface by coordination to surface hydroxy ligands (Sposito, 1989). Since illite is an Al containing clay mineral, the formation of Ni-Al layered double hydroxide (LDH) phases may also be expected. The importance of the formation of these precipitates has recently been demonstrated in spectroscopic studies of Ni sorption to Al bearing clay minerals and oxides (d'Espinose de la Caillerie *et al.*, 1995; Scheidegger *et al.*, 1998; Scheinost *et al.*, 1999). These phases are typically observed in a pH range below the pH where the solubility of ß-$Ni(OH)_2$ precipitates is exceeded. In the case of Ni sorption to pyrophyllite and other Al bearing minerals described by Scheinost *et al.* (1999), the Ni

phase that formed was unequivocally identified as a mixed Ni-Al LDH sheet, where the Al originated from the sorbent structure.

In the following the term *sorption* is used to describe the surface-mediated removal of Ni cations from solution. This includes adsorption processes at the illite clay sites and planar sites (*i.e.* formation of mononuclear inner- and outer-sphere Ni sorption complexes), as well as formation of Ni-Al LDH precipitates, which incorporate Al dissolved from the illite structure. Studies employing TEM showed that Co-Al LDH phases do not form coatings on Al_2O_3 and kaolinite surfaces but rather form 3-dimensional precipitate clusters that lack a preferred orientation with respect to the surfaces of these minerals, and in some cases are detached from the surface (Towle *et al.*, 1997; Thompson *et al.*, 1999). These results indicate that formation of Co-Al LDH is not a result of surface crowding, *i.e.* the precipitates do not consist of sorbed metal ions nucleated with metal ions on adjacent surface sites, since this would result in precipitate coatings on the mineral surface. For this reason, Ni-Al LDH formation may be considered as a separate sorption mechanism that occurs simultaneously with adsorption processes at the illite planar and edge sites (*i.e.* formation of inner-and outer-sphere Ni sorption complexes), instead of Ni-Al LDH precipitates being the products formed at these sites at high Ni loadings. We reported the Ni sorption density in the samples based on the total surface area of the illite clay. This was done only to allow for convenient comparison of the Ni sorption levels in the Ni/illite samples and not to imply a certain distribution of the Ni atoms at the illite surface.

In this study, we present macroscopic and spectroscopic data on Ni sorption in illite suspensions. As discussed above, Ni sorption in illite suspensions may proceed via a number of different mechanisms, which compete for Ni uptake. The Ni speciation in illite suspensions will therefore be determined by how effective each of the different sorption mechanisms competes for Ni uptake, which may be affected by a range of experimental parameters, including pH, reaction time, and ionic strength. Therefore, rather than limiting our systems to a single set of experimental parameters, we studied Ni sorption to illite as a function of pH, reaction time and ionic strength to determine the effect of these experimental parameters on the Ni sorption products formed in illite suspensions. X-ray absorption spectroscopy (XAS) was used to characterize the sorbed Ni bonding environment at the molecular scale.

3.3 Materials and Methods

The experiments were performed with Silver Hill Illite, Imt-1, obtained from the Source Clay Minerals Repository at the University of Missouri, Columbia, MO. After grinding in a ball mill for 2 weeks, the material was treated for removal of calcium carbonates, iron oxides and organic matter following the procedures described in Jackson (1956). We used the <2 μm fraction, which was isolated by sedimentation, and then saturated with Na. The clay was dialyzed for removal of excess salts and freeze-dried. The surface area of the clay was determined by both the N_2-BET method and the EGME method. The N_2-BET surface area was 17 $m^2 g^{-1}$, and the EGME surface area was 163 $m^2 g^{-1}$. The difference between both methods indicates that a

substantial amount of smectite-like phases was present in our illite clay fraction, constistent with the description of this illite by Srodon and Eberl (1984) as a mixture of illite and illite/smectite phases.

The sorption of Ni to illite was studied in batch experiments, using polyethylene reaction vessels. The following experimental parameters were varied: (1) pH: 4.5-8.0; (2) pH control: constant and drifting pH over time; (3) ionic strength: 0.1M $NaNO_3$ and 0.003M $NaNO_3$; and (4) reaction time: 3 hours, 24 hours, and 1 week. All studies were conducted under an N_2 atmosphere to eliminate effects of CO_2. The solid:solution ratio was 2 g L^{-1}, and the initial Ni concentration was 1 mM.

Metal sorption in mineral suspensions is often studied in systems where pH is not kept at a constant value during the time allowed for equilibration (*e.g.* Benjamin and Leckie, 1982; Roe *et al.*, 1991; Zachara *et al.*, 1993; O'Day *et al.*, 1996). In these systems, pH drifts due to metal sorption and sorbent mineral dissolution until equilibrium is reached. In the case of Ni sorption to clay minerals, both the Ni sorption reaction (Scheidegger *et al.*, 1998; Roberts *et al.*, 1999; Scheinost *et al.*, 1999) and the sorbent dissolution reaction (Scheidegger *et al.*, 1997; Ford *et al.*, 1999) may take weeks to reach equilibrium, during which time pH continuously drifts. Since pH is an important variable that may control both the extent and the mechanism of metal sorption (Bargar *et al.*, 1998; Strawn and Sparks, 1999; Roberts *et al.*, 1999), pH drift may affect the metal sorption product formed. We have studied the effect of pH drift on the Ni sorption mechanisms on illite by comparing the macroscopic and spectroscopic data obtained from systems where pH was not controlled to those from

systems where pH was held at a constant value over time. In the system with pH drift, different amounts of acid (0.1M HNO_3) or base (0.1M NaOH) were added to the Ni/illite suspensions at the beginning of the experiment, and pH and the Ni concentration remaining in solution were measured after 1d and 8d of reaction.

In the pH controlled system, pH was held constant by either using a pH stat apparatus (samples with pH>5 in the I=0.003M system), manual addition of 0.1M HNO_3 or 0.1M NaOH twice a day (pH=4.5 and 5.0 in both I=0.1M and 0.003M systems), or by using a 0.05M MES (pH=5.5-6.5) or 0.05M HEPES (pH=6.75-8.0) buffer concentration in the background electrolyte (I=0.1M system). MES and HEPES are organic buffers with pK_a values of 6.1 and 7.5, respectively. Preliminary studies showed no differences in Ni sorption as a function of time between Ni/illite systems equilibrated on a pH stat at pH=5.5 and 7.5 and Ni/illite systems where pH was maintained constant by using 0.05 M MES (pH=5.5) or 0.05 M HEPES (pH=7.5) in the background electrolyte. This indicated that the organic buffers did not interfere with the Ni sorption process(es) in the illite suspensions, which is consistent with results of other metal sorption studies using MES and organic buffers similar to HEPES (Baeyens *et al.*, 1995; Strawn *et al.*, 1998).

The buffer solutions were prepared by titrating a 0.05M buffer solution to the desired pH using a 10M NaOH solution, and then adding an appropriate amount of $NaNO_3$(s) to achieve a final I=0.1M. The needed amount of $NaNO_3$(s) was calculated by accounting for the buffer speciation at the pH value of interest, and the Na concentration resulting from the amount of 10M NaOH added to reach this pH.

The I=0.1M $NaNO_3$ suspensions were hydrated for 24 hours by stirring while open to a N_2 glove box atmosphere. Next, an appropriate amount of 0.1M $Ni(NO_3)_2$ was added to achieve an initial Ni concentration of 1 mM. For the system with non-controlled pH, 0.1M HNO_3 or 0.1M NaOH was added (prior to Ni addition) in different amounts to each sample. The suspensions were then sealed, placed in gas tight zipper bags inside the glove box, and transferred to a reciprocal shaker outside the glove box for equilibration. The I=0.003M $NaNO_3$ suspensions were hydrated on a reciprocal shaker for 22 hours, and then placed on the pH-stat apparatus. The suspensions were vigorously stirred with a magnetic stir bar and purged with N_2 to eliminate CO_2. The pH was maintained at the desired value using 0.1M NaOH. After 2 hours, an appropriate amount of Ni from a 0.1 M $Ni(NO_3)_2$ stock solution was added to achieve an initial Ni concentration of 1 mM.

Subsamples from the I=0.1M and I=0.003M systems were taken at the reaction times of interest. The samples were centrifuged and the supernatants were passed through a 0.2 μm filter. The filtered supernatants were then acidified and analyzed by ICP spectrometry for Ni. Nickel sorption was determined from the difference between the initial and final Ni concentrations.

The solids from select samples were analyzed by XAFS spectroscopy. The wet pastes were not washed to remove entrained electrolyte since in all samples the amount of Ni sorbed at the mineral surface was at least ~50 times higher than the amount of Ni in the entrained electrolyte. The samples were sealed and stored in a refrigerator to keep them moist for XAFS analysis.

XAFS spectra were recorded at Beamline X-11A of the National Synchroton Light Source, Brookhaven National Laboratory, Upton, NY. The electron storage ring was operated at 2.5 GeV with an average beam current of 180 mA. A Si(111) crystal was used as the monochromator. The premonochromator slit width was 0.5 mm, which yielded a resolution of about 0.5 eV. Higher order harmonics were suppressed by detuning 25% from the maximum beam intensity at 900 eV above the Ni K-edge of 8333eV.

The samples were scanned in fluorescence mode at the Ni K-edge using a Lytle detector. The samples were placed at a 45° angle to the incident beam, and a wide-angle collector with an ionization chamber was located at 90° off the incident beam. Fill-gases used were Ar for the Lytle detector and N_2 for the I_0 detector. A Co filter and soller slits were placed between the sample and the detector to reduce elastically scattered X-rays entering the fluorescence detector. The spectra were collected at room temperature. Three scans were collected per sample to improve the signal to noise ratio.

Background subtraction, Fourier filtering, and data fitting were accomplished with the program MacXAFS 4.0 (Bouldin *et al.*, 1995). The χ function was extracted from the raw data by fitting a linear function to the pre-edge region and a spline function to the post-edge region, and normalizing the edge jump to unity. The data were then converted from energy to k space and weighted by k^3 to compensate for the dampening of the XAFS amplitude with increasing k.

Data fitting was done in R space. *Ab initio* amplitude and phase functions for single shells were calculated using the FEFF7 code (Zabinsky *et al.*, 1995), in combination with ATOMS. Reference compounds used were β-$Ni(OH)_2$ (Johnson Mattey Co.), and α-$Ni(OH)_2$ prepared as described by Génin *et al.* (1991). The amplitude reduction factor was 0.83, as determined from fits to the experimental data of the reference compounds. Multishell fitting was done over ΔR=1.07-3.12 Å with Δk=3.2-13.6 $Å^{-1}$. For samples having only one shell, single shell fitting was performed over ΔR=1.07-2.30 Å with Δk=3.2-13.6 $Å^{-1}$. The Debye-Waller factors of the Ni-Ni and Ni-Al shells were fixed at 0.005 $Å^2$ in the case of multishell fitting. This constraint was proposed by Scheidegger *et al.* (1998) for fitting Ni-Al LDH precipitates. The resulting optimized R_{Ni-O} and R_{Ni-Ni} values are estimated to be accurate to ±0.02 Å, and the N_{Ni-O} and N_{Ni-Ni} values are estimated to be accurate to ±20%. The estimated accuracies for N_{Ni-Al} and R_{Ni-Al} are ±60% and ±0.06 Å, respectively. A discussion on the fitting procedure employed here and the accuracy estimates is given in Scheidegger *et al.* (1998). The deviation between the fitted and experimental spectra was quantified as :

$$\mathrm{Re}\,s = \frac{\sum_{i=1}^{N} | y_{\exp}(i) - y_{fit}(i) |}{\sum_{i=1}^{N} y_{\exp}(i)},$$

where N represents the number of data points, and y_{exp} and y_{fit} are the experimental and theoretical data points, respectively.

3.4 Results and Discussion

3.4.1 XAFS Data

Figure 3.1 shows the normalized, background-subtracted and k^3-weighted XAFS spectra that were collected for this study. The sorption density, Γ, is indicated along with the reaction conditions (pH, I, and reaction time) for each sample. The low pH samples 9 and 10 are dominated by the sinusoid resulting from oxygen backscattering from the first coordination shell of sorbed Ni. In the other samples, additional frequencies appear in the spectra due to the presence of Ni in the second coordination shell of the central Ni atom, which indicates that a Ni precipitate phase is present in these samples (Scheidegger *et al.*, 1998; d'Espinose *et al.*, 1995). The "cut-off" beat at about 8 $Å^{-1}$ recognizable for samples 1-4, and absent in the spectra of β-$Ni(OH)_2$ and α-$Ni(OH)_2$, identifies the Ni precipitates formed in the Ni/illite systems as Ni-Al LDH phases (Scheinost and Sparks, 2000). The differences between the XAFS spectra presented in Figure 3.1 indicate that the Ni bonding environment varies as a function of reaction conditions. Since XAFS provides the average bonding environment of all sorbed Ni atoms, this may be due to variable relative amounts of Ni bound in Ni-Al LDH versus mononuclear adsorbed Ni species. Additionally, there may be differences between the samples with respect to the composition or size of the Ni-Al LDH crystallites that form in the Ni-illite suspensions. The reaction condition-induced variation in the speciation of sorbed Ni will be evaluated in detail further in this chapter.

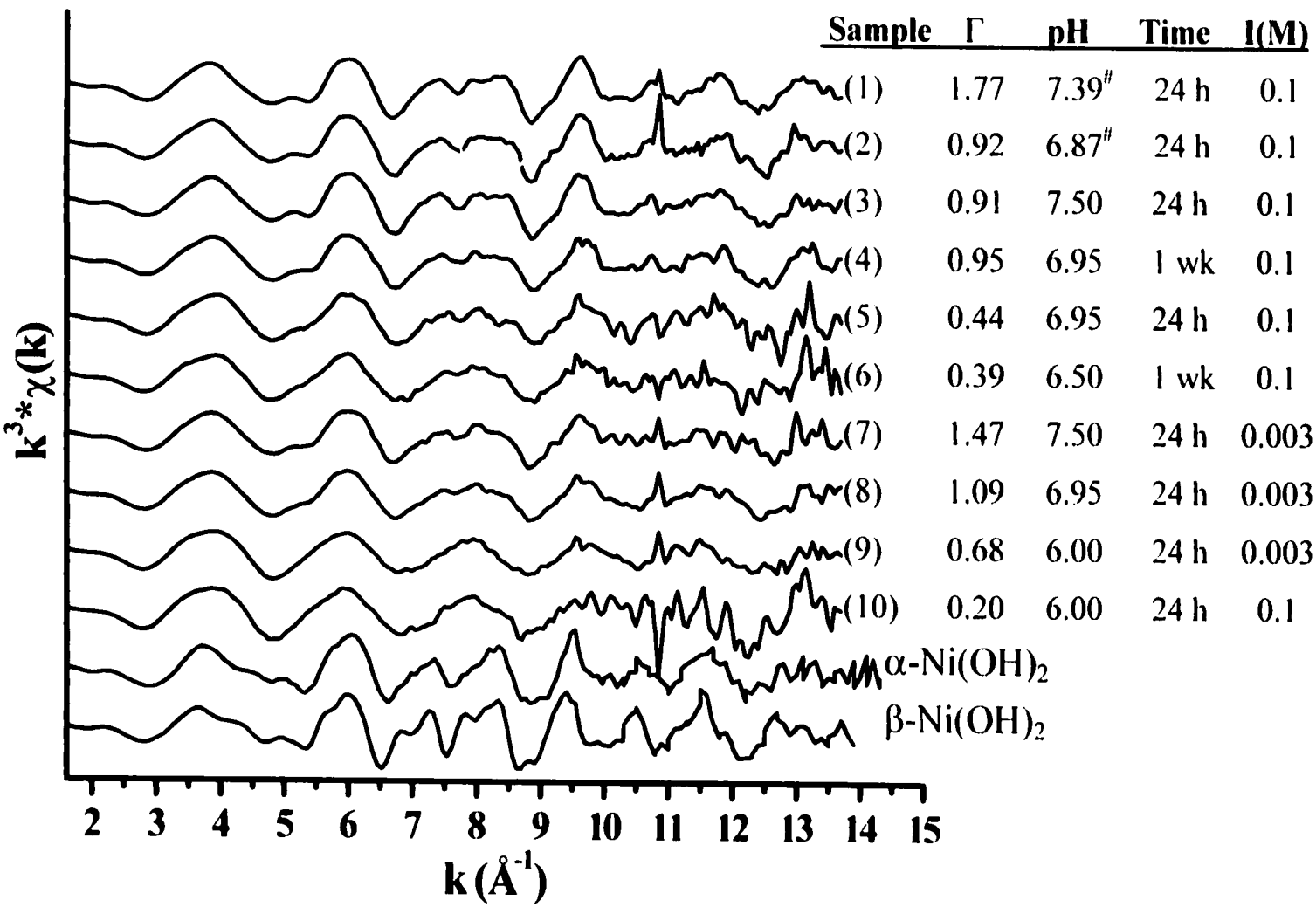

Figure 3.1 The XAFS data collected in this study

Table 3.1 Structural parameters derived from XAFS analysis. The sample numbers are the same as in Figure 3.1.

Sample	pH	Time	I (M)	Γ (μmol m^{-2})	Ni-O Shell¶ R# (Å)	N§	σ^{2}† (Å^2)	Ni-Ni Shell¶ R (Å)	N	σ^2 (Å^2)	Ni-Al Shell¶ R (Å)	N	σ^2 (Å^2)	Res
1	7.39	24 h	0.1	1.77	2.04	5.7	0.004	3.06	4.1	0.005	3.09	0.6	0.005	0.021
2	6.87	24 h	0.1	0.92	2.05	6.2	0.004	3.05	4.0	0.005	3.09	1.2	0.005	0.084
3	7.50	24 h	0.1	0.95	2.04	6.0	0.004	3.06	3.7	0.005	3.10	0.7	0.005	0.045
4	6.95	1 wk	0.1	0.90	2.04	6.0	0.005	3.06	3.2	0.005	3.10	1.5	0.005	0.036
5	6.95	24 h	0.1	0.44	2.06	5.7	0.003	3.04	2.5	0.005	3.11	1.3	0.005	0.074
6	6.50	1 wk	0.1	0.39	2.06	5.6	0.004	3.06	1.8	0.005	3.11	1.6	0.005	0.058
7	7.50	24 h	0.003	1.47	2.04	6.1	0.005	3.06	2.7	0.005	3.10	1.2	0.005	0.035
8	6.95	24 h	0.003	1.09	2.04	5.9	0.004	3.05	2.3	0.005	3.09	1.5	0.005	0.021
9	6.00	24 h	0.003	0.68	2.05	6.0	0.004	-	-	-	-	-	-	0.034
10	6.00	24 h	0.1	0.20	2.05	5.6	0.003	-	-	-	-	-	-	0.18
α-Ni(OH)$_2$					2.04	5.6	0.003	3.09	5.7	0.005	-	-	-	0.068
β-Ni(OH)$_2$					2.06	5.6	0.002	3.12	7.4	0.005	-	-	-	0.056

Interatomic distance, § coordination number, † Debye-Waller factor

¶ Accuracy estimates for first two shells: R ±0.02 Å, N ±20%; accuracy estimates for 3rd shell: R ±0.06 Å, N ±60%

Ni-Al LDH crystallites that form in the Ni-illite suspensions.

The structural parameters obtained from XAFS data fitting are presented in Table 3.1. The fit results for the Ni-O shell are essentially the same for all samples, with a radial distance of about 2.05 Å, and a coordination number of about 6. This indicates that Ni is present in an octahedral environment surrounded by 6 O atoms in all samples. The radial distance of the Ni-Ni shell is about 3.05 Å in all samples and is typical of Ni-Al LDH (Scheinost and Sparks, 2000). Differences exist in the Ni-Ni coordination numbers, indicating that the reaction conditions affected the amount and/or composition of the Ni-Al LDH phases formed. The radial distance of the Ni-Al shell is about 3.10 Å in all samples, consistent with the results of Scheidegger *et al.* (1998).

In the following material, the effects of pH, pH control, reaction time and ionic strength on the Ni sorption products formed in the illite suspensions will be discussed using the radial structure functions (RSF's) obtained by Fourier transformation of the k^3 weighted XAFS spectra presented in Figure 3.1. For convenient comparison, the RSF's relevant to each experimental parameter will be presented in a separate graph, along with the Fourier transforms of the theoretical spectra obtained from the fitting procedure.

3.4.2 Effect of pH Control

The effect of the pH control is demonstrated in Figure 3.2, which compares the pH edge of a system where pH was allowed to drift during reaction to a pH edge

where pH was held constant during reaction. All samples in Figure 3.2 were reacted for 24 hours at I= 0.1M. Both pH edges show a relatively steep increase in Ni sorption above pH ~6.5. At pH values <6.5, essentially no difference in Ni sorption is observed between the two pH edges. In the steep part of the edge (pH values >6.5), however, Ni sorption at a given pH is substantially higher for the edge with drifting pH than for the edge with constant pH. Two sets of data points from this higher pH range were analyzed by XAFS. Each set consisted of two data points that had similar final pH, but were reacted under different pH regimes. In all samples, the presence of Ni-Al LDH is observed, as indicated by the presence of a second neighbor peak in the radial structure functions (Figure 3.3). The solid lines in Figure 3.3 represent the Fourier transforms of the measured spectra, and the dotted lines those of the theoretical spectra derived with parameters obtained from the fitting procedure. A good agreement between the Fourier transformed XAFS functions and the theoretical fits is observed for all samples. The intensities of the second (Ni-Ni/Al) shells suggest that formation of Ni-Al LDH is the main mode of Ni sorption in these samples, especially in the samples with drifting pH and in the sample with constant pH=7.50, consistent with the results of Scheidegger *et al.* (1997, 1998).

The second shell in the RSF of the constant pH 6.95 sample is smaller than that of the constant pH 7.50 sample (Figure 3.3). Since the reaction time was the same for these samples and the amount of Ni sorbed was larger at pH 7.50 than at pH 6.95, this indicates that the rate of Ni-Al LDH formation increases with increasing pH.

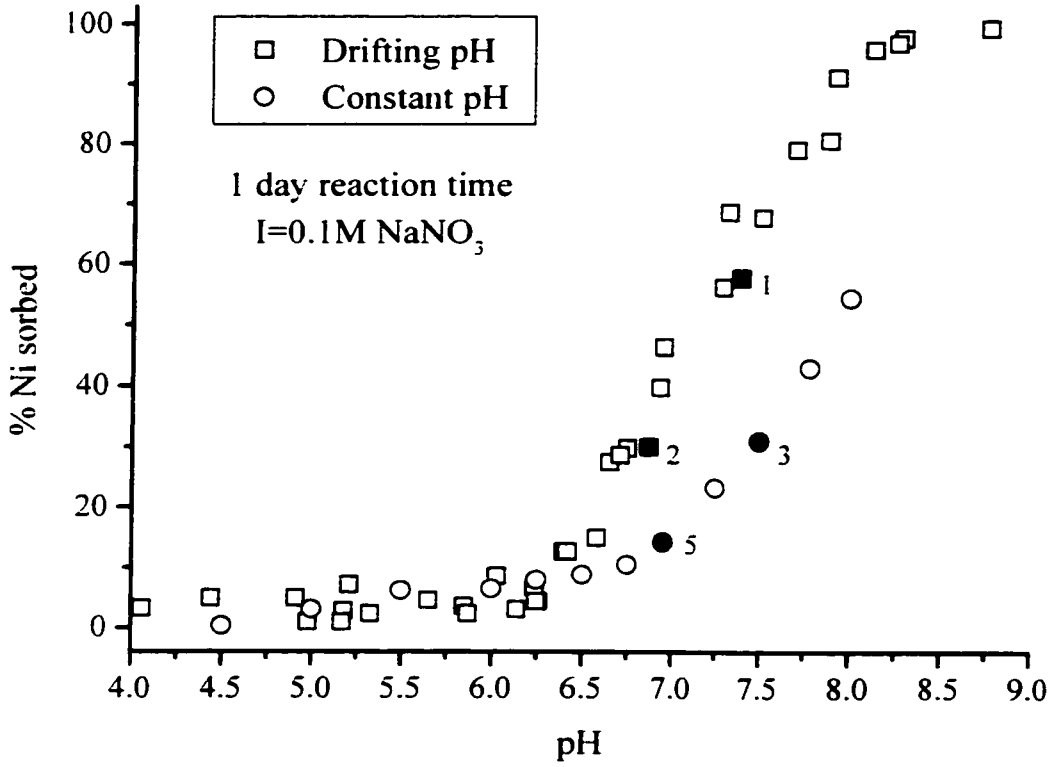

Figure 3.2 Macroscopic data on the effect of pH control on Ni sorption to illite. Filled datapoints were analyzed by XAFS; the sample numbers correspond to those in Figures 3.1 and 3.3.

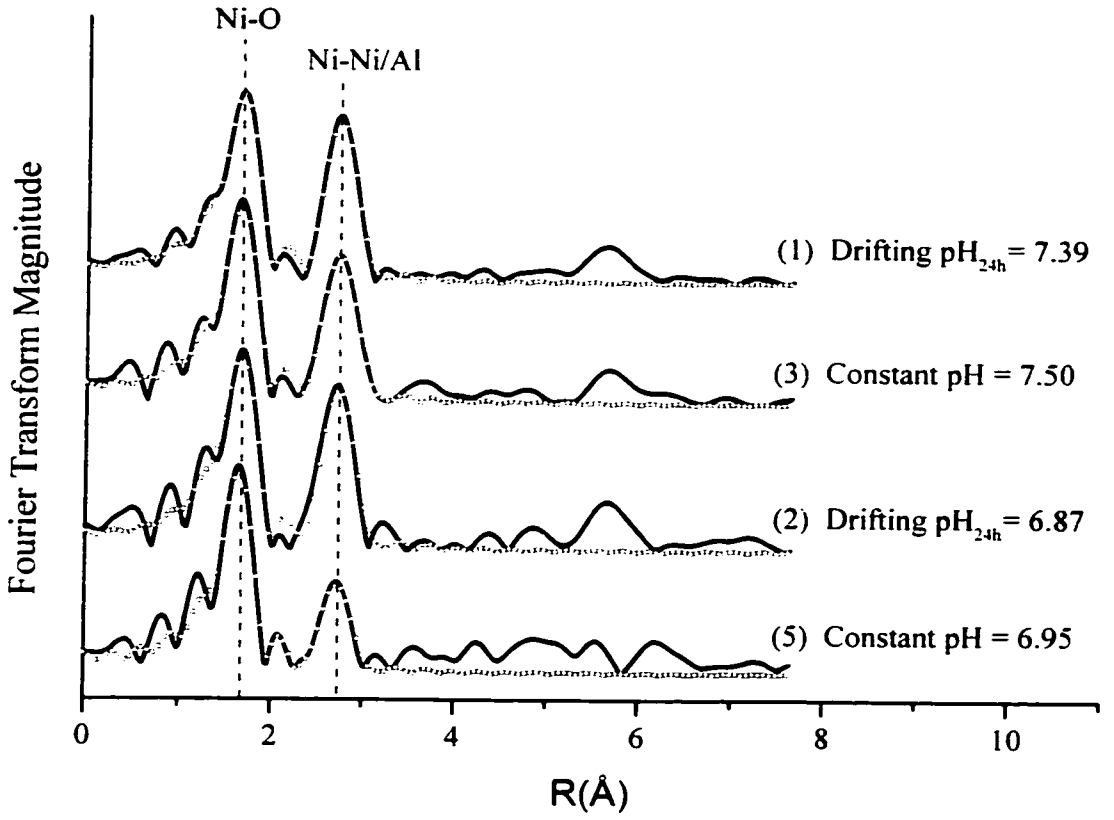

Figure 3.3 Radial structure functions (uncorrected for phase shift) of the filled datapoints in Figure 3.2. The solid lines represent the Fourier transforms of the measured spectra, and the dotted lines those of the theoretical spectra derived with parameters obtained from the fitting procedure. Sample numbers (in brackets) correspond to those in Figures 3.1 and 3.2.

The enhanced formation rate of Ni-Al LDH with increasing pH may explain why Ni sorption above pH 6.5 is higher in the edge with drifting pH than in the edge with constant pH, as follows. In a preliminary Ni/illite sorption experiment using a pH-stat apparatus, it was found that base was needed to maintain a constant pH of 7.50 over time. This indicates that formation of Ni-Al LDH is accompanied by release of H^+ ions into solution, although part of the base consumption in this experiment will have been due to illite dissolution, since the point of zero charge of illite is <7.50. Figure 3.4 shows Ni pH edges with non controlled pH for reaction times of 1 day and 8 days. The arrows in this figure track the drift in pH and Ni sorption between 1 day and 8 days of reaction for three samples in the pH range where Ni-Al LDH formation is observed. In all cases, we observe a pH drift to lower values that is accompanied by an increase in Ni sorption over time, consistent with the observation from the pH-stat experiment that Ni-Al LDH formation leads to H^+ release into solution (although part of the pH change occurring between 1 and 8 days is due to illite dissolution). These experimental results indicate that when pH is not controlled, high initial pH's continuously decrease with time due to Ni-Al LDH formation and illite dissolution. As a result, the pH measured after a 24 h reaction time, which is plotted on the x-axis in Figure 3.2, is lower than the initial pH at the start of the 24 h reaction time when pH is allowed to drift. In the presence of a buffer, however, the pH is maintained at the desired level during the 24 h reaction period. As a result, samples reacted for 24 h at constant pH effectively have been exposed to a lower pH value than samples that reach this pH after 24 h in the drifting pH regime. Since Ni-Al LDH formation

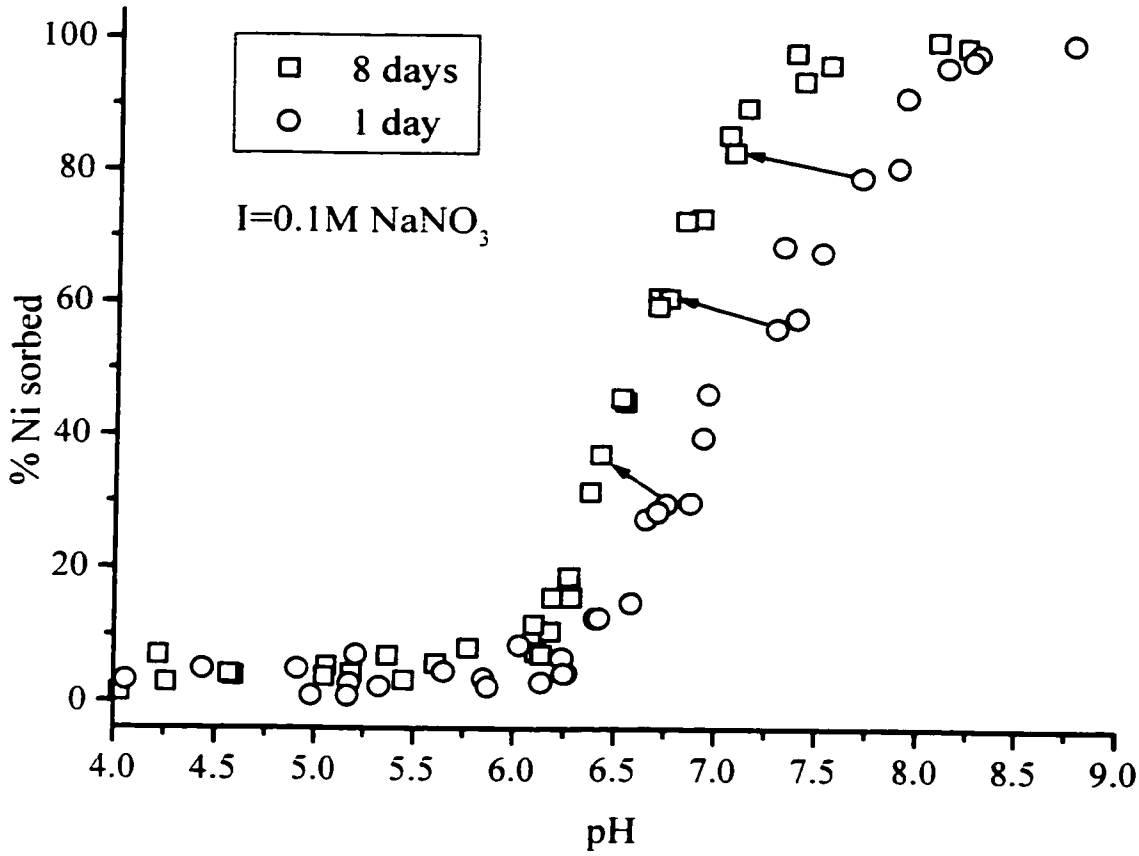

Figure 3.4 pH edges after 24 h and 8 days of reaction in a system with drifting pH over time. The arrows track the pH drift and Ni sorption of select samples over time.

proceeds faster at higher pH, more Ni-Al LDH is formed in the drifting pH samples than would be expected based on the pH measured after 24 hours of reaction. Comparison of the RSF's of drifting pH 6.87 vs. constant pH 7.50 shows that the intensity of the second peak is similar for these two samples. Since these samples have very similar Ni loadings (Figure 3.1), this suggests that the effective pH of the drifting pH 6.87 sample during the 24 h reaction period was close to pH=7.50.

A consequence of these findings is that modeling the kinetics of Ni sorption on clay minerals in the higher pH region will be more complicated when pH is not controlled. The change in pH over time will add an extra time dependency to the formation rate of Ni-Al LDH, since the formation rate is a function of pH. In turn, the change in pH over time itself will be affected by the formation rate of Ni-Al LDH, as well as by the rate of mineral dissolution, which also depends on pH, and is therefore also time dependent. Maintaining a constant pH over time will therefore significantly simplify the system in terms of modeling the Ni sorption kinetic behavior.

3.4.3 Effect of Reaction Time

The effect of reaction time is shown in Figure 3.5 for the system with I=0.1M where pH was kept constant over time. At low pH values (pH<6.25), no changes in the amount of Ni sorbed were observed between the samples taken at a reaction time of 3 hours and those taken at longer reaction times. At pH values >6.25, however, Ni sorption continuously increased with time. The XAFS data presented in Figure 3.6

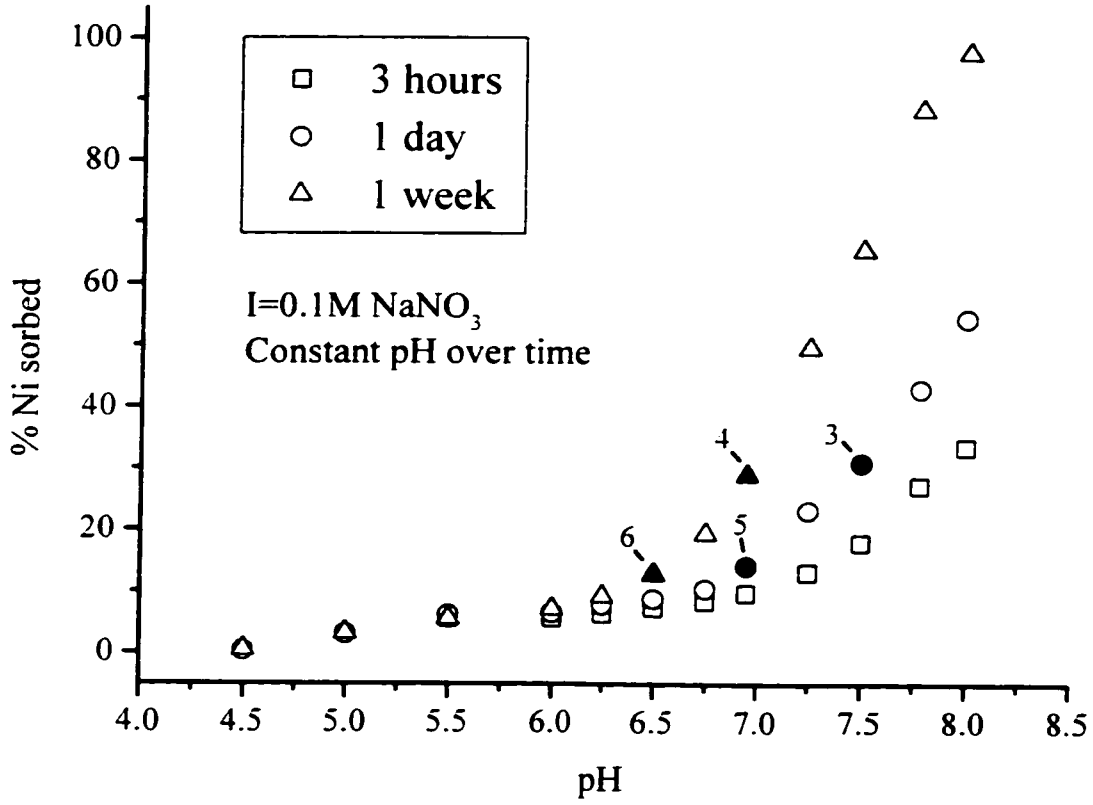

Figure 3.5 Macroscopic data on the effect of reaction time on Ni sorption. Filled datapoints were analyzed by XAFS; the sample numbers correspond to those in Figures 3.1 and 3.6.

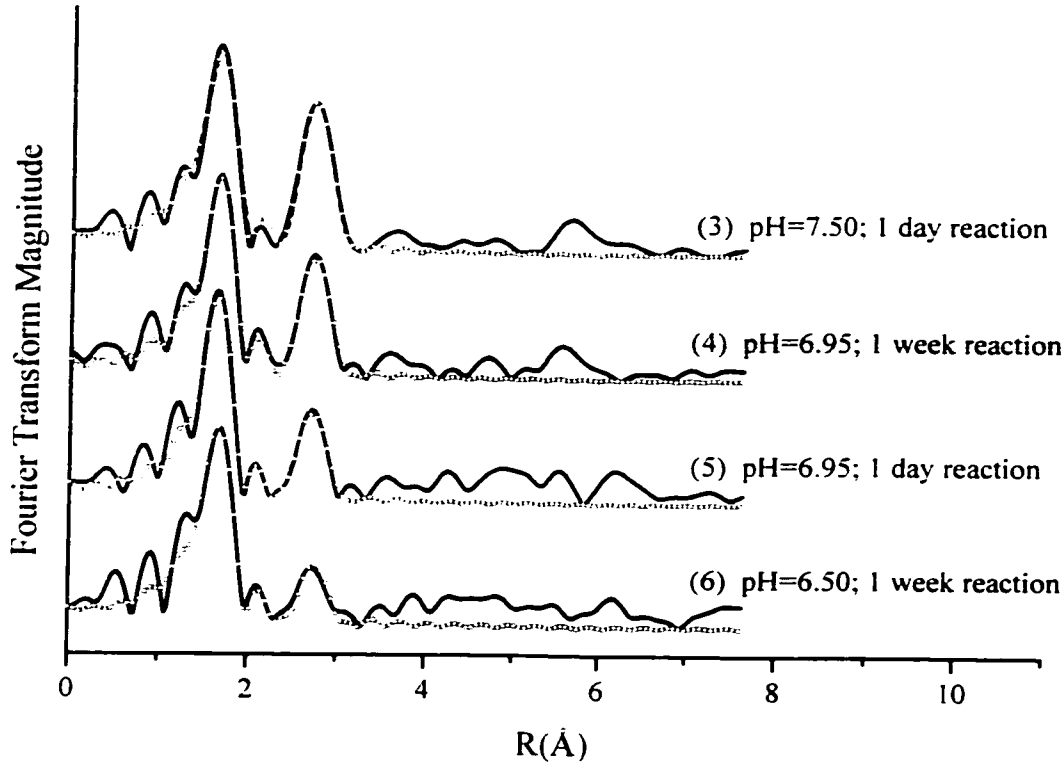

Figure 3.6 RSF's (uncorrected for phase shift) of the filled datapoints in Figure 3.5. The solid lines are the Fourier transforms of the measured spectra, and the dotted lines those of the theoretical spectra. The sample numbers in brackets correspond to those in Figures 3.1 and 3.5.

indicate that this is due to the formation of Ni-Al LDH. Two data points that had the same pH=6.95 but were reacted with Ni for different times (1 day and 1 week) show that the second Ni-Ni/Al peak in the radial structure function increases with time. This demonstrates the growth of the Ni-Al LDH precipitates over time, consistent with the time-resolved XAFS study on Ni sorption on clay minerals presented by Scheidegger *et al.* (1998). We observe the formation of these phases at a pH value as low as 6.50 after a reaction time of 1 week.

Comparison of the RSF's of two data points (pH=6.95 and pH=7.50) that have the same Ni loading but needed different reaction times (1 week and 1 day, respectively) to reach this Ni loading level due to the difference in pH, shows that the intensity of the second (Ni-Ni/Al) shell is larger for pH=7.50 than for pH=6.95. The same holds true for the sample reacted at pH=6.95 for 1 day vs. the sample reacted at pH=6.50 for 1 week, which also have similar Ni loadings. This demonstrates that the Ni bonding environment is different in these samples despite their very similar Ni loading levels. Three factors may explain this observation. First, formation of Ni-Al LDH phases as a Ni sorption mechanism may become more competitive with increasing pH relative to the other operative Ni sorption mechanisms (mononuclear inner- and outer-sphere adsorption at edge sites and planar sites). This may be related to the faster Ni-Al LDH precipitation at higher pH, which may make N-Al LDH formation more effective as a Ni sorption mechanism relative to Ni adsorption at the illite edge and planar sites. With increasing pH, Ni-Al LDH phases then would

increasingly contribute to the total amount of sorbed Ni, which would lead to the observed increase in second neighbor scattering. An alternative explanation is related to diffusion to illite interlayer sites. The difference between the BET and EGME surface areas determined for our illite clay fraction (17 and 163 $m^2 g^{-1}$ for BET and EGME, respectively) indicates the presence of a fairly large internal surface area. The BET method accounts for the external surface area, whereas the EGME method measures both the internal and external surface area. The difference between the two methods therefore represents the internal surface area of the clay, which contains planar sites at which outer-sphere Ni sorption would occur. Diffusion of reactants to internal surface sites may be slow, occurring on time scales of weeks, as has been suggested for Cs sorption to illite (Comans *et al.*, 1991). Therefore, due to the slower rate of Ni-Al LDH precipitation, and the longer reaction time allowed for the lower pH samples (1 wk vs. 1 day for the higher pH samples with similar Ni loadings), a relatively large fraction of nickel metal ions in these samples may be adsorbed as mononuclear outer-sphere complexes at illite interlayer sites, which would explain the smaller second-neighbor scattering in these samples relative to the higher pH samples with similar Ni loadings. However, for samples with pH $\leq$ 6, where no Ni-Al LDH formation occurs (as will be shown later), no difference in Ni sorption is observed between 1 wk and 3 h reaction times (Figure 3.2). This suggests that the illite interlayer sites are readily accessible, and that slow diffusion of Ni to illite interlayer sites does not play a role in the reduced second neighbor scattering observed for the samples reacted for 1 week.

Secondly, the composition of the Ni-Al LDH phases may be different at the two different pH values. Since the EXAFS contributions resulting from second-neighbor Al scattering are partly out of phase with those resulting from second-neighbor Ni scattering (d'Espinose de la Caillerie *et al.*, 1995; Scheidegger *et al.*, 1997), an increase in the Al content of the Ni-Al LDH phase would lead to an apparent decrease in overall second-neighbor scattering, and would therefore decrease the intensity of the second shell in the RSF (Scheinost and Sparks, 2000). As noted previously, the rate of formation of Ni-Al-LDH increases with increasing pH. The fast formation of Ni-Al LDH phases at pH 7.50 relative to pH 6.95 may lead to a lower Al content in the Ni-Al LDH phase formed at pH 7.50, since the amount of Al dissolved from the clay structure may be larger during 1 week of reaction at pH 6.95 than during 1 day of reaction at pH 7.50. Unfortunately, it is not possible to make a reliable estimate of the N_{Ni-Ni}/N_{Ni-Al} ratio from Ni-Al LDH EXAFS data, since the amplitude cancellation between the Ni and Al shells not only leads to apparent reduced second neighbor scattering, but also results in poorly constrained accuracies for the N_{Ni-Al} and R_{Ni-Al} values obtained from EXAFS data fitting (Scheidegger *et al.*, 1998).

Thirdly, the average cluster size of the Ni-Al LDH precipitate may be larger at higher pH (*i.e.* shorter reaction time). This would lead to an increase in the average number of second neighbors, and would therefore increase second neighbor scattering. Since XAFS probes the bonding environment of the central atom within an approximate 8Å radius (B. Boyanov, personal communication), it is sensitive to Ni-Al

LDH crystal size (with respect to N_{Ni-Ni}) only if the average radius of the Ni-Al LDH sheets is smaller than ~35 nm (A. Scheinost, personal communication). It should be noted, therefore, that a larger average Ni-Al LDH crystal size is indicated by larger second neighbor scattering only if the precipates are within this size scale. In an EXAFS study on Co sorption on kaolinite, where $Co(OH)_2$-like phases formed that are similar to the Ni-Al LDH phases we observe, O'Day *et al.* (1994) hypothesized that the formation of smaller precipitate clusters occurred over time on the kaolinite clay fraction (< 2 μm fraction). Similar to our findings, a decrease in Co-Co scattering for long-term samples (reacted for 45 days) was observed as compared to short-term samples (reacted for 24 h). O'Day *et al.* (1994) hypothesized that the short-term sorption products may be large, metastable multinuclear complexes, or a disordered hydrous precipitate resulting from fast Co sorption from solution. The surface species may reorganize over time to form smaller complexes that are bonded directly to the surface, which would account for the decrease in average Co backscattering over time. This mechanism may also occur in our system and explain the lower Ni-Ni scattering for the 7 day sample (pH=6.95) as compared to the 24 h sample (pH=7.50). An important difference in our study compared to the study by O'Day *et al.* (1994), however, is that we compare the effect of time for samples with different pH's, whereas pH was the same for the 24 h and 48 d samples in O'Day's study, which both had essentially 100% Co sorbed. Our data show that Ni-Al LDH precipitation proceeds faster at higher pH. A fast precipitation process generally leads to many small crystals, whereas slow precipitation causes a few large crystals to grow (Morse

and Casey, 1988; Putnis, 1992). This would lead to a higher average N_{Ni-Ni} for low pH (slow precipitation) as compared to high pH (fast precipitation) in our samples. Since we observe the opposite, it is not likely that differences in crystal size can explain the observed difference in Ni-Ni scattering between these samples. More likely, the possible differences with respect to the amount or composition of the Ni-Al LDH phases discussed above are responsible for the observed difference.

3.4.4 Effect of Ionic Strength

Ionic strength has a substantial effect on Ni sorption as a function of pH, as demonstrated in Figure 3.7. At any given pH value, Ni sorption is higher for I=0.003M than for I=0.1M.

The radial structure functions of selected samples in Figure 3.7 are given in Figure 3.8. The samples selected had the same pH but different ionic strengths.At pH 6.0, no differences between the RSF's of low I and high I samples are apparent above the noise level. The noise level of the I=0.1M sample at this pH is relatively high, however, due to its low Ni loading level. Possible differences with the I=0.003M sample may therefore not be visible.

The XAFS results of pH=6.95 and pH=7.50 show the formation of Ni-Al LDH precipitates at both low I and high I. However, at both pH values, the second Ni-Ni/Al peak is smaller for I=0.003M as compared to I=0.1M, although the total Ni uptake is higher at I=0.003M. This suggests substantial outer-sphere adsorption of Ni at low

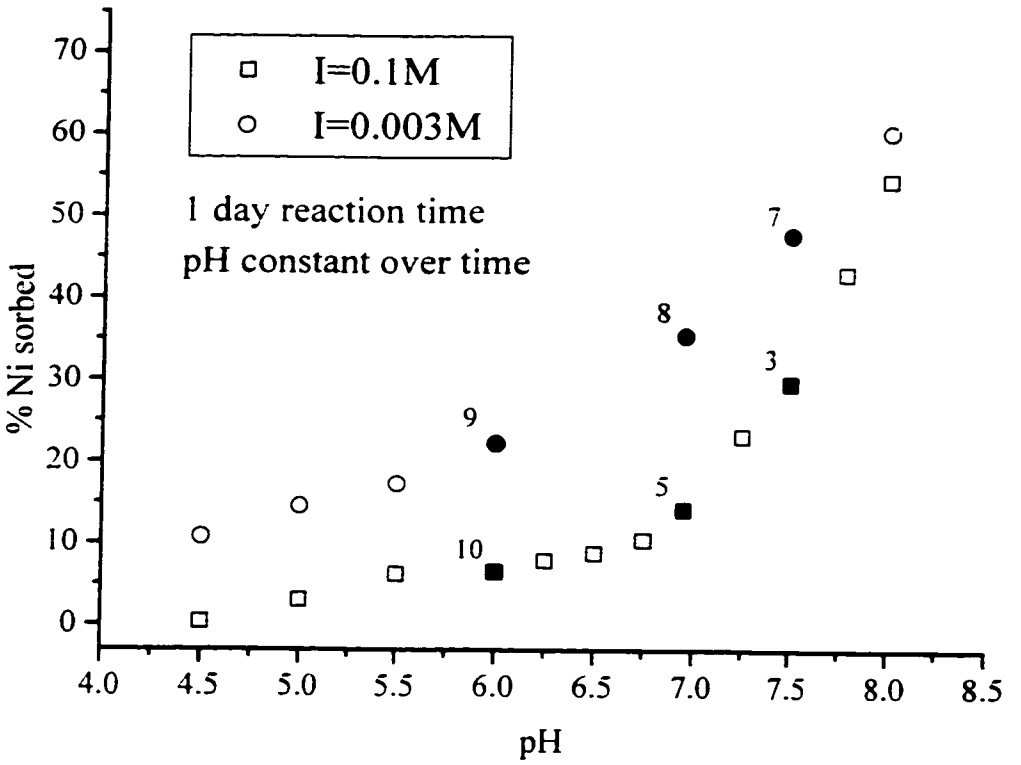

Figure 3.7 Macroscopic data on the effect of ionic strength on Ni sorption. Filled datapoints were analyzed by XAFS; the sample numbers correspond to those in Figures 3.1 and 3.8.

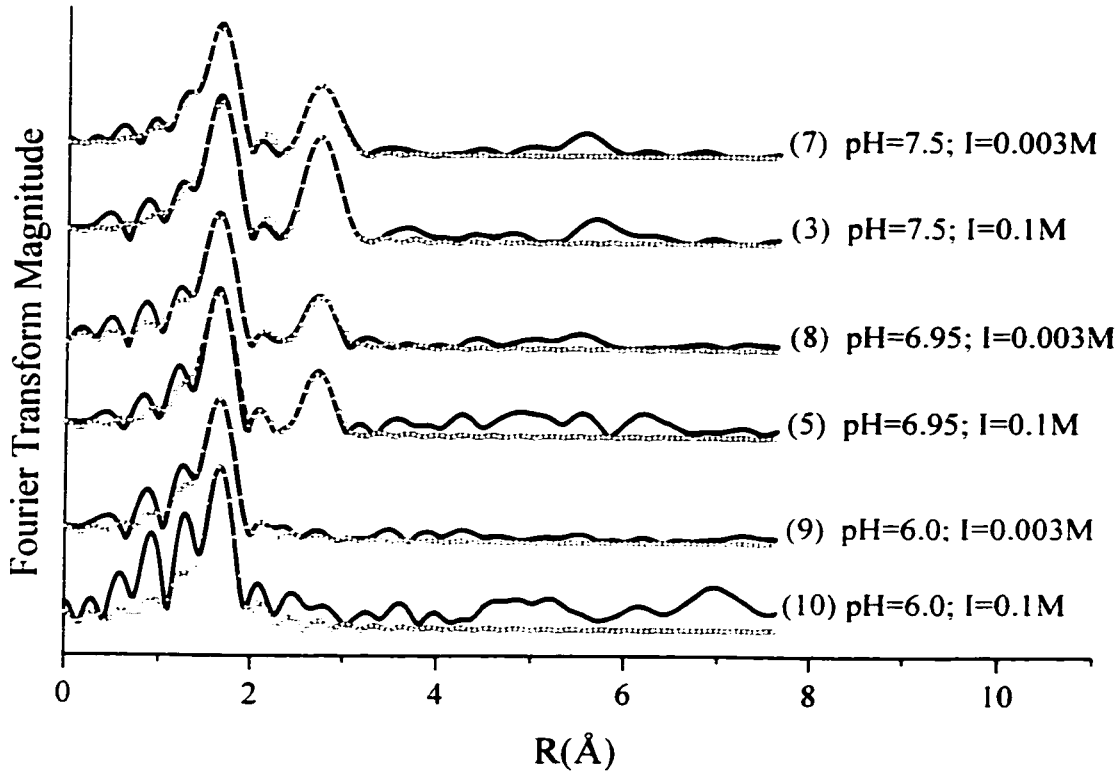

Figure 3.8 RSF's (uncorrected for phase shift) of the filled datapoints in Figure 3.7. The solid lines are the Fourier transforms of the measured spectra, and the dotted lines those of the theoretical spectra. The sample numbers correspond to those in Figures 3.1 and 3.7.

ionic strength. The potential of illite for cation exchange is mainly associated with the interlayer region, which contains planar sites at which outer-sphere Ni sorption would occur. As noted previously, the illite clay fraction used in this study contains a fairly large interlayer region, as indicated by the difference between the BET and EGME surface areas (17 and 163 $m^2 g^{-1}$ for BET and EGME, respectively). At high ionic strength (I=0.1M), outer-sphere Ni sorption is suppressed due to the high concentration of Na ions, that compete with Ni ions for planar sites. At low ionic strength (I=0.003M) the concentration of Na ions is low, and Ni can more effectively compete for the outer-sphere sorption sites. The XAFS data suggest that the resultant increase in outer-sphere Ni complexes leads to a decrease in the importance of Ni-Al LDH formation as a Ni sorption mechanism, as reflected in the smaller second peak in the RSF's. A similar observation was made by Papelis and Hayes (1996) for Co sorption on montmorillonite, which is a strongly swelling clay mineral with an even higher potential for outer-sphere metal sorption than illite. Note that it is still possible in our system that the absolute amount of Ni-Al LDH formed is the same at low and high I. The total Ni sorption is higher at low I and XAFS provides an average bonding environment of all sorbed Ni atoms. An increase in outer-sphere Ni sorption with the same amount of Ni present in Ni-Al LDH will therefore lead to a decrease in the relative contribution of Ni-Al LDH to the total amount of Ni sorbed, which would result in the observed lower (average) Ni-Ni scattering.

3.5 Conclusions

Our XAFS data show that the formation of mixed Ni-Al LDH precipitates is an important Ni sorption mechanism in Ni/illite systems at pH values >6.25. The rate of formation of these phases was found to increase with increasing pH, and the precipitates continued to grow over time. Comparison between samples that had the same Ni loading, but were reacted for different reaction times and at different pH values, showed enhanced second neighbor scattering at higher pH. This either indicated a relative increase in the importance of Ni-Al LDH precipitation as a Ni sorption mechanism relative to other (mononuclear) Ni sorption mechanisms with increasing pH (shorter reaction time), and/or a higher Al content in the Ni-Al LDH phase formed at longer reaction times (lower pH). Our data suggest that at low Na concentrations (*i.e.* low ionic strength), significant outer-sphere Ni sorption occurred, leading to an overall increase in Ni sorption and a reduced contribution of Ni-Al LDH phases to the overall amount of Ni sorbed.

3.6 References

Baeyens, B, and M.H. Bradbury. 1995. A quantatative mechanistic description of Ni, Zn and Ca sorption on Na-montmorillonite. Report PSI Ber. 95-11: Paul Scherrer Institut, Villigen, Switzerland.

Bargar, J.R., G.E. Brown Jr., and G.A. Parks. 1998. Surface complexation of Pb(II) at oxide-water interfaces: III. XAFS determination of Pb(II) and Pb(II)-chloro adsorption complexes on goethite and alumina. Geochimica et Cosmochimica Acta, 62, 193-207.

Benjamin, M.M., and J.O. Leckie. 1982. Effects of complexation by Cl, SO_4, and S_2O_3 on adsorption behavior of Cd on oxide surfaces. Environonmental Science and Technology, 16, 162-170.

Bolt, G.H., M.G.M. Bruggenwert, and A. Kamphorst. 1979. Adsorption of cations by soil. p. 54-90. *In* G.H. Bolt and M.G.M. Bruggenwert (ed.) Soil Chemistry. A. Basic Elements. Elsevier Scientific Publishing Company, Amsterdam, The Netherlands.

Bouldin, C., L. Furenlid, and T. Elam. 1995. MacXAFS – An EXAFS analysis package for the MacIntosh. Physica B, 209, 190-192.

d'Espinose de la Caillerie, J.B., M. Kermarec, and O. Clause. 1995. Impregnation of γ-alumina with Ni(II) and Co(II) ions at neutral pH: hydrotalcite-type formation and characterization. Journal of the American Chemical Society, 117, 11471-11481.

Comans, R.N.J., M. Haller, and P. Depreter. 1991. Sorption of cesium on illite – nonequilibrium behavior and reversibility. Geochimica et Cosmochimica Acta, 55, 433-440.

Fanning, D.S., V.Z. Keramidas, and M.A. El-Dosoky. 1989. Micas. p. 551-634. *In* J.B. Dixon and S.B. Weed (ed.) Minerals in Soil Environments. SSSA Book Series No 1. 1989, Soil Science Society of America, Madison, WI.

Ford, R.G., A.C. Scheinost, K.G. Scheckel, and D.L. Sparks. 1999. The link between clay mineral weathering and the stabilization of Ni surface precipitates. Environonmental Science and Technology, 33, 3140-3144.

Génin, P., A. Delahaye-Vidal, F. Portemer, K. Tekaia-Elhsissen, and M. Figlarz. 1991. European Journal of Solid State Inorganic Chemistry, 28, 505-518.

Jackson, M.L. 1956. Plant and Soil Analysis. Advanced Course. University of Wisconsin, Madison, WI.

McBride, M.B. 1994. Environmental chemistry of soils. Oxford University Press, New York.

Morse, J.W., and W.H. Casey. 1988. Ostwald processes and mineral paragenesis is sediments. American Journal of Science, 288, 537-560.

O'Day, P.A., C.J. Chisholm-Brause, S.N. Towle, G.A. Parks, and G.E. Brown Jr. 1996. X-ray absorption spectroscopy of Co(II) sorption complexes on quartz (α-SiO_2) and rutile (TiO_2). Geochimica et Cosmochimica Acta, 60, 2515-1532.

Papelis, C., and K.F. Hayes. 1996. Distinguishing between interlayer and external sorption sites of clay minerals using X-ray absorption spectroscopy. Colloids and Surfaces, 107: 89-96.

Putnis, A. 1992. Introduction to mineral sciences. Cambridge University Press, Cambridge, UK.

Roberts, D.R., A.M. Scheidegger, and D.L. Sparks. 1999. Kinetics of mixed Ni-Al precipitate formation on a soil clay fraction. Environmental Science and Technology, 33, 3749-3754.

Roe, A.L., K.F. Hayes, C.J. Chisholm-Brause, G.E. Brown Jr., G.A. Parks, K.O. Hodgson, and J.O. Leckie. 1991. In situ X-ray absorption study of lead ion surface complexes at the goethite-water interface. Langmuir 7: 367-373.

Scheidegger, A.M., G.M. Lamble, and D.L. Sparks. 1997. Spectroscopic evidence for the formation of mixed-cation hydroxide phases upon metal sorption on clays and aluminum oxides. Journal of Colloid and Interface Science, 186, 118-128.

Scheidegger, A.M, D.G. Strawn, G.M. Lamble, and D.L. Sparks. 1998. The kinetics of mixed Ni-Al Hydroxide formation on clays and aluminum oxides: a time-resolved XAFS study. Geochimica et Cosmochimica Acta, 62, 2233-2245.

Scheinost, A.C., R.G. Ford, and D.L. Sparks. 1999. The role of Al in the formation of secondary Ni precipitates on pyrophyllite, gibbsite, talc and amorphous silica: A DRS study. Geochimica et Cosmochimica Acta, 63, 3193-3203.

Scheinost, A.C., and D.L. Sparks. 2000. Formation of layered single- and double-metal hydroxide precipitates at the mineral/water interface: A multiple-scattering XAFS analysis. Journal of Colloid and Interface Science, 223, 167-178.

Sparks, D.L. 1995. Environmental Soil Chemistry. Academic Press, San Diego, CA.

Sposito, G. 1989. The chemistry of soils. Oxford University Press, New York..

Srodon , J., and D.D. Eberl. 1984. Illite. p. 495-544. *In* S.W. Bailey (ed.) Micas. Mineralogical Soc. Am. Washington, DC.

Strawn, D.G., A.M. Scheidegger, and D.L. Sparks. 1998. Kinetics and mechanisms of Pb(II) sorption and desorption at the aluminum oxide-water interface. Environmental Science and Technology, 32, 2596-2601.

Strawn, D.G. and D.L. Sparks. 1999. The use of XAFS to distinguish between inner- and outer-sphere lead adsorption complexes on montmorillonite. Journal of Colloid and Interface Science, 216, 257-269.

Thompson, H.A., G.A. Parks, and G.E. Brown Jr. 1999. Dynamic interactions of dissolution, surface adsorption, and precipitation in an aging cobalt(II)-clay-water system. Geochimica et Cosmochimica Acta, 63, 1767-1779.

Towle, S.N., J.R. Bargar, G.E. Brown Jr., and G.A. Parks. 1997. Surface precipitation of Co(II) (aq) on Al_2O_3. Journal of Colloid and Interface Science, 187, 62-82.

Zabinsky, S.I., J.J. Rehr, A. Ankudinov, R.C. Albers, and M.J. Eller. 1995. Multiple-scattering calculations of X-ray absorption spectra. Physical Reviews B, 52, 2995-3006.

Zachara, J.M., S.C. Smith, J.P. McKinley, and C.T. Resch. 1993. Cadmium sorption on specimen and soil smectites in sodium and calcium electrolytes. Soil Science Society of America Journal, 57, 1491-1501.

Chapter 4

SPECTROSCOPIC STUDIES OF PB(II)-SULFATE INTERACTIONS AT THE GOETHITE-WATER INTERFACE

4.1 Abstract

We used a combination of in situ attenuated total reflectance Fourier transform infrared (ATR-FTIR) spectroscopy and X-ray absorption fine structure (XAFS) spectroscopy to conduct molecular scale studies on Pb(II)-sulfate interactions at the goethite-water interface between pH4.5 and 6.0. Both the ATR-FTIR studies (probing sorbed SO_4 in a flow cell setup) and the EXAFS studies (probing sorbed Pb) indicated that Pb-SO_4 ternary complexes form at the goethite surface. Based on the combined information from the IR and XAFS studies, a number of possible Pb-SO_4 ternary complex configurations are presented and discussed. In addition to forming ternary complexes with SO_4, Pb also promotes SO_4 sorption to goethite via electrostatic effects, which are more pronounced at lower Pb concentrations and higher pH values.

4.2 Introduction

Soil solutions often contain numerous metal cations and anions simultaneously, each of which may be able to sorb on variable charge surfaces present in the soil matrix. Numerous macroscopic studies have shown that anions may have a dramatic effect on metal sorption behavior (*e.g.* Webster *et al.*, 1998; Ali and Dzombak, 1996; Benjamin and Leckie, 1982), and, *vice versa*, that metal cations may significantly alter the sorption behavior of anions (*e.g.* Ali and Dzombak, 1996; Bolan *et al.*, 1993; Marcano-Martinez and McBride, 1989; Balistrieri and Murray, 1981). Metal sorption in some cases increases (*e.g.* Barrow and Leckie, 1981; Marcano-Martinez and McBride, 1989; Gunneriusson *et al.*, 1994), and in other cases decreases (*e.g.* Davis and Leckie, 1978; Elrashdi and O'Connor, 1982; Boekhold *et al.*, 1993) in the presence of non-inert anions, depending on the particular adsorbent, pH range, and the type and concentration of the metals and ligands being studied. Decreased metal sorption is generally explained by competition between metal-ligand complexation in solution and metal complexation to surface sites, or by competition between anions and metal ions for surface sorption sites. Mechanisms suggested to explain promotive effects of anions on metal sorption include the formation of ternary complexes, reduction of the surface potential by anion sorption, making the surface more attractive to metal sorption, and the formation of Me-ligand precipitates.

Only a few spectroscopic studies addressing co-adsorption of metal cations and anions at mineral surfaces have been reported in the literature. Clark and McBride (1985) used a combination of extraction experiments and electron spin resonance

spectroscopy to study Cu-PO_4 interactions at the allophane surface, and suggested the formation of Cu-PO_4 surface complexes with Cu chemisorbed to the surface. Zhengbin *et al.* (1997) investigated Cu sorption on goethite in the presence of the organic tryptophan ligand using diffuse reflectance infrared spectroscopy, and found evidence for the formation of a Cu-ligand surface complex, where Cu was chemisorbed to the surface and bonded simultaneously to ligand functional groups. Bargar *et al.* (1998) used XAFS to study Pb sorption on goethite and γ-alumina as affected by chloride, and found evidence for the formation of ternary Pb-Cl complexes on goethite at pH values below 6, whereas $PbCl_2$ precipitation was observed for γ-alumina. Weesner and Bleam (1998) combined electrophoretic mobility measurements with XAFS spectroscopy to study the coadsorption of Pb with SO_4 and PO_4 on goethite and boehmite. Phosphate induced $PbPO_4$ precipitation on both surfaces, whereas the role of sulfate was less conclusive. Sulfate sorption appeared to cause no changes in the chemical environment of Pb sorbed to the boehmite surface, but did lead to changes in the mechanism of Pb sorption to goethite, possibly due to the formation of Pb-SO_4 surface complexes or clusters.

The aim of this study was to provide more insight on the mechanisms involved in the co-adsorption of Pb^{2+} and SO_4^{2-} on goethite. To this end, we used ATR-FTIR spectroscopy to probe the sorbed SO_4 bonding environment, and XAFS spectroscopy to characterize the chemical environment of sorbed Pb. A recent study by Peak *et al.* (1999) showed that the sulfate sorption mechanism to goethite depends on pH. Experiments were therefore performed over a range of pH-values.

4.3 Materials and Methods

4.3.1 Goethite Preparation

The goethite used in this study was synthesized by titrating 50 mL of a 1M ferric nitrate solution with 450 mL of 1M KOH, and aging the resultant ferric oxide suspension for 2 weeks at 25°C (Schwertmann *et al.*, 1985). Next, the goethite suspension was centrifuged, washed with DDI-H_2O and resuspended in 0.4 M HCl for 2h to remove any remaining ferrihydrite. The goethite was then centrifuged, and washed with DDI-H_2O. Finally, the goethite was dialyzed to remove excess salts, and freeze-dried. The material was confirmed to be goethite via IR spectroscopy. The goethite had a N_2-BET surface area of 63.5 $m^2 g^{-1}$, and a point of zero salt effect of 8.4, as determined via potentiometric titration in 0.1, 0.01 and 0.005M sodium perchlorate backgrounds (Peak *et al.*, 1999).

4.3.2 Reaction Conditions

Experiments were performed at pH values ranging between 4.5 and 6.0, using a background electrolyte of 0.01M NaCl. To eliminate effects of CO_2, the experiments were carried out under N_2 conditions, using either a glove box with a N_2 atmosphere, or a continuous N_2 flow into the reaction vessels. The Pb and SO_4 solution concentrations were chosen such that solutions were undersaturated with respect to $PbSO_4$(s) (anglesite), as determined via speciation calculations in MINEQL. All chemicals used were reagent grade.

4.3.3 ATR-FTIR Data

The FTIR experiments were conducted to probe the molecular environment of SO_4 sorbed at the goethite surface. The data were collected on a Perkin-Elmer 1720x spectrometer equipped with a purge gas generator and a liquid N_2-cooled MCT detector. Spectra were collected using the flow cell technique described by Peak *et al.* (1999), and Hug and Sulzberger (1994). A 45° ZnSe ATR crystal was coated with about 2.5 mg of goethite, and placed inside the flow cell. The flow cell was placed on the horizontal ATR sample stage inside the IR spectrometer, and connected to a reaction vessel containing 1 L of background electrolyte. The reaction vessel was N_2-purged and the solution pH was adjusted to the desired value. The solution in the reaction vessel was continuously mixed using a magnetic stir bar. The solution pH was monitored throughout each experiment, and adjusted if necessary.

To start the experiment, the background electrolyte was flown through the flow cell at a flow rate of about 1 mL min^{-1}. The effluent from the flow cell was collected as waste. A background spectrum consisting of the combined absorbance of the ZnSe crystal and the goethite deposit was collected every 15 minutes. Typically after about 3 hours, there was no difference between successive background spectra, indicating that the goethite coating had equilibrated with the background electrolyte. At this time, the final background spectrum was collected as the average of 1000 scans at a 4 cm^{-1} resolution, and the sorption experiment was started by injection of sulfate into the reaction vessel. All successive spectra were collected as a ratio to this background spectrum.

The goethite deposit on the ZnSe crystal was first equilibrated with a 30μM SO_4 solution concentration. The appropriate amount of a 1 M Na_2SO_4 stock solution needed to achieve this concentration in the reaction vessel was calculated from the flow rate and the time necessary to stabilize the goethite deposit. The sorption of SO_4 to the goethite deposit was monitored by collecting spectra every 10 minutes. When the intensity of the spectra of sorbed SO_4 was stable over time, typically after about 2 hours after SO_4 injection, the final spectrum was collected and Pb was added to the reaction vessel.

The addition of Pb to the system was done in increments, with Pb solution concentrations increasing from 5μM to 1mM. The Pb concentrations in solution were reached by adding appropriate amounts of a 15 mM $PbCl_2$ stock solution to the reaction vessel connected to the flow cell. For every level of [Pb] in solution, the SO_4 sorption to the goethite deposit was monitored until there was no further increase in the infrared spectra of sorbed SO_4 over time. The final spectrum was then collected, the Pb concentration in the reaction vessel was raised to the next level, and the SO_4 was allowed to reach a new sorption equilibrium with the goethite in the flow cell.

4.3.4 EXAFS Data

We used EXAFS spectroscopy to probe the molecular environment of Pb sorbed at the goethite surface. Preparation of the EXAFS samples was done in a N_2-purged glove box using boiled DDI-water. Pb was reacted with goethite for 24 h in the presence and absence of sulfate at pH5.0 and pH6.0. For the samples without SO_4,

the goethite concentration was 0.4 g L^{-1}, and the Pb concentration was 100 μM. Pb sorption to goethite in the presence of SO_4 was done at a goethite concentration of 0.1 g L^{-1}, and Pb and SO_4 concentrations of 25 μM and 4.5mM, respectively.

XAFS spectra were recorded at Beamline X-11A of the National Synchroton Light Source, Brookhaven National Laboratory, Upton, NY. Spectra were collected at the Pb L_{III} edge using a Si(111) crystal monochromator. The premonochromator slit width was set at 0.5 mm. Higher order harmonics were suppressed by detuning 25% from the maximum beam intensity. The samples were scanned in fluorescence mode at room temperature using a Kr filled Lytle detector equipped with an As filter and 6 layers of Reynolds Al foil. At least five scans were collected per sample.

Background subtraction, Fourier filtering, and data fitting were accomplished with the program WinXAS97, in combination with the FEFF7 code. The χ-function was extracted from the raw data by fitting a linear function to the pre-edge region and a 7-knot spline function to the post-edge region, and normalizing the edge jump to unity. The data were converted to k space and weighted by k^3. Structural parameters were extracted with fits to the standard EXAFS equation by multi-shell fitting in R space. The reference compound used was β-$Pb(OH)_2$. The amplitude of the theoretical data was adjusted by a factor 0.65.

4.4 Results and Discussion

4.4.1 ATR-FTIR Data

Figures 4.1- 4.3 show the effect of Pb addition on the FTIR spectra of sorbed SO_4 at the goethite surface at pH4.5-6.0. At all three pH values, SO_4 sorption increases upon metal addition, as evidenced from the increasing IR absorbance of sorbed SO_4 with increasing metal solution concentration. Comparison of the spectra that were collected prior to metal addition shows the effect of pH on the SO_4 sorption mechanism on goethite discussed by Peak *et al.* (1999). At pH6.0, the spectrum of sorbed SO_4 shows 2 peaks: a small ν_1 peak at 975 cm^{-1}, and a broad ν_3 peak centered at approximately 1105 cm^{-1}. This spectrum is representative of SO_4 sorbed in an outer-sphere fashion at the goethite surface (Peak *et al.*, 1999). Lowering the pH to pH5.0 and pH4.6 results in a more sharply defined ν_1 band, and splitting of the ν_3 band in 2 distinct peaks at 1055 and 1133 cm^{-1}, and a shoulder at 1170 cm^{-1}. This indicates the formation of inner-sphere SO_4 surface complexes, with increasing inner-sphere complexation as pH decreases. The inner-sphere complex has C_{2v} symmetry and is either a monodentate bisulfate complex, or a monodentate sulfate complex interacting with a proton on an adjacent goethite surface site (Peak *et al.*, 1999).

Metal addition not only addition not only raises the overall SO_4 sorption to the goethite surface, but also appears to result in a gradual change of the IR spectrum of sorbed SO_4 (Figures 4.1-4.3). In order to obtain the IR spectrum of the complexes that form at the goethite surface as a result of Pb addition, we subtracted the SO_4 IR

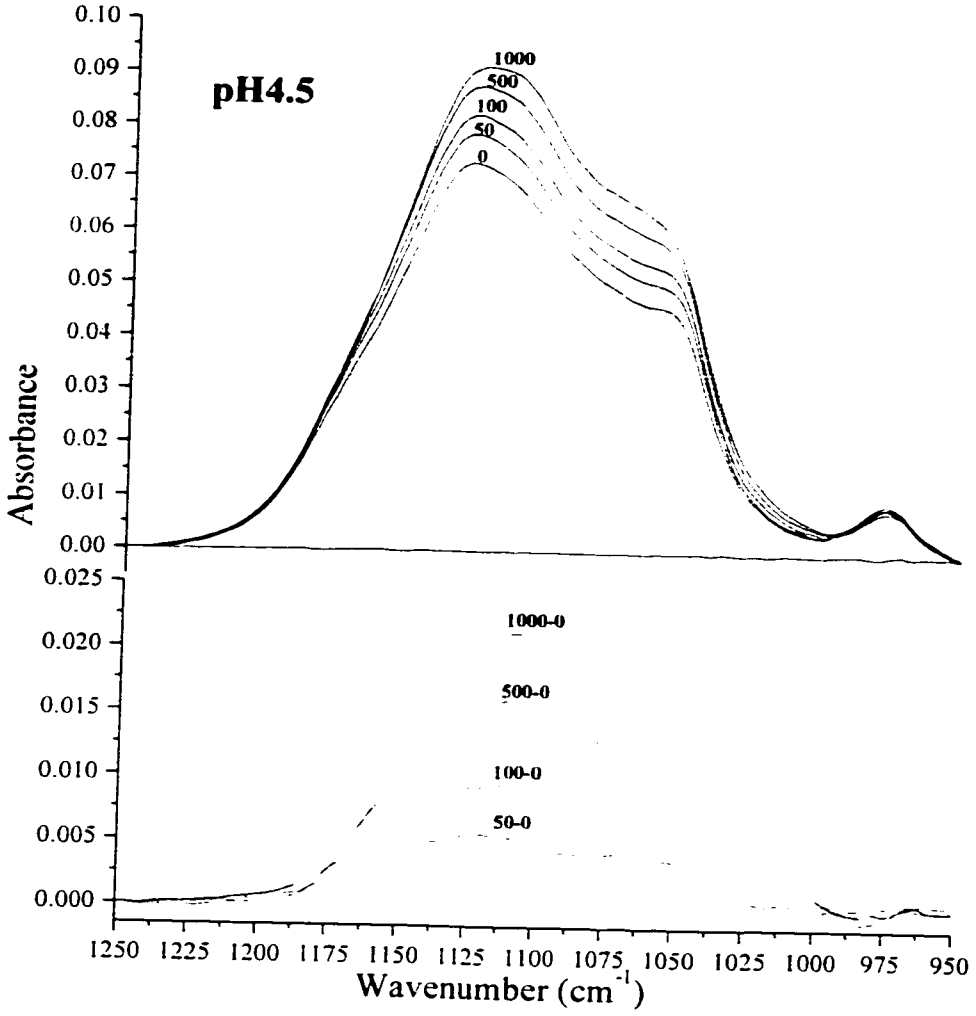

Figure 4.1 Spectrum of sorbed SO_4 as a function of Pb addition at pH4.5 (top). The numbers denote the Pb solution concentration in μM. The spectra in the bottom part of the graph are the difference spectra between the sulfate spectra at the various levels of Pb solution concentration and the spectrum collected prior to Pb addition.

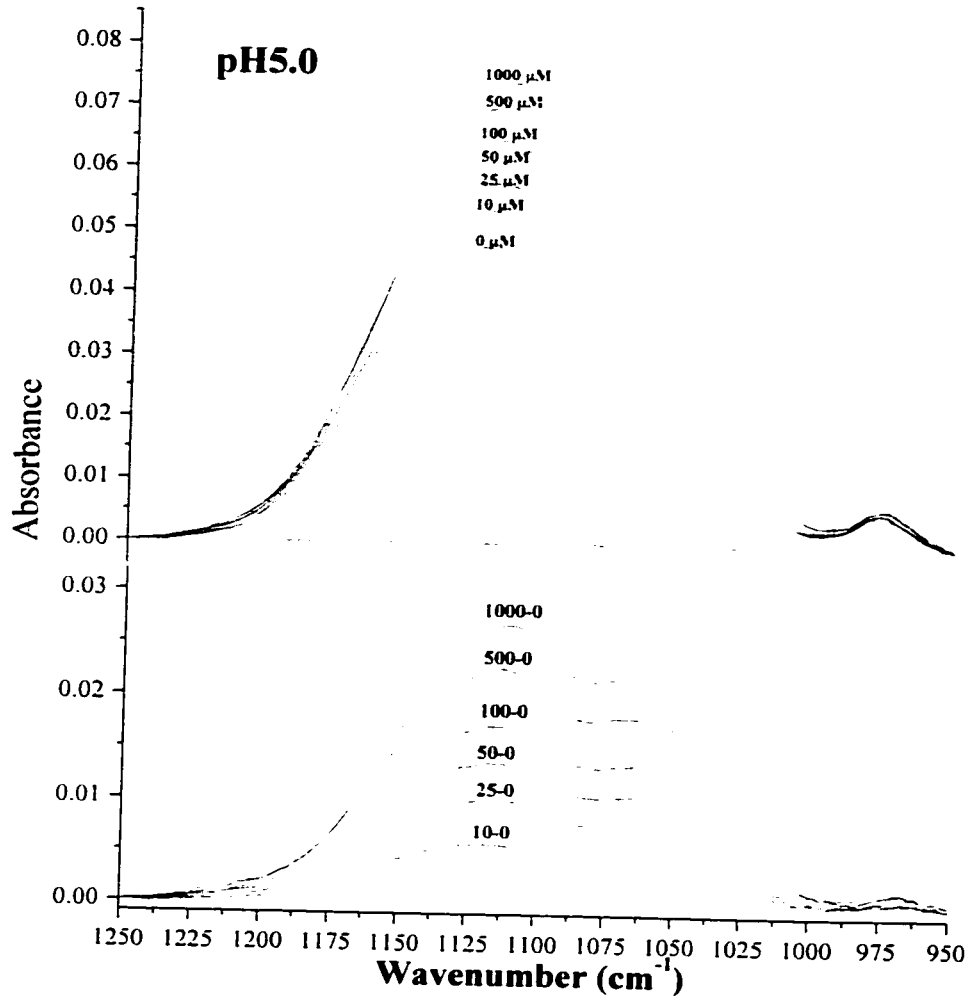

Figure 4.2 Spectrum of sorbed SO_4 as a function of Pb addition at pH5.0. The spectra in the bottom part of the graph are the difference spectra.

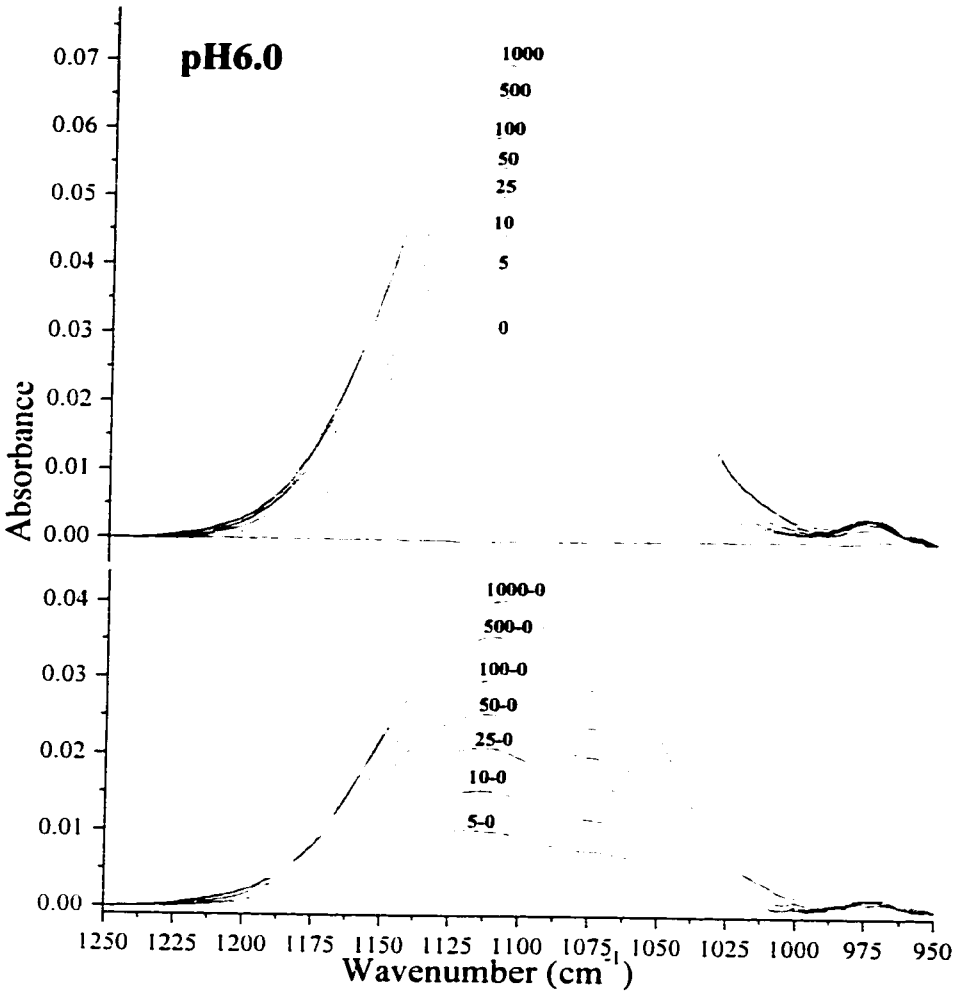

Figure 4.3 Spectrum of sorbed SO_4 as a function of Pb addition at pH6.0. The spectra in the bottom part of the graph are the difference spectra.

spectrum collected prior to metal addition from the spectra obtained upon increasing the Pb solution concentrations. The resultant difference spectra are also shown in Figures 4.1-4.3. At all three pH values, raising the Pb solution concentration leads to the appearance of two frequencies at ≈ 1110 and 1065 cm^{-1} in the IR difference spectra. This type of ν_3 splitting is not observed in the absence of Pb (Figures 4.1-4.3), which indicates that Pb addition leads to the formation of an additional inner-sphere SO_4 sorption complex at the goethite surface.

To evaluate the SO_4 sorption complexes forming upon Pb addition, Figure 4.4 compares the difference spectrum of the spectra obtained at 1 and 0 mM Pb additions to the following SO_4 reference spectra: (i) SO_4 sorbed on goethite in the absence of Pb at pH3.5. At this low pH value, a relatively large fraction of sorbed SO_4 is bonded in an inner-sphere fashion, and as a result, the IR absorbances characteristic of inner-sphere SO_4 complexes at the goethite surface are well-resolved; (ii) SO_4 sorbed on hematite at pH6.0. This spectrum is very similar to the IR spectra reported by Hug (1997) for SO_4 sorption on hematite, and represents an inner-sphere monodentate SO_4 surface complex; (iii) SO_4 sorption complexes formed on goethite in the absence of Pb as a result of increasing the SO_4 solution concentration from 30 μM to 150 μM (pH4.5), to 200 μM (pH5.0), or to 1 mM (pH6.0). These spectra were collected as the difference spectrum of sorbed SO_4 spectra obtained at 30 μM and those obtained at the raised SO_4 solution concentrations. No Pb was present in these systems, and spectra were collected at pH 4.5, 5.0 and 6.0. Increasing the SO_4 concentration in solution

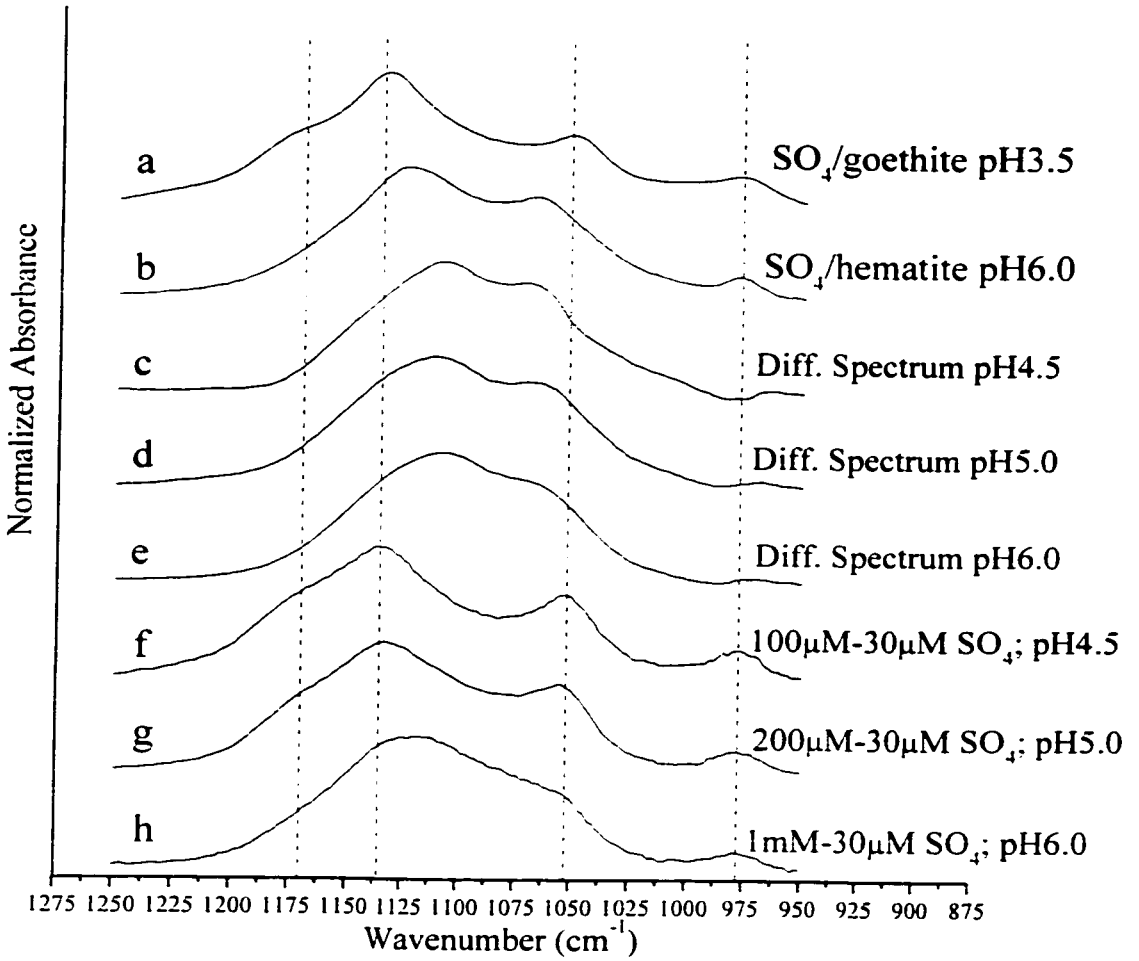

Figure 4.4 The difference spectra between the SO_4 spectra obtained at 1mM and 0 mM Pb concentrations (c, d, and e) compared to spectra of inner-sphere SO_4 complexes on goethite and hematite (a and b). Spectra f, g, and h are checks on possible surface loading effects, as described in the text.

leads to increased sorption of SO_4 at the goethite surface, as is the case for increasing the metal solution concentration. Raising the SO_4 concentration from 30 μM to 1000 μM at pH6.0 leads to a similar increase in SO_4 sorption as raising the Pb concentration from 0 to 1mM at a sulfate concentration of 30 μM at pH6.0, as judged from the increase in the integrated absorbance of the IR spectra (data not shown). At pH5.0, the sulfate concentration has to be raised from 30 μM to 200 μM to achieve the same approximate increase in SO_4 adsorption obtained upon raising the Pb solution from 0 to 1mM at a SO_4 concentration of 30μM, and at pH6.0 the sulfate concentration needs to be increased from 30 to 100 μM. Comparing the difference spectra of the Pb-containing systems to those of the Pb-free systems therefore isolates the effect of Pb addition from possible effects of SO_4 surface loading on the SO_4 sorption mechanism at the goethite surface.

The inner-sphere SO_4 complexes forming as a result of 1mM Pb addition is different from the inner-sphere complex that forms at the goethite surface when no Pb is present, as shown by comparison to the sulfate spectrum obtained at pH3.5 (Figure 4.4). The degree (band positions) and possibly the type (number of bands) of ν_3 splitting are different for the inner-sphere SO_4 complexes formed in the presence and absence of high Pb levels. In the absence of Pb, the ν_3 band splits in three peaks centered at 1055, 1133 and 1170 cm^{-1}. In the presence of Pb, however, ν_3 band splitting results in peaks located at 1110 and 1070 cm^{-1}. The appearance of these frequencies upon Pb addition is not due to a surface loading effect, since they do not

show up in the difference spectra obtained from increasing the SO_4 solution concentrations (Figure 4.4). We therefore attribute the appearance of ν_3 bands at 1110 and 1070 cm^{-1} to the formation of a Pb-SO_4 ternary complex at the goethite surface.

The ν_3 band splitting of the Pb-SO_4 ternary complexes forming at the goethite surface is similar, although not identical, to the ν_3 band splitting of the inner-sphere SO_4 complex that forms at the hematite surface (Figure 4.4), indicating that the SO_4 present in the ternary complexes has monodentate-like symmetry. For further characterization of the structure of the goethite-Pb-SO_4 ternary complexes, Pb L_{III} EXAFS analyses were performed.

4.4.2 EXAFS Data

Figure 4.5 shows the k^3-weighted χ-data (Figure 4.5a) and the radial structure functions obtained by Fourier-transformation of the k^3-weighted χ-spectra (Figure 4.5b) for the XAFS samples analyzed in this study. Both pH and the presence of SO_4 appear to influence the Pb sorption mode at the goethite surface. The pH effect is evident from the difference in the RSF's of the samples reacted at pH5.0 and pH6.0. The RSF of the sample reacted at pH6.0 shows two peaks, whereas an additional third shell is observed at pH5.0 (Figure 4.5b). The first peak in both samples represents the first-shell oxygen atoms surrounding the sorbed Pb atom, and the second and third shells indicate the presence of Fe atoms in the local coordination environment of sorbed Pb, consistent with the formation of inner-sphere Pb complexes at the goethite

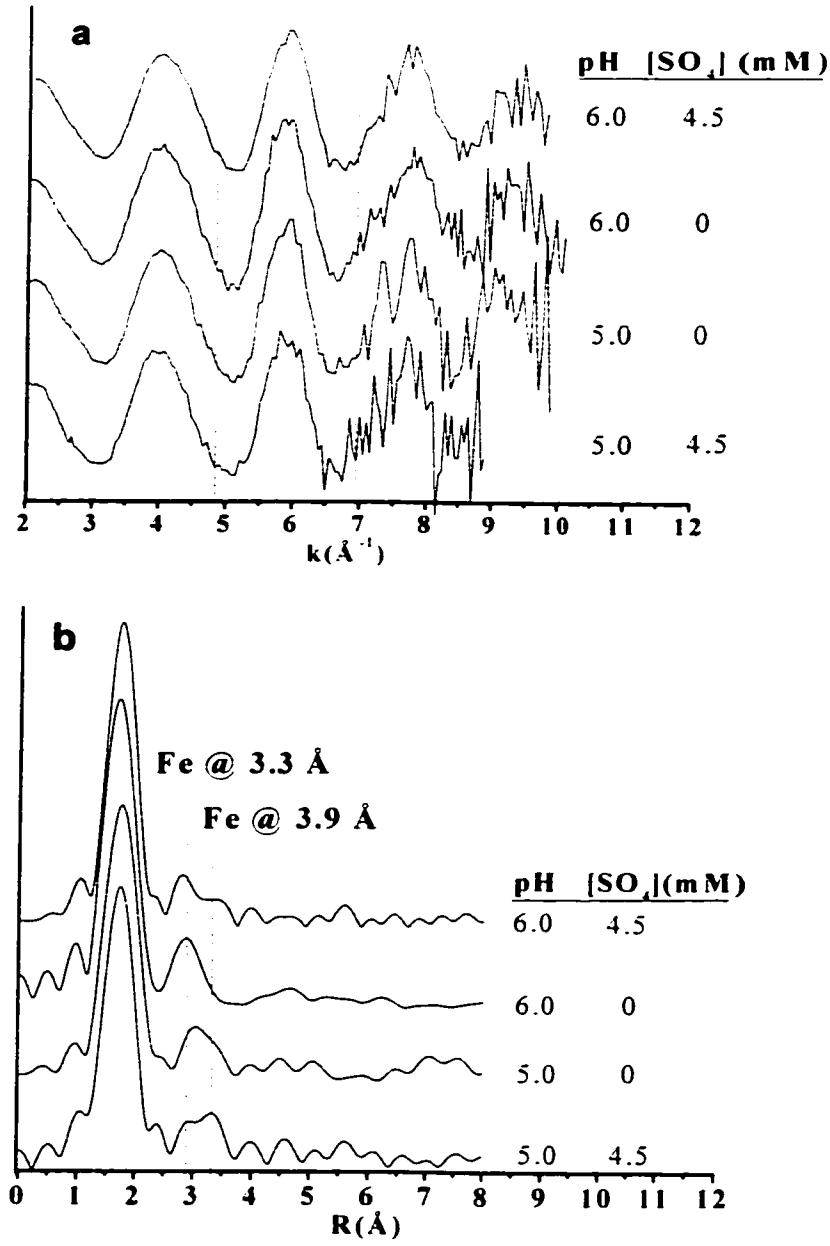

Figure 4.5 The χ-spectra of the XAS samples collected in this study (a), and the RSF's obtained by Fourier-transforming these spectra (b).

surface. Data fitting results for the pH6.0 sample indicated 2-3 O atoms at a distance of ~2.3Å, and ~1 Fe at a distance of ~3.3Å from the central Pb atom, consistent with the results of Bargar *et al.* (1997) for Pb sorption on goethite. The Pb-Fe distance of 3.3Å is characteristic of Pb bonding to edges of FeO_6 octahedra, *i.e.* the Pb atoms are coordinated to 2 surface oxygens on adjacent corners of FeO_6 octahedra (Bargar *et al.*, 1997, 1998). Data fitting indicated that the additional peak appearing in the pH5.0 spectrum was due to the presence of additional Fe at a radial distance of ~3.9Å from the central Pb atom. This Pb-Fe distance is consistent with inner-sphere Pb bonding in a binuclear bidentate fashion (*i.e.* corner sharing) to FeO_6 octahedra at the goethite-water interface (Bargar *et al.*, 1997, 1998).

The effect of SO_4 addition becomes clear by comparing the RSF's of the samples reacted in the absence and presence of SO_4 at pH5.0 and 6.0. At both pH values, SO_4 addition results in increased scattering of Fe atoms located at 3.9Å from the central Pb atom, as indicated by the increase of the third shell in the RSF's of the SO_4 containing samples relative to the SO_4-free samples. This is similar to the results of Bargar *et al.* (1998), who observed the appearance of this peak at high Cl concentrations (0.1M NaCl) at pH=6, but not in the absence of Cl. The increased coordination of Pb to Fe atoms located at ~3.9Å was attributed to the formation of Pb-chloro ternary complexes on goethite, where both Pb and Cl ions form inner-sphere bonds at the goethite surface. The presence of Fe scattering from a 3.9Å radial

distance is expressed in the χ-spectra by subtle additional features appearing between 4.8 and 5.0 $Å^{-1}$, and between 6.5 and 7.0 $Å^{-1}$ (Figure 4.5b).

4.4.3 Discussion

Our ATR-FTIR results indicate that Pb-SO_4 ternary complexes form at the goethite surface, and that the SO_4 ions in these complexes are bonded in an inner-sphere fashion having C_{3v} or lower symmetry. Our XAFS studies show that the presence of high SO_4 concentration leads to the formation of Pb inner-sphere complexes that are bonded in a corner-sharing fashion to the FeO_6 octahedra at the goethite surface. The combined information obtained from these studies points to the formation of Pb-SO_4 ternary complexes of either of the configurations shown in Figure 4.6.

The ATR-FTIR results indicated that formation of Pb-SO_4 ternary complexes results in splitting of the SO_4 ν_3 bands in at least two peaks, indicating inner-sphere SO_4 bonding. Therefore, in order to be consistent with the IR results, configuration B in Figure 4.4 would require Pb-SO_4 bonding to be strong and mostly covalent. In configuration A however, covalent bonding occurs between Fe and SO_4 (monodentate inner-sphere bonding as observed for SO_4 on hematite (Figure 4.4 and Hug, 1997), and as a result, only a more electrostatic interaction between Pb and SO_4 would be required to explain the IR data. We collected the FTIR spectra of a number of $Me(II)SO_4^0(aq)$ solution complexes in an attempt to characterize the nature of M(II)-

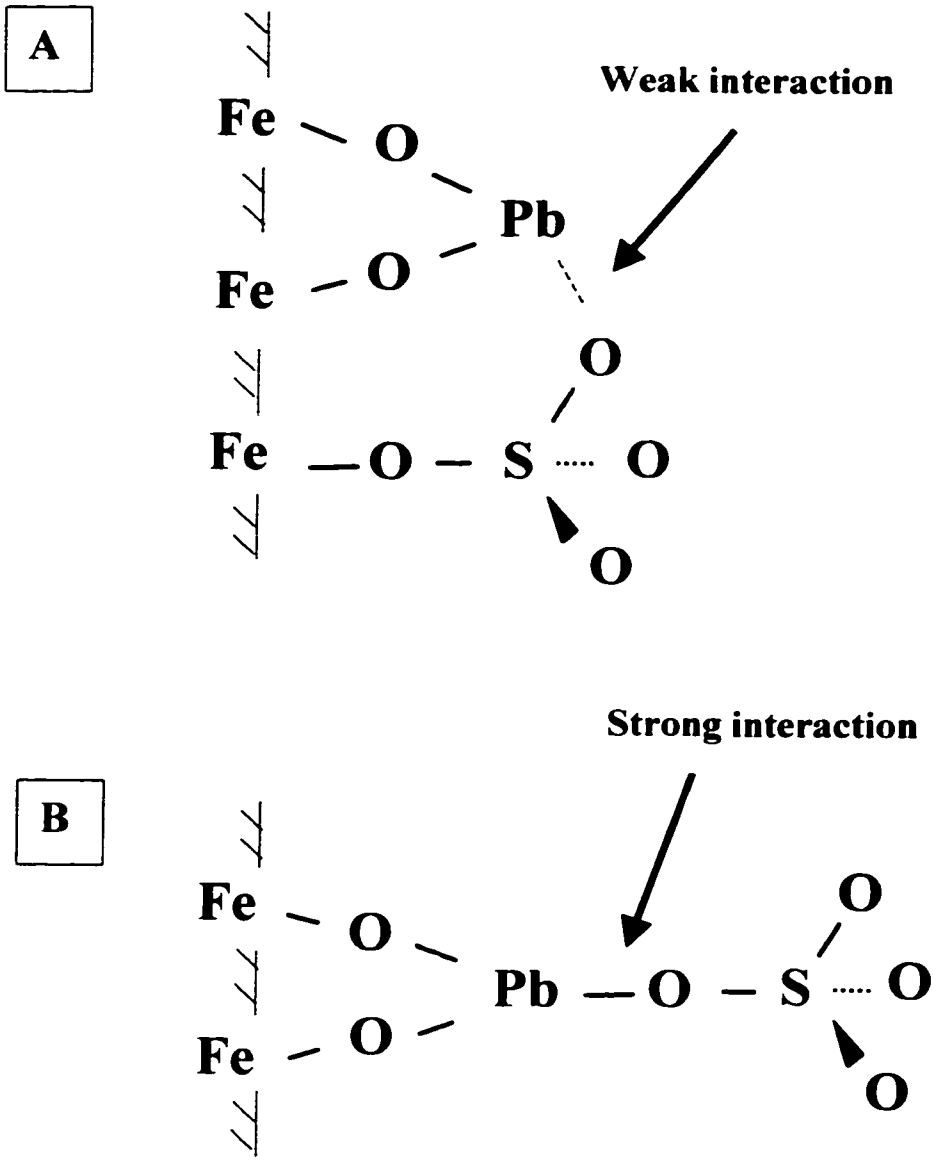

Figure 4.6 Possible Pb-SO_4-goethite ternary complexes based on the combined information from the IR and XAFS data.

SO_4 complexation. Unfortunately, it was not possible to collect an FTIR scan for $PbSO_4^0$(aq), due to the low solubility of $PbSO_4$(s): precipitation of $PbSO_4$(s) reduced the SO_4 solution concentrations below the detection limit of the IR spectrometer. The FTIR spectra of $CdSO_4^0$(aq), $MnSO_4^0$(aq), and $NiSO_4^0$(aq) are shown in Figure 4.7. Also shown are the FTIR spectra of HSO_4^-(aq), SO_4^{2-}(aq), and the spectrum of the SO_4-Pb ternary complex forming at the goethite surface upon Pb addition at pH5.0. The general appearance of the spectra of the $MeSO_4^0$(aq) solution complexes is close to that of sulfate in aqueous solution, indicating that T_d symmetry is largely retained. The ν_1 bands are slightly active, and the ν_3 bands show a small shift towards higher wavenumbers relative to the spectrum of SO_4^{2-}(aq), but no distinct splitting of the ν_3 bands is observed. This indicates that Me(II)-SO_4 ion pairing in solution is mainly due to electrostatic interactions, which lead to small distortions of the SO_4 octahedra. In contrast, the HSO_4^-(aq) spectrum shows strong splitting of the ν_3 band, which indicates a strong distortion of the SO_4 octahedron, consistent with strong covalent bonding between H^+ and SO_4^{2-}.

If it is assumed that Pb-SO_4 bonding is mostly electrostatic, as is observed for the Me(II)-SO_4 complexes shown in Figure 4.7, then only configuration A can account for the IR spectrum observed for the Pb-SO_4 ternary complexes. This can be considered an analogue to the inner-sphere SO_4 configuration forming on goethite in the absence of co-adsorbed metal cations proposed by Peak *et al.* (1999). In this configuration, sulfate is bonded as a monodentate complex interacting with a proton

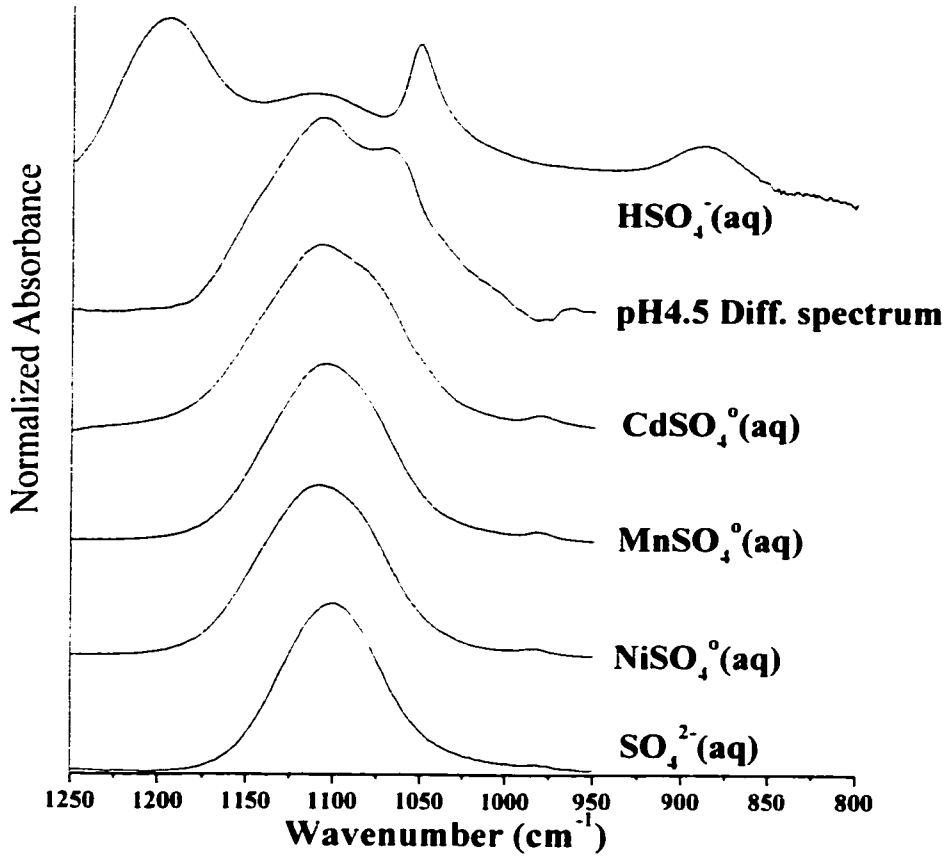

Figure 4.7 Comparison of the degree of ν_3 band splitting between the pH4.5 difference spectrum and a number of aqueous SO_4 standards.

on an adjacent goethite surface site. The strong Fe(III)-SO_4 (Hug, 1997) and H-SO_4 (Figure 4.7) interactions result in a relatively large splitting of the SO_4 ν_3 bands (Figure 4.4). Replacing the strong H-SO_4 interaction with a relatively weak Pb-SO_4 interaction, as in configuration A in Figure 4.6, leads to less-distorted SO_4 tetrehedra with monodentate-like (C_{3v}) symmetry, which is consistent with the IR spectra we observe for the Pb-SO_4 ternary complexes.

However, the Me(II)SO_4^0(aq) spectra presented in Figure 4.7 may not be representative of the $PbSO_4^0$(aq) spectrum. The logK values of the Me(II)-SO_4 association reactions (Me^{2+}(aq) + SO_4^{2-}(aq) $\leftrightarrow$ $MeSO_4^0$(aq)) range between 2.1 and 2.4 for the metals shown in Figure 4.7, whereas the logK value for Pb is 2.8, which indicates that Pb has a higher affinity for sulfate complexation than the other metals. Furthermore, the solubility of $PbSO_4$(s) is significantly lower than the solubilities of the $MeSO_4$ salts of the metals appearing in Figure 4.7. Complexation between Pb^{2+} and SO_4^{2-} ions is therefore expected to be more covalent than for the $MeSO_4$ complexes in Figure 4.7, and as a result, configuration B may also be responsible for the IR spectrum observed for the Pb-SO_4 ternary structure.

Although the frequencies occurring at 1070 and 1110cm^{-1} appear in the difference spectra at all three pH values, there are differences between the difference spectra obtained at different pH's shown in Figures 4.1-4.3. At pH6.0, the ν_3 bands are less well resolved than at pH5.0 and 4.5, suggesting the presence of an additional frequency in the pH6.0 spectrum. To isolate this frequency, the difference spectrum

obtained at pH6.0 was subtacted from the difference spectrum obtained at pH5.0. The resultant difference spectrum (not shown) was very similar to the outer-sphere SO_4 spectrum shown in Figure 4.3 (pH6.0, no Pb addition). This indicates that at pH6.0, 1mM Pb addition not only leads to formation of ternary Pb-SO_4 complexes, but also results in increased SO_4 outer-sphere sorption. At pH4.5, the difference spectrum has a negative ν_1 absorbance, and the spectrum shows dips (relative to the difference spectrum obtained at pH5.0) at 1133, 1150, and 1070cm^{-1}, which are the ν_3 band locations of the SO_4 inner-sphere complex forming in the absence of Pb (Figure 4.4). The negative absorbances at these spectral locations indicate that part of the SO_4 sorbed initially (*i.e.*, before Pb addition) as inner-sphere complexes is replaced by or transformed into Pb-SO_4 ternary complexes upon a 1mM Pb addition at pH4.5.

An analysis of the difference spectra between different levels of Pb addition is shown in Figure 4.8 to further characterize the effect of Pb addition on SO_4 sorption to the goethite surface. Shown in this figure are the successive difference spectra between the spectra obtained at Pb solution concentrations of 0, 10μM, 100μM, 500μM, and 1000μM at pH5.0. Also shown is the difference spectrum obtained from subtracting the SO_4 spectrum at a 2500μM Pb solution concentration (not shown in Figure 4.2) from the SO_4 spectrum with 500μM Pb present. Several points can be made from this figure. Between [Pb] = 0 and 500μM, the frequencies characteristic of SO_4 present in Pb-SO_4 ternary complexes are more sharply defined for the difference spectra of higher Pb concentrations. Further increasing the Pb solution concentration

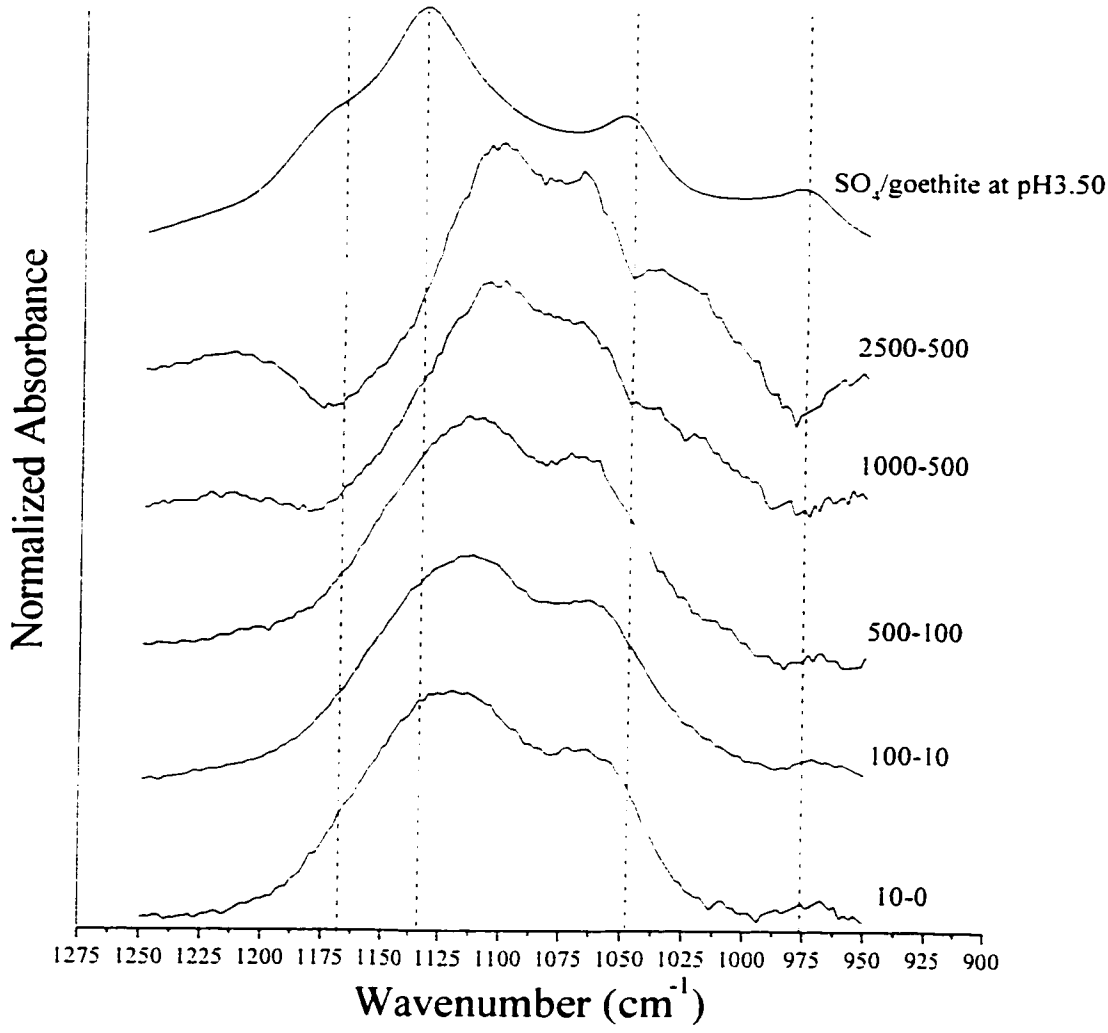

Figure 4.8 Difference spectra between successive Pb additions at pH5.0. The numbers in the figure legends refer to the Pb solution concentrations in μM. The dotted lines locate the ν_1 and ν_3 bands of sulfate inner-sphere complexes with C_{2v} symmetry.

from 500 to 1000 μM leads to negative absorbances at the spectral locations of the ν_3 bands of the inner-sphere SO_4 complex forming in the absence of Pb, which is even more pronounced in the difference spectra of the 500 and 2500 Pb concentrations. The relatively broad peaks for the difference spectra obtained by incremental Pb increases of 10-0 and 100-10 μM Pb indicates that at these relatively low Pb concentrations, increased SO_4 sorption not only occurs due to formation of Pb-SO_4 complexes, but also via additional inner-sphere and outer-sphere SO_4 complexation. Evidence for increased SO_4 inner-sphere complexation (in the same configuration as in Pb-free systems, *i.e.*, with C_{2v} symmetry, and without Pb involved in the surface complex) at low Pb concentrations is also provided by comparison of the difference spectrum of the spectra obtained at 1000 and 0 μM Pb at pH 5.0 (Figure 4.2) to the difference spectrum of the spectra obtained at 1000 and 500 μM Pb (Figure 4.8). Negative absorbances at the ν_3 band spectral locations of C_{2v} inner-sphere SO_4 complexes are observed for the 1000-500 spectrum, but not for the 1000-0 spectrum. Transformation of C_{2v} inner-sphere complexes into SO_4-Pb ternary complexes, as indicated by negative ν_3 band absorbances of the former complexes, would appear in both the 1000-0 and 1000-500 spectra if no additional SO_4 inner-sphere complexation had occurred as a result of 500 μM Pb addition. However, negative absorbances only appear in the 1000-500 spectrum, which indicates the formation of inner-sphere SO_4 complexation (C_{2v} symmetry) upon raising the Pb solution from 0-500 μM, followed by transformation of these inner-sphere complexes into Pb-SO_4 ternary complexes

when the Pb solution concentration is further raised to 1mM. Similar analyses were done on the pH4.5 and pH6.0 systems (not shown). The main differences with respect to the pH5.0 system were: (i) At pH4.5, the negative ν_3 absorbances in the 1000-500 and 2500-500 difference spectra are much stronger than at pH5.0, whereas at pH6.0 they are much weaker. Moreover, at pH4.5, negative ν_3 absorbances already appear in the 500-100 spectrum, which is not the case at pH5.0 and 6.0; (ii) As noted before, part of the initial (*i.e.*, before Pb addition) SO_4 sorbed as inner-sphere complexes at pH4.5 is transformed into Pb-SO_4 ternary compexes when raising the Pb solution concentration from 0 to 1mM Pb, as evidenced by the negative absorbances in the 1000-0 difference spectrum (Figure 4.3). This was not observed at pH5.0 and 6.0; (iii) relatively strong increases in SO_4 outer-sphere sorption upon Pb addition are observed in the difference spectra at pH6.0.

These results indicate that Pb affects SO_4 sorption via electrostatic effects as well as by ternary complex formation, and that the relative impacts of these mechanisms are a function of the pH and the level of Pb addition. The analysis described in the previous paragraph indicates that, although ternary complex formation is observed at all three pH values studied here, it appears to be promoted (relative to the importance of electrostatic effects in the overall additional SO_4 sorption resulting from Pb addition) at lower pH values given a certain Pb solution concentration. The electrostatic effect of Pb sorption is readily explained by the fact that Pb is bonded to the goethite surface as inner-sphere complexes (as indicated by our EXAFS data, as well as by Bargar *et al.*, 1997). Pb sorption will therefore create additional positive

surface charge, which results in a more favorable situation for SO_4 sorption. Given a certain Pb solution concentration level, more Pb sorption, and therefore a larger change in surface charge, is expected at higher pH, which may explain the relatively large electrostatic effect at higher pH. The transformation of inner-sphere SO_4 complexes (with C_{2v} symmetry) into Pb-SO_4 ternary complexes observed at low pH and high Pb additions suggest a surface crowding effect, where interactions occur between sorbed Pb and inner-sphere SO_4 sorption complexes that lead to the formation of ternary complexes. At lower pH's, transformation of inner-sphere SO_4 complexes from C_{2v} symmetry to ternary complexes is observed at lower Pb solution concentrations than at higher pH, indicating a more direct interaction between SO_4 and Pb (*i.e.*, the formation of ternary complexes) given a certain Pb solution concentration at low pH relative to high pH. This may be due to the fact that more inner-sphere SO_4 sorption occurs at lower pH than at higher pH, both in absolute and relative terms, and suggests that Pb sorption to goethite is more affected by the presence of SO_4 at lower pH than at higher pH.

4.5 References

Ali M.A., and D.A. Dzombak (1996). Interactions of copper, organic acids, and sulfate in goethite suspensions. Geochimica et Cosmochimica Acta, 60, 5045-5053.

Balistrieri L.S., and J.W. Murray (1981). The surface chemistry of goethite (α-FeOOH) in major ion seawater, American Journal of Science 281, 788-806.

Bargar J.R., G.E. Bown Jr., and G.A. Parks (1997). Surface complexation of Pb(II) at oxide-water interface: II. XAFS and bond-valence determination of mononuclear Pb(II) sorption products and surface functional groups on iron oxides. Geochimica et Cosmochimica Acta 61, 2639-2652.

Bargar J.R., G.E. Brown Jr., and G.A. Parks (1998). Surface complexation of Pb(II) at oxide-water interfaces: III. XAFS determination of Pb(II) and Pb(II)-chloro adsorption on goethite and alumina. Geochimica et Cosmochimica Acta 62, 193-207.

Benjamin M.M., and J.O. Leckie (1982). Effects of complexation by Cl, SO_4, and S_2O_3 on adsorption behavior of Cd on oxide surfaces. Environmental Science and Technology 16, 162-170.

Bolan N.S., J.K. Syers, and M.E. Mumner (1993).Calcium-induced sulfate adsorption by soils. Soil Science Society of America Journal 57, 691-696.

Hug S.J., and B. Sulzberger (1994). In-situ Fourer-transform infrared spectroscopic evidence for the formation of several different surface complexes of oxalate on TiO_2 in the aqueous phase. Langmuir 10, 3587-3597.

Hug S.J. (1997) In situ Fourier transform infrared measurements of sulfate adsorption on hematite in aqueous solutions. Journal of Colloid and Interface Science, 188, 415-422.

Marcano-Martinez E., and M.B. McBride (1989). Calcium and Sulfate retention by two oxisols of the Brazilian Cerrado. Soil Science Society of America Journal 53, 63-69.

Peak D., R.G. Ford, and D.L. Sparks. (1999). An in situ ATR-FTIR investigation of sulfate bonding mechanisms on goethite. Journal of Colloid and Interface Science 218, 289-299.

Schwertmann U., P. Cambier, and E. Murad (1985) Clays and Clay Minerals 33, 369-

Webster J.G., P.J. Swedlund, and K.S. Webster (1998) Trace metal adsorption onto an acid mine drainage iron(III) oxy hydroxy sulfate Environmental Science and Technology 32, 1361-1368.

Weesner F.J., and W.F. Bleam (1998). Binding characteristics of Pb^{2+} on anion-modified and pristine hydrous oxide surfaces studied by electrophoretic mobility and

X-ray absorption spectroscopy. Journal of Colloid and Interface Science 205, 380-389.

Zhengbin Z., W. Wei, I. Liansheng, F. Youjun, and W. Zhijian (1997). Studies of ternary surface complexes at liquid-solid interfaces in seawater. III. Comparative studies of the E(%)-pH curves and the diffuse reflectance ir spectra of the α-FeOOH-Cu(II)-tryptophan system. Journal of colloid and interface science 190, 1-8.

Chapter 5

THE EFFECTS OF PH AND IONIC STRENGTH ON PB(II) SORPTION MECHANISMS AT THE AMORPHOUS SILICA-WATER INTERFACE

5.1 Abstract

Pb sorption to amorphous SiO_2 was studied as a function of pH and ionic strength using XAS to characterize the sorption products formed. Macroscopic data showed that Pb sorption increased with increasing pH and decreasing ionic strength. The XAS data indicated that the mechanism of Pb sorption to the SiO_2 surface was strongly pH dependent. At low pH (pH=3.5-4.5), predominantly outer-sphere Pb sorption was observed, along with some inner-sphere Pb sorption to high affinity surface sites. Between pH4.5 and 5.5, Pb outer-sphere sorption systematically decreased with increasing pH, and sorption became increasingly inner-sphere. At pH>6.3, no outer-sphere sorption was observed. Nucleation was observed at pH>5.25. The average coordination number of the Pb-Si shell did not increase with pH, indicating either an increase in the disorder with respect to the Pb-Si distance, or outer-sphere adsorption of positively charged Pb-hydroxy clusters with increasing pH. Although lowering the ionic strength from I=0.1 to I=0.005M lead to a strong increase

Although lowering the ionic strength from I=0.1 to I=0.005M lead to a strong increase in Pb sorption, the XAS data showed that it did not strongly influence the average local coordination environment of sorbed Pb at a given pH. Increasing the Pb concentration in the electrical double layer above the SiO_2 surface due to increased outer-sphere Pb sorption may lead to increased inner-sphere Pb sorption as well, resulting in similar average Pb bonding environments at low and high ionic strength.

5.2 Introduction

Determining the mechanisms of heavy metal retention on solid surfaces is important in understanding and predicting the speciation, mobility and bioavailablity of these contaminants in natural environments. Metal sorption to mineral phases is known to occur via a number of mechanisms. These include electrostatic interactions, leading to outer-sphere metal sorption complexes, the formation of chemical bonds between the metal ions and surface functional groups, leading to inner-sphere metal sorption complexes, and the formation of multi-nuclear metal phases (Bargar *et al.*, 1996, 1997; Papelis and Hayes, 1997; Towle *et al.*, 1997; Scheidegger *et al.*, 1998; Xia *et al.*, 1998; Strawn and Sparks, 1999). Important controls on the speciation of heavy metals in mineral suspension are provided by the time allowed for reaction, the suspension pH, and the ionic strength of the system.

In soil environments, hydrous oxides such as silica usually form high surface area particles that may coat other soil materials, and therefore may strongly influence the surface charasteristics of field soils. Spectroscopic studies of Pb sorption to Fe-

on these minerals (Bargar *et al.*, 1997a,b; Strawn *et al.*, 1998). XAS studies of Cr(III), Co(II) and Cu(II) sorption to silica and quartz have shown the formation of multinuclear metal hydroxide sorption products upon contact with these SiO_2 phases (Fendorf *et al.*, 1994; O'Day *et al.*, 1996; Xia *et al.*, 1997, 1998; Cheah *et al.*, 1998). These studies, however, were performed under a limited set of reaction conditions with respect to pH and ionic strength, whereas these experimental parameters may have a significant effect on the mechanism(s) of metal sorption to SiO_2 (Kosmulski, 1997). Moreover, the results of these studies may not apply to the mechanism(s) involved in the interaction between Pb and amorphous SiO_2. In the case of Pb and Ni sorption to Al_2O_3, for instance, Ni forms precipitate phases, whereas Pb forms inner-sphere adsorption complexes under similar reaction conditions (Scheidegger *et al.*, 1998; Bargar *et al.*, 1997a; Strawn *et al.*, 1998). The aim of this study was therefore to study the mechanism of Pb sorption to amorphous SiO_2 as a function of pH and ionic strength (I), using XAS spectroscopy to characterize the Pb sorption products formed.

5.3 Materials and Methods

The amorphous SiO_2 used was Zeo49, obtained from the J.M. Huber Corporation. This silica has been used as a sorbent in previous metal sorption studies (*e.g.* Huang and Rhoads, 1988; Schulthess and Huang, 1990), and has a reported BET surface area of 280 $m^2\ g^{-1}$, and an average particle diameter of 9 μm (Huang and

Roads, 1988). A slight Al contamination is present in this material, which has a molar Si/Al ratio of 400 (Huang and Rhoads, 1988).

Pb sorption studies were performed in a N_2-purged glove box, using boiled DI water for sample and reagent preparation. The silicate concentration was 7 g L^{-1}, and the initial Pb solution concentration was 2 mM. The experimental parameters that were varied were pH (pH=4-7) and the background electrolyte (I= 0.1M and 0.005M $NaClO_4$). Prior to reaction with Pb, the amorphous SiO_2 material was hydrated in the background electrolyte for 24 h at pH4.0. Next, an appropriate amount of a 0.1M $Pb(ClO_4)_2$ stock solution was added to achieve a Pb solution concentration of 2 mM. The suspension was then titrated to higher pH by stepwise addition of 0.1M NaOH. After each pH increment, 5 mL aliquots were transferred from the main reaction vessel to 30 mL centrifuge tubes. The centrifuge tubes were placed on an end-over-end rotator operating at 20 rpm, for a reaction time of 24h. After equilibration, the final suspension pH was measured, and the samples were centrifuged at 15000 rpm for 10 minutes. The supernatants were filtered through 0.2 μm filters, acidified, and analyzed for Pb using AA spectrometry. The amount of Pb sorbed was calculated from the difference between the initial and final Pb concentrations.

Preparation of the XAS samples was done using the same procedure as described above, except that total volumes of 60 mL were used for these samples. To avoid Pb desorption, the wet pastes resulting after centrifugation were not washed to remove non-sorbed Pb in the entrained electrolyte. In the sample with the lowest Pb loading, the amount of Pb in the entrained electrolyte represented ≈3% of total Pb

present in the sample, with the percentage going down to essentially 0% for the high Pb loading samples. The XAS spectra were therefore strongly dominated by sorbed Pb, with negligible contributions of non-sorbed Pb present in entrained electrolyte.

XAFS spectra were recorded at Beamline X-11A of the National Synchroton Light Source, Brookhaven National Laboratory, Upton, NY. Spectra were collected at the Pb L_{III} edge (8333 eV) using a Si(111) crystal monochromator. The premonochromator slit width was set at 0.5 mm. Higher order harmonics were suppressed by detuning 25% from the maximum beam intensity. The samples were scanned in fluorescence mode at room temperature using a Kr filled Lytle detector equipped with an As filter. At least five scans were collected per sample.

Background subtraction, Fourier filtering, and data fitting were accomplished with the program WinXAS, in combination with the FEFF 7.0 code. The χ-function was extracted from the raw data by fitting a linear function to the pre-edge region and a 6-knot spline function to the post-edge region, and normalizing the edge jump to unity. The data were converted to k space and weighted by k^3. Structural parameters were extracted with fits to the standard EXAFS equation by multi-shell fitting in k-space. The reference compound used was β-$Pb(OH)_2$(s). The amplitude reduction factor used in the fitting procedure was 0.65.

The Pb/SiO_2 EXAFS data revealed that several different Pb sorption complexes were simultaneously present at the SiO_2 surface, as will be shown later. Two Pb-O shells were present in most samples, separated by about 0.2Å. Strong correlations between the optimized $N_{Pb\text{-}O}$ and $R_{Pb\text{-}O}$ values of the first and second O

shells resulted. Similarly, overlapping Pb-Si and Pb-Pb shells were present in some samples, leading to correlations between the R and N values of these shells. As a result, the accuracies of the optimized fitting parameters are difficult to estimate, which is further complicated by the lack of good reference materials for Pb^{2+}(aq). The fitting results obtained from our EXAFS analyses therefore do not necessarily present a very accurate description of the Pb speciation at the SiO_2 surface. Nevertheless, in combination with the raw XAS data, they provide useful information on the sorption processes of Pb occurring at the amorphous SiO_2 surface as a function of pH and I.

5.4 Results and Discussion

5.4.1 pH edges

Figure 5.1 compares the Pb/SiO_2 pH edges of the I=0.1M $NaClO_4$ and the I=0.005M $NaClO_4$ systems. Clearly, there is an ionic strength effect, with higher Pb sorption for the I=0.005M $NaClO_4$ system over most of the pH range. A similar ionic strength effect on metal sorption to silica has been reported in other studies (*e.g.* Kosmulski, 1997). This type of ionic strength dependence is commonly interpreted as indicating the occurrence of outer-sphere metal sorption. Since the Na ions present in the background electrolyte can compete with metal ions for outer-sphere sorption sites, there will be less metal sorption when the ionic strength (*i.e.* the Na concentration) is raised. In only few studies, however, the hypothesis of outer-sphere metal sorption as suggested by ionic strength dependent sorption has been tested using spectroscopic techniques characterizing the metal bonding mechanisms at the molecular level. In a

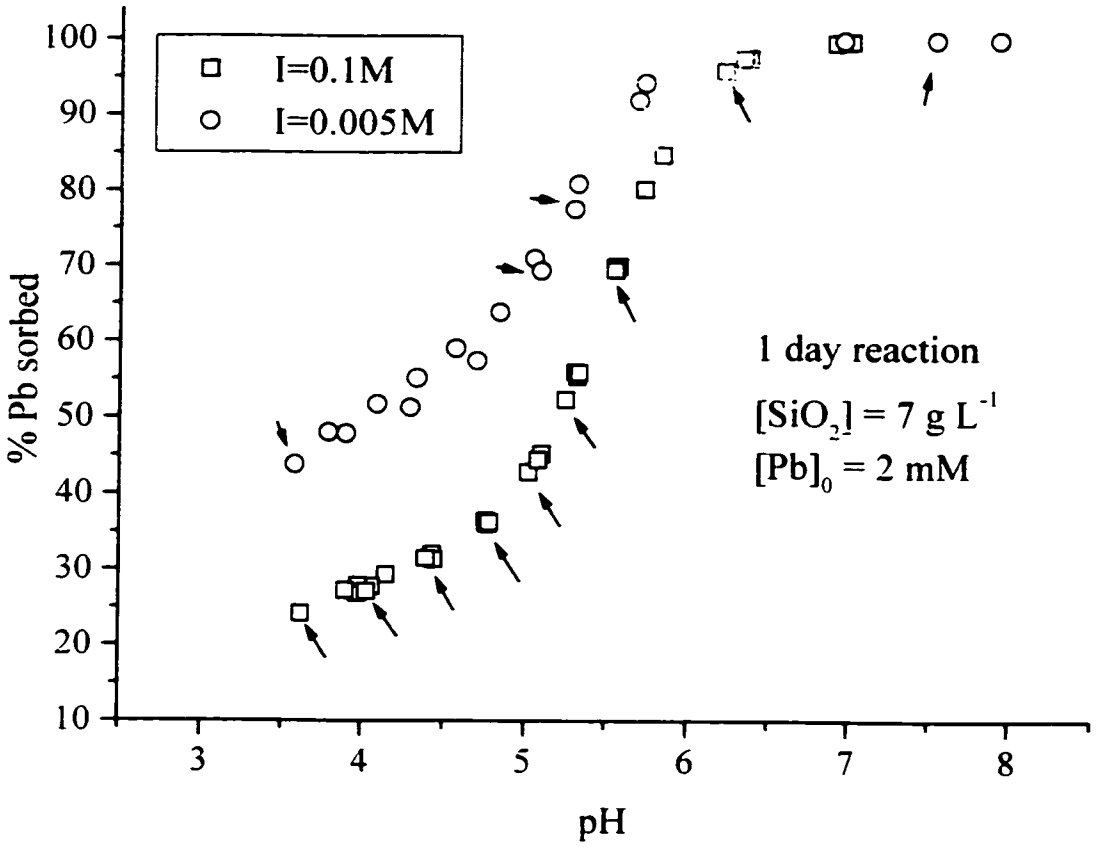

Figure 5.1 Comparison of the pH edges of Pb sorption to SiO_2 at I=0.1M and I=0.005M. The arrows denote the samples analyzed by XAS.

study of Pb sorption to montmorillonite, which is a strongly swelling clay mineral, Strawn and Sparks (1999) reported highly ionic strength dependent Pb sorption, and used XAS to demonstrate the occurrence of Pb outer-sphere complexes at low ionic strength. Similarly, Papelis and Hayes (1996) used XAFS to demonstrate the importance of outer-sphere Co complexes on montmorillonite at low ionic strength, explaining the increased Co sorption as I was lowered. To test the hypothesis of outer-sphere Pb sorption on silica, we performed XAS analysis of Pb/SiO_2 samples over a range of pH values. The samples analyzed by XAFS are indicated by arrows in Figure 5.1 and span the pH range between 3.5 and 7.5.

5.4.2 XANES Data

Figure 5.2 presents the near-edge spectra, normalized for the edge-jump, of the I=0.1M samples analyzed by XAS, along with those of the reference compounds Pb^{2+} (aq) and $Pb_4(OH)_4^{4+}$ (aq). Samples with low pH (3.5-4.5) have spectra that are similar, although not identical, to free Pb^{2+}(aq), suggesting that the dominant sorbed Pb species at low pH values retain their solvation water shells, *i.e.* they form outer-sphere complexes at the amorphous SiO_2 surface. As pH increases beyond pH4.5 to pH 6.3, the Pb/SiO_2 XANES spectra increasingly resemble the XANES spectrum of $Pb_4(OH)_4^{4+}$. Between pH 4.5 and 5.8, the Pb/SiO_2 spectra appear to be intermediate between the spectra of the two reference compounds, whereas the Pb/SiO_2 spectrum at pH 6.3 is essentially identical to the spectrum of $Pb_4(OH)_4^{4+}$. The Pb atoms in $Pb_4(OH)_4^{4+}$ have a distorted trigonal pyramidal coordination environment with

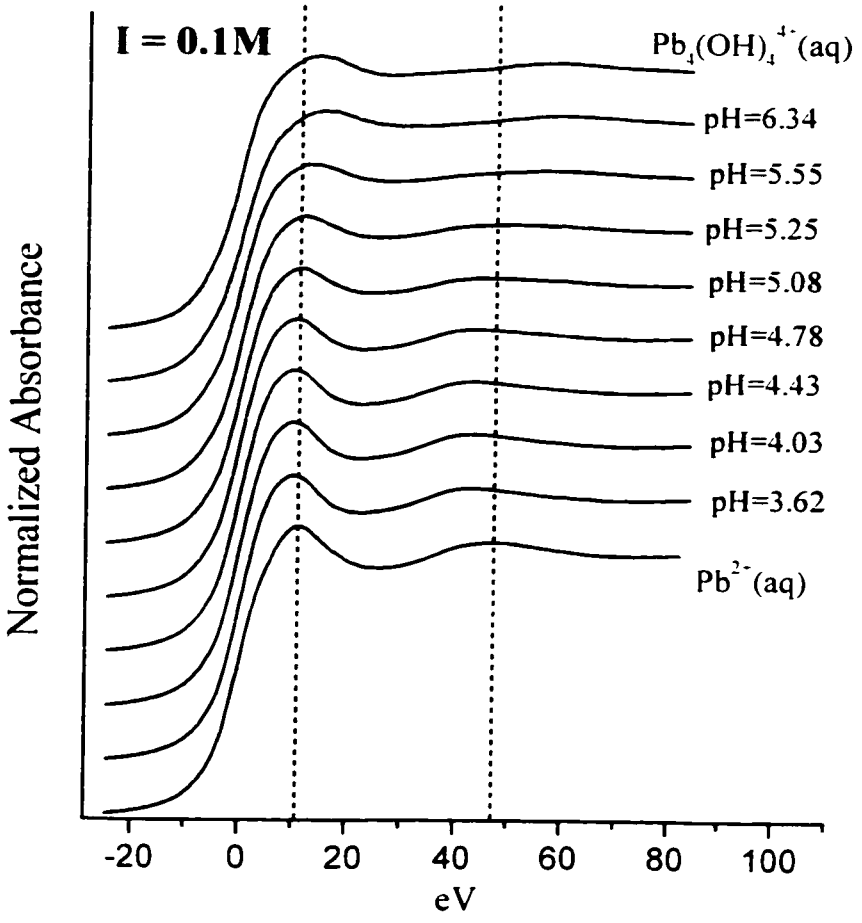

Figure 5.2 The XANES spectra (normalized for edge jump) of the I=0.1M Pb/SiO_2 samples and the Pb^{2+}(aq) and $Pb_4(OH)_4^{4+}$ (aq) reference compounds.

hydroxide ions as coordinating ligands (Bargar *et al.*, 1997a). This Pb coordination environment has been observed for Pb inner-sphere adsorption complexes at Al oxide surfaces (Bargar *et al.*, 1997a), as well as for multinuclear Pb complexes forming at the montmorillonite surface (Strawn and Sparks, 1999). The increasing resemblance between the $Pb_4(OH)_4^{4+}$ and Pb/SiO_2 spectra with increasing pH therefore indicates the formation of Pb inner-sphere adsorption complexes and/or multinuclear Pb complexes at the SiO_2 surface as pH increases.

The overall results of the XANES analysis suggest predominant outer-sphere Pb sorption at pH's up to about 4.5, the formation of Pb inner-sphere sorption complexes and/or multinuclear Pb complexes in addition to Pb outer-sphere complexes as pH increases from pH 4.5 to pH6, and predominant Pb inner-sphere adsorption or nucleation at pH>6. For a quantitative description of the Pb sorption processes at the amorphous SiO_2 surface, EXAFS analyses were performed on the XAS data collected.

5.4.3 EXAFS Data

The k^3-weighted χ-spectra of the samples analyzed by XAS in this study are presented in Figures 5.3 and 5.4, along with the best fits obtained from the fitting procedure. The χ structures show distinct changes as pH increases from 3.5 to 6.5. The low pH samples are dominated by O shell backscattering, with the signal amplitude strongly decreasing at $k>8$ $Å^{-1}$, which indicates high structural and thermal disorder, and a lack of heavy backscatterers in the coordination shell of the sorbed Pb

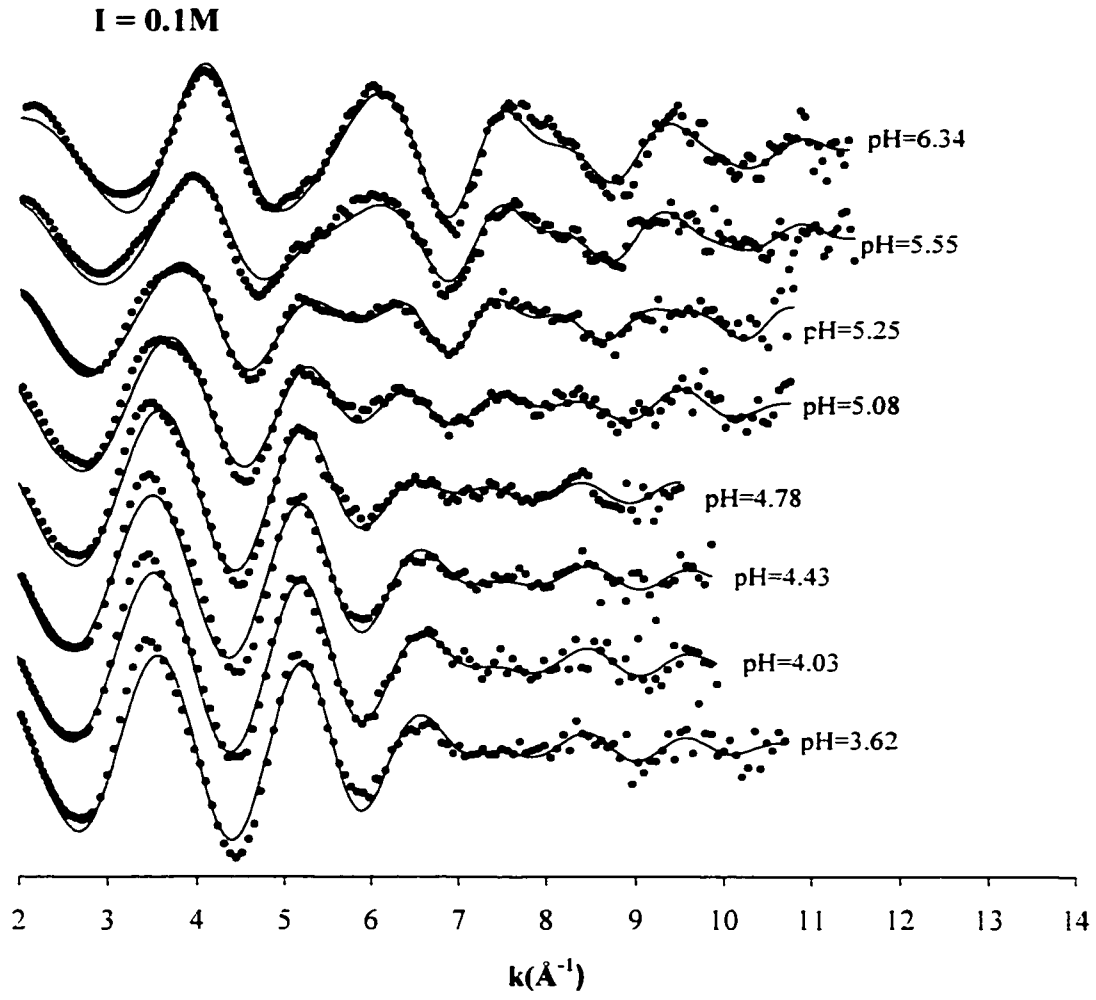

Figure 5.3 The raw χ spectra of the I=0.1M samples analyzed by XAFS (dotted lines), along with the theoretical χ spectra obtained from data fitting (solid lines).

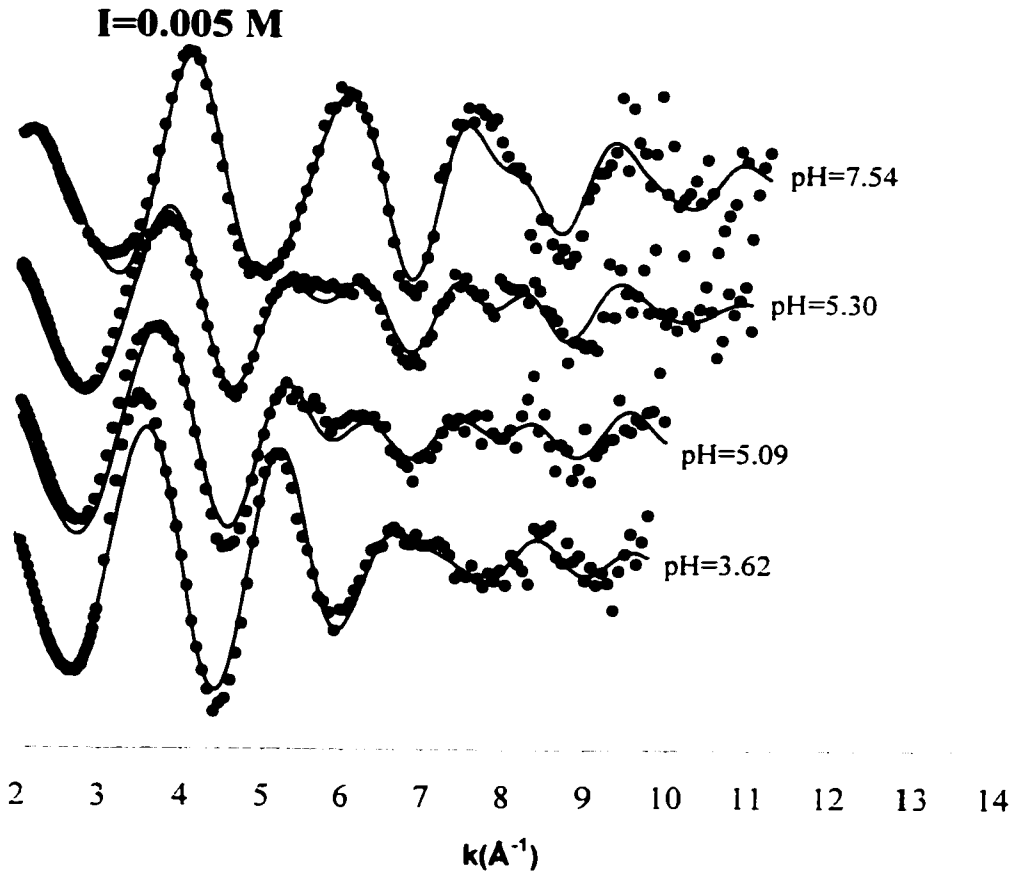

Figure 5.4 The raw χ spectra of the I=0.005M samples analyzed by XAFS (dotted lines), along with the theoretical χ spectra obtained from data fitting (solid lines).

metal cations (Yu *et al.*, 1991; Strawn and Sparks, 1999). As pH increases, pronounced features appear in the higher k range, indicating the presence of heavy backscatterers in the local coordination environment of sorbed Pb in these samples.

To analyze the frequencies appearing in the χ spectra presented in Figures 5.3 and 5.4, the k^3-weighted spectra were Fourier transformed. The resultant radial structure functions (uncorrected for phase shift) are shown in Figure 5.5. A broad first-shell O peak is observed for the low pH samples, along with a small second shell. Between pH 4 and 5.5, a second O shell appears in the RSF's, at a shorter radial distance than the O shell observed in the low pH samples. This O shell becomes more pronounced with increasing pH, and is the dominant O shell at pH 6.3. At pH>5, two features appearing at about 3.2 (on the shoulder of the Si shell) and 3.8 Å indicate Pb-Pb scattering in this pH range.

The EXAFS fitting results are presented in Table 5.1. At low pH, reasonable fits were obtained by fitting 2 shells: a Pb-O and a Pb-Si shell. The optimized $R_{Pb\text{-}O}$ values of these samples ($R_{Pb\text{-}O}$=2.5 Å) are similar to the $R_{Pb\text{-}O}$ of the Pb^{2+}(aq) standard ($R_{Pb\text{-}O}$=2.49 Å; fit not shown). This value, along with the high $N_{Pb\text{-}O}$ and Debye-Waller factor found for this shell, is consistent with Pb sorbed in an outer-sphere fashion (Bargar *et al.*, 1996; Strawn and Sparks, 1999). The presence of Si backscattering indicates that part of the total sorbed Pb in these samples is sorbed as inner-sphere complexes. Based on the results of Bargar *et al.* (1996, 1997a) and Strawn and Sparks (1999), we expect the $R_{Pb\text{-}O}$ of the inner-sphere complexes to be shorter (by about 0.2 Å) than the $R_{Pb\text{-}O}$ of the outer-sphere complexes. It was possible

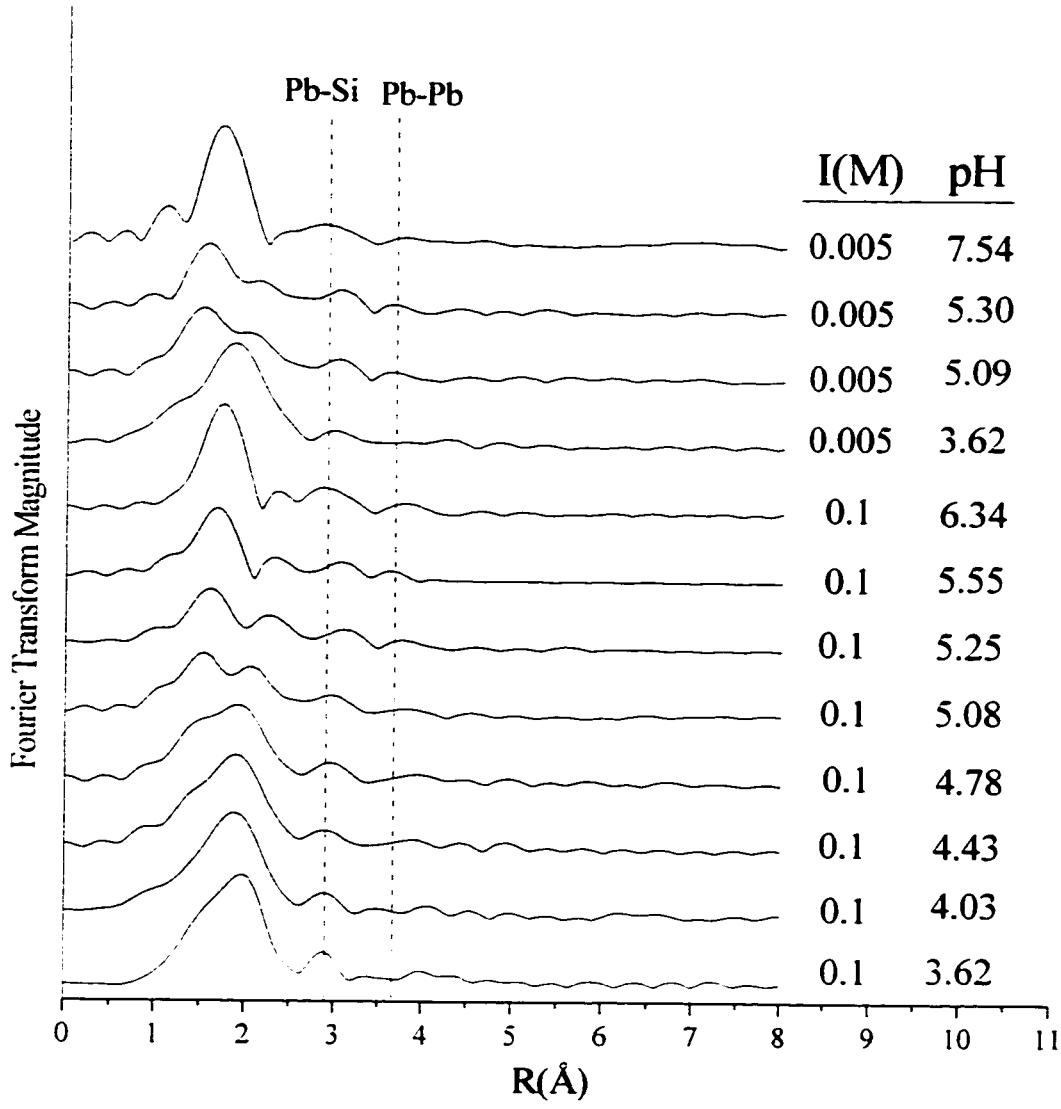

Figure 5.5 The radial structure functions (RSF's) obtained by Fourier transformation of the raw k^3-weighted χ spectra presented in Figures 5.3 and 5.4.

Table 5.1 The EXAFS fitting results of the Pb/SiO_2 samples.

I(M)	pH	Pb-O			Pb-O			Pb-Si			Pb-Pb		
		N	R(Å)	$\sigma^2(Å^2)$	N	R(Å)	$\sigma^2(Å^2)$	N	R(Å)	$\sigma^2(Å^2)$	N	R(Å)	$\sigma^2(Å^2)$
0.005	7.54	-	-	-	2.2	2.26	0.01	0.7	3.43	0.01	0.7	3.74	0.01
0.005	5.30	3.5	2.48	0.025	1.3	2.26	0.01	0.9	3.44	0.01	0.4	3.74	0.01
0.005	5.09	4.4	2.48	0.025	0.9	2.26	0.01	0.8	3.42	0.01	-	-	-
0.005	3.58	6.1	2.49	0.025	-	-	-	0.6	3.42	0.01	-	-	-
0.1	6.34	-	-	-	2.1	2.27	0.01	0.9	3.42	0.01	0.7	3.74	0.01
0.1	5.55	2.4	2.53	0.025	1.8	2.28	0.01	0.6	3.44	0.01	0.6	3.74	0.01
0.1	5.25	3.8	2.53	0.025	1.4	2.29	0.01	0.8	3.42	0.01	0.8	3.78	0.01
0.1	5.08	4.7	2.5	0.025	0.9	2.26	0.01	0.9	3.42	0.01	-	-	-
0.1	4.78	5.8	2.51	0.025	0.4	2.29	0.01	0.8	3.43	0.01	-	-	-
0.1	4.43	6.3	2.51	0.025	-	-	-	0.8	3.41	0.01	-	-	-
0.1	4.03	6.7	2.52	0.025	-	-	-	0.9	3.41	0.01	-	-	-
0.1	3.62	7.3	2.53	0.025	-	-	-	0.9	3.41	0.01	-	-	-

to fit a small number of O atoms at a radial distance of 2.25-2.30 Å. However, the R and N values of this additional O shell were very strongly correlated to the R and N values of the outer-sphere O shell. Moreover, including this shell only marginally decreased the least-squares residual of the fit. We therefore did not report this shell in Table 5.1.

The spectra of the samples reacted in the pH range 4.5-5.5 all required two O shells to obtain reasonable fits (Table 5.1). The first O shell had the same radial distance as the dominant O shell present in the low pH samples 1-3 (R_{Pb-O}=2.5 Å), and the second O shell had a R_{Pb-O} of about 2.28 Å, which is consistent with Pb present in a distorted trigonal coordination environment. These findings indicate that Pb sorption in the pH range 4.5-5.5 occurs via both inner- and outer-sphere complexation, and that both types of sorption complexes are simultaneously present at the amorphous SiO_2 surface in this pH range. Inspection of the RSF's in Figure 5.5 and the fitting results presented in Table 5.1 shows that the O shell indicative of Pb inner-sphere complexation (with R_{Pb-O}=2.28 Å) inreases relative to the O shell of Pb sorbed as outer-sphere complexes (R_{Pb-O}) as pH increases, indicating an increase in the importance of Pb inner-sphere sorption with increasing pH. Besides the two O shells, a Si shell at 3.45 Å was required to obtain good fits for these samples, and for the pH5.25 and pH5.55 samples, Pb-Pb scattering also had to be included for a good fit (Table 5.1).

The samples reacted at pH6.3 and pH7.5 show only one O peak , with a radial distance of about 2.28 Å (Figure 5.5 and Table 5.1). This indicates that outer-sphere

Pb sorption did not play a role in the Pb uptake at these high pH values. Additional scattering in these samples resulted from the presence of Si and Pb in the local coordination environment of sorbed Pb, at radial distances also found in the other samples (Table 5.1).

The combined XANES and EXAFS analysis of these samples show a strong pH effect on the Pb sorption mechanism to amorphous SiO_2. At low pH, substantial outer-sphere Pb sorption occurs, along with some (mononuclear) inner-sphere complexation. As pH increases from 4.4 to 6.3, the importance of outer-sphere Pb complexation systematically decreases, and inner-sphere Pb complexes and multinuclear Pb sorption products become increasingly important. The outer-sphere metal sorption observed in the pH range 3.5-5.5 can be explained by the low pH_{PZC} of amorphous SiO_2, which is estimated at about 2.0 (Parks, 1967). Huang and Rhoades (1988) measured the pH_{PZC} of the amorphous SiO_2 used in this study to be slightly lower than 2 ($\approx$1.3), probably due to Al^{3+} for Si^{4+} substitution in the SiO_2 structure, which had a Si/Al molar ratio of 400. As a result, the amorphous SiO_2 surface was negatively charged in the entire pH range applied in this study, allowing for the observed formation of outer-sphere Pb sorption complexes.

The optimized $R_{Pb\text{-}Si}$ is essentially the same in all samples ($\approx$3.42 Å). Coordination of Pb to the edge of a Si tetrahedron would result in a $R_{Pb\text{-}Si}$ value of about 2.45 Å, as calculated based on an O-O edge distance in Si tetrahedra of 2.62-2.64 Å (O'Day *et al.*, 1996), and the $R_{Pb\text{-}O}$ value of 2.3 Å found in the fitting procedure. We therefore conclude that Pb does not form edge-sharing inner-sphere

complexes with Si-tetrahedra, presumably due to strong Si^{4+}-Pb^{2+} repulsion in this configuration, but rather forms monodentate or corner-sharing complexes. It is interesting to note that the EXAFS data analysis results (Table 5.1) suggest that the average number of Si backscatterers is the same throughout the whole pH range. This suggests a larger disorder in the (average) local coordination environment of the inner-sphere Pb sorption complexes formed at higher pH. The amorphous nature of the SiO_2 likely results in a large number of potential sites for inner-sphere Pb sorption, with slightly different $R_{Pb\text{-}Si}$ values. At low pH, only the most reactive sites with a high affinity for Pb sorption will be active in inner-sphere Pb complexation. It is likely that these high affinity sites have very similar $R_{Pb\text{-}Si}$ values. As pH increases, also sites with less affinity for Pb become active in Pb complexation, and it is likely that this leads to an increase in the range of $R_{Pb\text{-}Si}$ values of the inner-sphere Pb sorption complexes present. The resultant increase in destructive interference between Si scattering signals from slightly different radial distances may explain why the overall second neighbor Si scattering does not increase with increasing pH. An alternative explanation is that the Pb polymers forming at higher pH are not attached to the silica surface via chemical Pb-surface bonds, but form positively charged $Pb_4(OH)_4^{4+}(aq)$ complexes that are electrostatically held in the electrical double layer of the negatively charged SiO_2 surface. An increase in Pb-Si coordination with increasing pH due to increased inner-sphere Pb complexation could then be countered by a simultaneous increase in $Pb_4(OH)_4^{4+}$ sorption, resulting in similar average Si scattering with increasing pH.

While pH has a strong effect on the mechanisms of Pb sorbed to the amorphous SiO_2 surface, ionic strength does not appear to strongly influence the average local coordination environment of sorbed Pb at a given pH, as shown by the similarity in the χ structures and RSF's of low and high I samples with the same pH (Figures 5.3-5.5). This indicates that the increase in Pb sorption observed by lowering the ionic strength from I=0.1 to 0.005M (Figure 5.1) is due to increases in both inner- and outer-sphere Pb complexation. In the case of Pb and Co sorption to montmorillonite, lowering I has been shown to dominantly favor outer-sphere Pb complexation (Papelis and Hayes, 1996; Strawn and Sparks, 1999). The difference between amorphous SiO_2 and montmorillonite in this respect may be due to the strong separation of inner- and outer-sphere sites on montmorillonite, where sites for outer-sphere sorption are located in the internal surface area of the clay, whereas inner-sphere sorption sites are located on the clay edges. At the amorphous SiO_2 surface, however, such a strong spatial separation of inner- and outer-sphere sites does not exist. Increasing the Pb concentration in the electrical double layer above the SiO_2 surface due to increased outer-sphere Pb sorption may therefore, via mass action, drive additional inner-sphere Pb sorption as well.

5.5 References

Bargar, J.R., S.N. Towle, G.E. Brown Jr., and G.A. Parks. 1996. Outer-sphere Pb(II) adsorbed at specific surface sites on single crystal α-alumina. Geochimica et Cosmochimica Acta, 60, 3541-3547.

Bargar, J.R., G.E. Brown Jr., and G.A. Parks. 1997a. Surface complexation of Pb(II) at oxide-water interfaces: I. XAFS and bond-valence determination of mononuclear and polynuclear Pb(II) sorption products on aluminum oxides. Geochimica et Cosmochimica Acta, 61, 2617-2637.

Bargar J.R., G.E. Bown Jr., and G.A. Parks. 1997b. Surface complexation of Pb(II) at oxide-water interface: II. XAFS and bond-valence determination of mononuclear Pb(II) sorption products and surface functional groups on iron oxides. Geochimica et Cosmochimica Acta, 61, 2639-2652.

Cheah, S.F., G.E. Brown Jr., and G.E. Parks. 1998. XAFS spectroscopy study of Cu(II) sorption on amorphous SiO_2 and γ-Al_2O_3: Effect of substrate and time on sorption complexes. Journal of Colloid and Interface Science, 208, 110-128.

Fendorf, S.E., G.M. Lamble, M.G. Stapleton, M.J. Kelley, and D.L. Sparks. 1994. Mechanisms of Chromium(III) on silica. 1. Cr(III) surface structure derived by extended X-ray absorption fine structure spectroscopy. Environmental Science and Technology, 28, 284-289.

Huang, C.P., and E.A. Rhoads. 1988. Adsorption of Zn(II) onto hydrous aluminosilicates. Journal of Colloid and Interface Science, 131, 289-306.

Kosmulski, M. 1997. The effect of the ionic strength on the adsorption isotherms of nickel on silica. Journal of Colloid and Interface Science, 190, 212-223.

O'Day P.A., C.J. ChisholmBrause, S.N. Towle, G.A. Parks, and G.E. Brown Jr. 1996. X-ray absorption spectroscopy of Co(II) sorption complexes on quartz (α-SiO_2) and rutile (TiO_2). Geochimica et Cosmochimica Acta, 60, 2515-2532.

Parks, G.A. 1967. Aqueous surface chemistry of oxided and complex oxide minerals - Isoelectric point and zero point of charge. In "Equilibrium Concepts in Natural Water Systems" (W. Stumm, ed.). Advances in Chemistry Series No. 67, pp 121-160. American Chemical Society, Washington, DC

Papelis, C., and K.F. Hayes. 1996. Distinguishing between interlayer and external sorption sites of clay minerals using X-ray absorption spectroscopy. Colloids and Surfaces A, 107, 89-96.

Scheidegger, A.M., D.G. Strawn, G.M. Lamble, and D.L. Sparks. 1998. The kinetics of mixed Ni-Al hydroxide formation on clay and aluminum oxide minerals: A time-resolved XAFS study. Geochimica et Cosmochimica Acta, 62 , 2233-2245.

Schulthess, C.P. and C.P. Huang. 1990. Adsorption of heavy metals by silicon and aluminum oxide surface on clay minerals. Soil Science Society of America Journal, 54, 679-688.

Strawn, D.G., A.M. Scheidegger, and D.L. Sparks. 1998. Kinetics and mechanisms of Pb(II) sorption and desorption at the aluminum oxide-water interface. Environmental Science and Technology, 32, 2596-2601.

Strawn, D.G., and D.L. Sparks. 1999. The use of XAFS to distinguish between inner- and outer-sphere lead sorption complexes on montmorillonite. Journal of Colloid and Interface Science, 216, 257-269.

Towle, S.N., J.R. Bargar, G.E. Brown Jr., and G.A. Parks. 1997. Surface precipitation of Co(II)(aq) on Al_2O_3. Journal of Colloid and Interface Science, 187, 62-82.

Xia K., A. Mehadi, R.W. Taylor, and W.F. Bleam. 1997. X-ray absorption and electron paramagnetic resonance studies of Cu sorbed to silica: Surface-induced precipitation at low surface coverages. Journal of Colloid and Interface Science, 185, 252-257.

Xia K., R.W. Taylor, W.F. Bleam, and P.A. Helmke. 1998. The distribution of Cu(II) on boehmite and silica surfaces: Correlating EPR signal loss with the effective Bohr magneton number of sorbed ions. Journal of Colloid and Interface Science, 199, 77-82.

Yu, Y.H., T. Tyliszczak, and A.P. Hitchcock. 1990. Pb L3 EXAFS and near-edge studies of lead metal and lead oxides. Journal of Physics and Chemistry of Solids, 51, 445-451.

Chapter 6

Summary and Future Research Needs

The research presented in this dissertation showed the importance of characterizing metal sorption reactions to clay minerals and oxides as a function of the reaction conditions applied to the metal-mineral sorption system. Dramatic changes in both the extent and mechanisms of metal sorption were found to occur within ranges of pH, ionic strength, and reaction times relevant to natural soil and aquatic systems. This indicates that in most systems, there is no such thing as "the" metal-mineral sorption reaction. Instead, sorption mechanisms should be defined and modeled with due attention to the reaction conditions imposed on the system, taking into account that several different retention mechanisms may be simultaneously operative. The presence of non-inert co-adsorbing oxyanions, as well as competition between mineral surfaces for metal uptake, both of which are situations commonly found in field soils, were found to strongly influence the metal speciation in the model systems presented here. This demonstrates the importance of doing basic research on systems that are more realistic with respect to what is going on in the field in order to understand the behavior of metal contaminants in natural systems.

Continued research on model systems and more complex systems is needed to put constraints on modeling efforts of metal speciation, reactivity and bioavailability in environmental settings. The use of spectroscopic tools is highly useful, if not a prerequisite, in this respect, since they provide truly mechanistic information on the reaction mechanisms studied. The continued development of these tools will lead to increased sensitivity, enabling analysis at the relatively low contaminant levels commonly found in soils. The development of synchroton sources with high fluxes in the hard X-ray energy range, such as the recently opened 3rd generation light source at Argonne National Laboratory, provides opportunities for combining high resolution microscopy with XAFS measurements at the sub-micron scale, which is ideal for studying metal speciation in field contaminated soils. Combining the mechanistic information from bulk XAFS analyses of model systems with μ-XAFS data of real soils will provide a solid basis for testing, adjusting and calibrating current mechanistic models on metal contaminant behavior in soils.